March 2018

MODELING DEFORMATION BEHAVIOR AND STRENGTH CHARACTERISTICS OF SAND-SILT MIXTURES: A MICROMECHANICAL APPROACH

Mehrashk Meidani
University of Massachusetts Amherst

MODELING DEFORMATION BEHAVIOR AND STRENGTH CHARACTERISTICS OF SAND-SILT MIXTURES: A MICROMECHANICAL APPROACH

A Dissertation Presented

by

MEHRASHK MEIDANI

Submitted to the Graduate School of the

University of Massachusetts Amherst in partial fulfillment

of the requirements for the degree of

DOCTOR OF PHILOSOPHY

February 2018

Civil Engineering

MODELING DEFORMATION BEHAVIOR AND STRENGTH CHARACTERISTICS OF SAND-SILT MIXTURES: A MICROMECHANICAL APPROACH

A Dissertation Presented

by

MEHRASHK MEIDANI

Approved as to style and content by:

_____

Ching S. Chung, Chair

_____

Don J. DeGroot, Member

_____

Byung H. Kim, Member

_____

Richard N. Palmer, Department Head

Civil and Environmental Engineering Department

ABSTRACT

MODELING DEFORMATION BEHAVIOR AND STRENGTH CHARACTERISTICS OF SAND-SILT MIXTURES: A MICROMECHANICAL APPROACH

FEBRUARY 2018

MEHRASHK MEIDANI

B.Sc., CHAMRAN UNIVERSITY

M.Sc., SHIRAZ UNIVERSITY

Ph.D., UNIVERSITY OF MASSACHUSETTS AMHERST

Directed by: Professor Ching S. Chang

This dissertation is comprised of six chapters. In the first chapter the motivation of this research, which was modeling the deformation behavior and strength characteristics of soils under internal erosion, is briefly explained. In the second chapter a micromechanis-based stress-strain model developed for prediction of sand-silt mixtures behavior is presented. The components of the micromechanics-based model are described and undrained behavior of six different types of sand-silt mixtures is predicted for several samples with different fines contents. The need for a more comprehensive compression model for sand-silt mixtures is identified at the end of this chapter. This desired compression model should be able to explicitly consider the fines content of the mixture and incorporates particle crushing effects as well. In the third chapter a new hypothesis of active and inactive void ratios in granular material and its application in modeling compressibility is examined and a compression model for sands is proposed. In the fourth

chapter the concept of inactive void ratio is extended to sand-silt mixtures and a new model is developed for compression of these mixtures that can explicitly consider the fines content in its formulation. After the validity of the new hypothesis of active and inactive voids in granular material is verified in chapters 3 and 4, the model is further developed in chapter 5 to incorporate the effects of particle crushing on the compressibility of granular material. The sixth chapter is conclusion of this work and recommendations for future investigations.

TABLE OF CONTENTS

Page

LIST OF TABLES

Table Page

LIST OF FIGURES

Figure Page

CHAPTER 1

INTERNAL EROSION AND UNDRAINED INSTABILITY IN SAND-SILT MIXTURES

1.1. Introduction

This research started with a National Science Foundation project to study the deformation behavior and strength characteristics of sand-silt mixtures under the effects of internal erosion. A micromechanics-based model was adopted to be developed and used to predict the undrained behavior sand-silt mixtures, which are the most prone class of soils to the internal erosion.

Sand-silt mixtures are very abundant in nature as well as in earthfill structures and the fines content in these mixtures can be in various proportions. About 80% of shoreline areas in the world are covered by sediments such as silty and sandy soils (Brandes, 1999). Mine tailing facilities are also among the places where silty sands, usually at very loose state and in high fines contents, are found (Yamamuro and Covert, 2001). In the North American continent, 75% of sedimentary deposits are floodplain silt and sandy silt.

Only in the United States, more than 160 million people live close to shorelines and river banks and are protected from the seasonal floods by levees and embankments (as of census 2008, see Figure 1). Most of these levees and embankments are built of sand-silt mixtures. New Orleans levee failures during hurricane Katrina in 2005 is an example of the catastrophe that can happen due to the instability and loss of shear strength in sand-silt mixtures.

Most of the natural soil deposits are formed in still or running waters. When non-

plastic fines are present in sand fabric, they increase the likelihood of forming metastable structures under certain deposition conditions. Terzaghi (1956) mentioned this fact and showed some failures of submarine large slopes in the presence of fines. In 1988 Saguenay earthquake, liquefaction occurred in sandy-silt and silty-sand soils in Quebec-Canada (Troncoso, 1988). In 1983, The Nerlerk berm in Canada slid due to liquefaction in silty sand (Sladen et al., 1985).

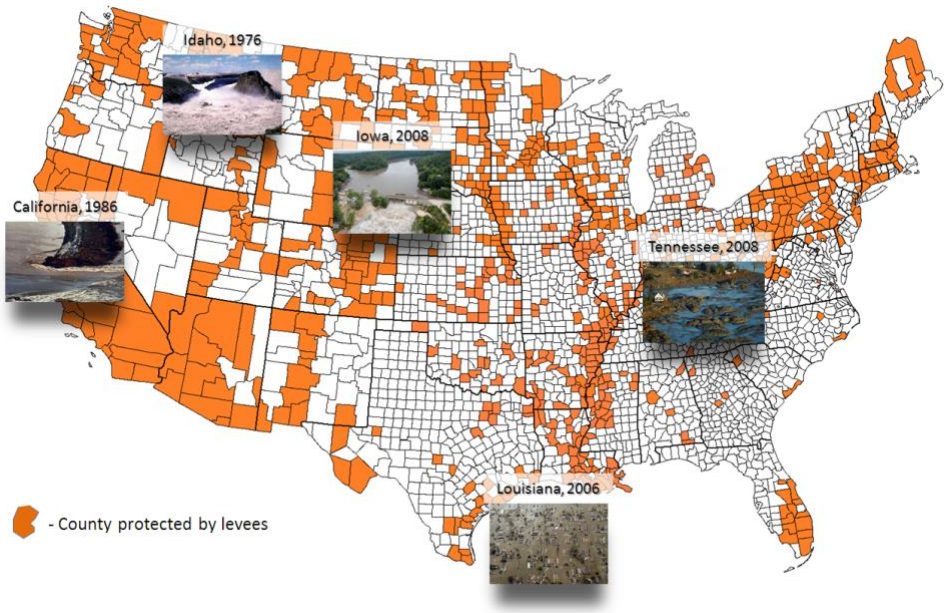

Figure 1- Counties protected by levees in the United States and some of the failure cases [after Chang and Meidani, 2012].

One of the main reasons that contribute to the loss of shear strength of such soil mixtures is loss of fines due to internal erosion (Ke and Takahashi, 2015; Ke et al., 2016). When fines are washed out from the soil as a result of seepage, the initial fabric of the soil is changed and its void ratio increases. Incremental or continuous volume change (collapse) may occur in the soil as well. Increase of soil void ratio causes the shear strength of the soil to decrease. Settlement as a consequence of displacing the fine

particles due to internal erosion can also lead to overtopping. Figure 2 shows a schematic cross section of an embankment which has gone through internal erosion. The pictures show the onset of failure in the earth structure due to internal erosion and its complete collapse.

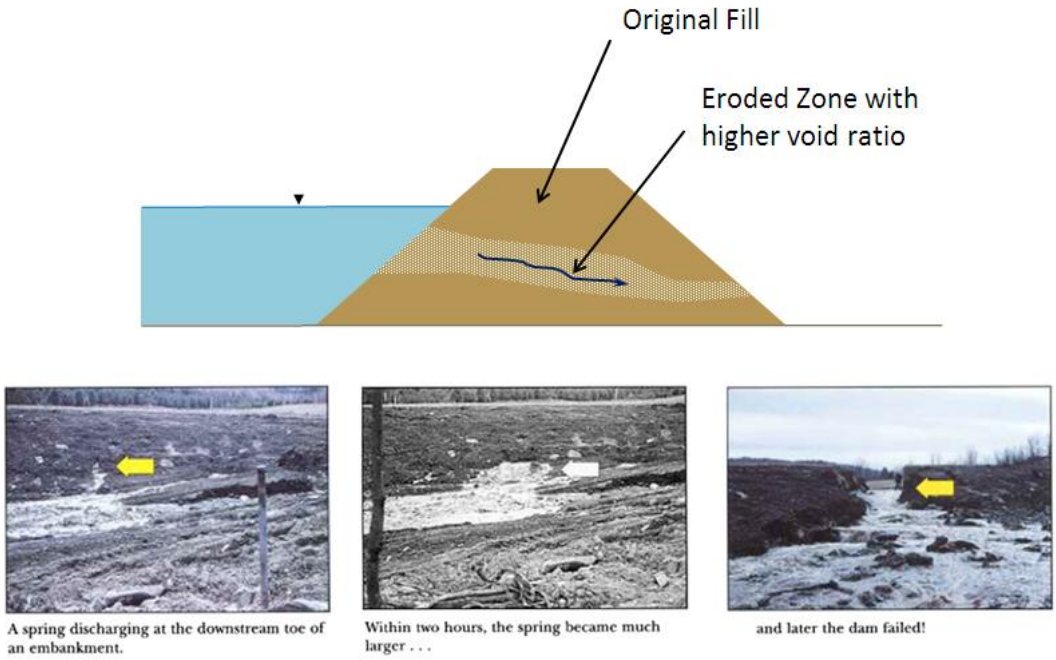

Figure 2- Internal erosion in soil and consequent failure [after Chang and Meidani, 2012].

1.2. Undrained behavior of sand-silt mixtures

In the past two decades, due to the frequent failures of levees associated with storms and floods, the monotonic undrained behavior of such soils has drawn more attention from the geotechnical community. Some of these works are listed in Table 1 in a timely order. However, there are very few works which included the effect of internal erosion on the deformation behavior and shear strength of eroded soils, either theoretically or experimentally (e.g. Pham, 2008; Fujiswa, 2009; Shwiyhat, 2010; Chang, 2012; Putman

et al., 2012; Shire & O'Sullivan, 2012; Ke and Takahashi, 2016).

Based on the results of triaxial tests for isotropic consolidated specimens and subsequently loaded under monotonic undrained conditions, the stress-strain behavior of sand-silt mixtures can be classified into four general distinct types as shown in Figure 3.

Type 1 indicates a complete loss of shear strength during shear, which is also named static liquefaction (or *collapsive behavior* in this thesis). During shear, pore water pressure develops and accumulates due to contractive tendency of the soil. As a result, the shear strength of soil drops drastically because of the largely decreased effective confining pressure.

In Type 2, after soil reaches the pick deviator stress (q_{peak}), it continues to deform with decreasing shear strength until it reaches a residual strength at critical state condition. This behavior may be called *partially collapsive*. A special case for this type of behavior is perfectly plastic shearing when the soil does not lose any shear strength once it reaches q_{peak} and the residual strength and q_{peak} are equal.

Type 3 of behavior shows a temporary loss of shear strength after its initial peak. For a relatively large range of axial strains, the soil remains weaker than its initial peak strength. This stage is called quasi-steady state in the literature. As the shearing continues, the soil dilates and gradually gains strength. The final residual strength could be even higher than the first peak strength. However, the lowest residual strength after the peak should be considered in the stability analyses. This behavior can be called *temporally collapsive*.

In Type 4, soil shows a complete hardening behavior which is also called *dilative response*. In this type of behavior, the stiffness of soil may reduce temporarily after the yield point but soil continues to gain strength towards the critical state condition.

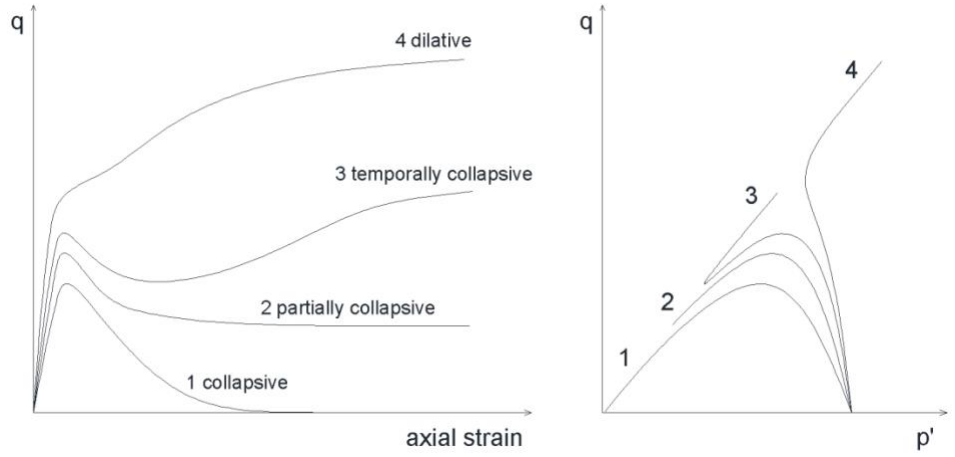

Figure 3- Four different types of undrained behavior observed in sand-silt mixtures [after Chang and Meidani, 2013].

These four types of behavior are mainly governed by (1) the initial void ratio, (2) amount of fines in the mixture, (3) the way that soil was deposited, and (4) the effective stress level that is applied to the soil.

It is well-known that void ratio alone is not correlated well with the various types of behavior of sand-silt mixtures because fines content has a significant influence on the soil microstructure (Thevanayagam et. al, 2002). Usually, if fines content in the mixture is less than 25%, the coarse grains form a network of connecting particles and the behavior of the mixture is mainly controlled by that network (*case i* in Figure 4). If fines content is higher than 35%, the coarse particles become dispersed in the mixture and the behavior of the soil is mainly dominated by a network of fine particles (*case ii* in Figure 4). There are also intermediate cases in which the soil matrix is neither coarse nor fine grain

dominated, as is shown in *case iii* of Figure 4. Therefore, a proper index to correlate the behavior should include both void ratio and fines content. For this purpose, inter-granular and inter-fine void ratios are defined in the literature for sand-silt mixtures to represent the void ratio of the dominant matrix.

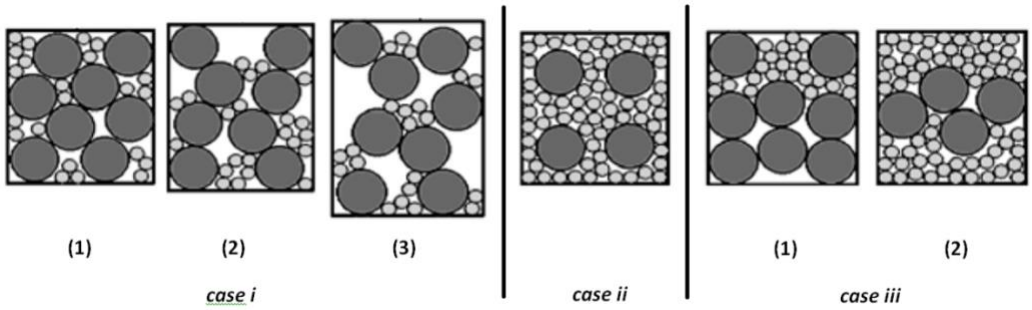

Figure 4- Intergranular soil mixture classification (after Thevanayagam et al., 2002).

Kuerbis et al. (1989) defined skeleton void ratio (e_c) for coarse-grain dominated matrices as:

$$e_c = \frac{e + f_c}{1 - f_c} \tag{1}$$

where f_c is the fines content ($d_{50} \leq 0.075$mm) in decimal figures, and e is the global void ratio of the mixture. Mitchell (1993) and Vaid (1994) later called e_c "intergranular void ratio".

Thevanayagam (1998) and Thevanayagam and Mohan (2000) defined inter-fine void ratio (e_f) for fine-grain dominated matrices as:

$$e_f = \frac{e}{f_c} \tag{2}$$

The intergranular and interfine void ratios, compared to the global void ratio, have been shown to be useful in correlating the aforementioned four different types of stress-

strain behavior for sand-silt mixtures. However, as demonstrated by Thevanayagam et al. (2002), these indices fail to characterize the behavior of sand-silt mixtures in some situations. In order to find a better index to characterize the behavior of sand-silt mixtures, Thevanayagam et al. (2002) proposed two "equivalent intergranular contact void ratios", $(e_c)_{eq}$ and $(e_f)_{eq}$, for the mixtures with low and high fines contents, respectively. However, they also concluded that there was no unique index suitable for characterizing the behavior of the sand-silt mixtures.

Besides the aforementioned work, some researchers tried to correlate particular characteristics of the stress-strain behavior with density indices. For example, Yang et al. (2006) correlated the peak stress ratios of samples with low and high fines content with intergranular and interfine void ratios, respectively. The correlations are reasonably good using the experimentally measured data by Yang (2004). Intergranular void ratio index has also been used by Belkhatir et al. (2010) to correlate residual undrained shear strength of silty Chlef sands (f_c=0 to 50%). Their results show a linear decrease in undrained shear strength of the sample with an increase in intergranular void ratio.

Since the approach of using density indices shows shortcomings when describing the overall behavior of sand-silt mixtures, a general stress-strain model for these materials could be more desirable. As the physics underlying the behavior of all the granular materials is the same, the constitutive models for sand can be used for sand-silt mixtures with some modification that consider the influence of fines on the mixture behavior.

To date, there have been very few works on the stress-strain modeling of sand-silt mixtures. Yamamuro and Lade (1999) proposed a simple modification to their single hardening model yield surface formulation, which leads to the prediction of silty sands

behavior. However, their prediction is restricted to the mixtures with 20% fines content. Thus, the proposed yield surface in their model may be only valid for 20% fines content, and the yield surface may take different shapes for other fines contents. Chang and Yin (2011) proposed a more general model that can be used for simulating the behavior of silty sands with low fines contents, by adopting a micromechanical model approach for sands (Chang and Hitcher, 2005). They considered the contribution of different amount of fines to the magnitude of plastic sliding between sand particles during shear. The model worked well for predicting the behavior of silty sand. However, this model was developed for coarse-grain dominated mixtures, i.e. f_c<25% (case i in Fig. 2) and would not be applicable for higher fines contents (cases ii or iii in Fig. 2).

In the following sections, first we describe the general approach in modeling the behavior of granular materials. Then following in Chapter 3, we explain our micromechanics-based model for sand-silt mixtures. Subsequently, the calibration procedure of model parameters is provided and the applicability of this new model is evaluated by comparing the simulation results with the experimental measurements for two different types of sand-silt mixtures from the literature (Yang 2004 and Konishi et al. 2007).

The adopted micromechanics based model (Chang and Hicher, 2005) has two elementary building blocks: (1) the inter-particle contact model that defines the relationship between inter-particle forces and displacements for two contacting grains; and (2) utilizing a mean-field analysis, the overall stress-strain relationship of the packing is obtained from integration of the contact behaviors in all orientations.

This approach has also been used by other researchers to construct elastic and elasto-plastic multi-scale constitutive models. Elastic stress-strain models can be found in the works of Jenkins (1988), Walton (1987), Rothenburg and Selvadurai (1981), Chang (1988), Emeriault and Cambou (1996), Liao et al. (2000), Kruyt and Rothenburg (2002), and Tran et al. (2012). For elasto-plastic stress-strain models, the behavior at inter-particle level is more complex. These types of models can be found in the works by Jenkins and Strack (1993), Matsuoka and Takeda (1980), Nicot and Darve (2007), Maleej et al. (2009), Misra and Yang (2010), Zhu et al. (2010), and Zhang and Zhao (2011).

Compared with the discrete element method (DEM), the first advantage of this approach is that we do not need to know the detailed configuration of entire packing at particle level as the input information. Instead, the packing configuration in our approach is represented by the distribution of contacts orientations, which can be estimated from conventional laboratory test results (e.g. compression and extension triaxial tests). The second advantage of this approach is that the computational effort is much less for the integration process using a mean-field analysis, and in some simple elastic cases, closed form solutions can be derived.

The shortcomings of this approach, compared with DEM, result from three assumptions: (1) the contact force is either estimated from the applied stresses using a static hypothesis, or from the applied strains using an affine deformation assumption (i.e. kinematic hypothesis). In either case, the interaction of neighboring particles at local contacts is not considered and the inter-particle contact force can be regarded as an average measure; (2) the mean-field analysis does not consider the correlations between

force vector and branch vector; (3) the mean-field analysis does not consider the physical mechanisms of particle rotation and rolling.

It seems that the first and second assumptions cannot be resolved without prior knowledge of grains configuration details in a packing. For the third assumption, the necessary understanding about the complex mechanism of interaction between particles rotation and sliding has not been achieved yet. Therefore, these shortcomings are embedded in the approach of mean-field analysis and cannot be removed at the present time.

For modeling the elasto-plastic behavior of sand, the above-mentioned assumptions prevent the mean-field method from correctly predicting the behavior. To overcome this problem, a density state variable (defined as a function of the critical state void ratio) was introduced for the packing and the amount of inter-particle plastic sliding was assumed to be dependent on this variable (Chang and Hicher, 2005). Using this assumption, the induced error by the mean-field method can be corrected and the mean-field analysis can be used to successfully model the salient features of the stress-strain behavior of sand. This approach is rather empirical but it can capture the essence of the phenomenon.

In the mean-field analysis, only mean particle size is used and particle size distribution is not accounted for. Thus, the mean-field analysis is acceptable for the materials which has relatively uniform particle size distribution (e.g. poor graded sand). It is questionable whether this method can be applied to materials with a broad range of particle sizes. Looking into the literature, very few work were found to be devoted to study the behavior of material with a broad range of particle sizes. As an example, Shaebani et al. (2012) showed that for modeling elastic stiffness of a packing with a broad range of particle

sizes, the use of mean particle size is not appropriate. They included the moments of particle size distribution in the mean-field analysis in order to calculate the elastic stiffness of the packing. Their analysis was limited to elastic conditions, and still contained the three assumptions mentioned above.

Another study on the effect of particle size distribution was performed by Chang and Yin (2011), focused on the elasto-plastic modeling of sand mixed with small amounts of silt ($f_c < 25\%$). In this work the mean-field analysis by Chang and Hicher (2005) was adopted; The effect of fines particles was considered through the use of a density state variable (or the critical state void ratio) of the overall packing. It was shown that for a sand-silt mixture, the density state is a function of fines content. A model based on this approach has been found to be applicable to several types of sand-silt mixtures under triaxial drained and undrained conditions (Chang and Yin, 2011).

Chang and Yin (2011) work is focused on the behavior of mixtures with small amount of fines ($0\% < f_c < 25\%$). In this work, we adopt mean-field analysis to model the behavior of sand-silt mixtures with high amount of fines ($25\% < f_c < 100\%$).

For the full range of fines content, the characteristics of void ratio change of a packing is very different for the following three ranges of fines contents:

For the case of sand mixed with small amounts of silt ($f_c < 25\%$), most of the fines are filling the voids between sand particles. The dominant grains network is primarily comprised of sand particles. The silt particles are mainly floating in the voids of that network. So, deformation of the packing is controlled by the displacement of sand particles.

For the case of sand mixed with intermediate amounts of silt (25% < f_c < 35%), the fines almost fill all the voids, and start to separate the sand grains. The dominant network of sand grains starts to be destroyed while a network of silt grains starts to form. In this range of fines contents, the dominant grains network is not solely comprised of either sand or silt particles. It is difficult to determine whether the dominant network is made of fine or coarse particles.

For the case of mixtures with high silt content (f_c > 35%) the sand grains become isolated and float in a network of silt grains. Therefore, the silt grains form a *dominant grain network*. Deformation of the packing is controlled by the displacement of the silt particles. The presence of sand particles within a dominant network of silt particles has two major effects on the mechanical behavior of these mixture: (1) the presence of coarse particles has considerable influence on the amount of particle sliding between fines, which is closely related to the characteristics of void ratio change. A method is proposed to model the influence of coarse particles on the characteristics of void ratio change; (2) since the mixture is treated as a network of fine grains, the contact density, *N/V*, is referred to the total number of contacts between fine grains per unit volume. A method for estimation of *N/V* is described. Details of these two aspects are given below.

1.3. Void ratio change characteristics for sand-silt mixtures

In a packing with single sized spherical particles, the void ratio can range from 0.35 for a tight rhombohedral structure to 0.91 for a loose cubical packing structure (Graton and Fraser, 1935). In a mixture comprised of two different sphere sizes (bimodal packing), the change of minimum void ratio as a function of fines content has been shown by the classic theory of Furnas (1931). Yu et al. (1993), Podcreck and Sharma

(1996), and Rassouly (1999) have also studied the minimum void ratio of packing with two sized spherical particles. These studies were developed for bimodal packing with spherical particles, which are not applicable to sand-silt mixtures since the sand and silt particles are not generally spherical. Oakeshott and Edwards (1994) used perturbation theory to describe packing of mixtures with non-spherical particles. Their model is qualitative and the particle shapes do not resemble the real soil grains. It is considered that, even if a quantitative model exists, it is not practical to measure the shape of each particle in the soil. Therefore, in this paper we adopted a phenomenological approach to describe the void ratio change characteristics for sand-silt mixtures.

Chang and Yin (2011) proposed a method to predict the initial void ratio of a sand-silt mixture after the specimen is prepared in laboratory. The prediction requires the silt content of the mixture, and the void ratio of sand, which is prepared by the same preparation method and effort. The method is valid for silty sand with low amounts of fines (f_c<25%)

Here a method is proposed that can predict the initial void ratio of sand-silt mixtures with high amount of fines (f_c >35%). Since the fine grain dominated matrices (i.e. f_c >35%) with isolated and floating coarse grains have very different microstructures compared with coarse grain dominated packings (i.e. f_c <25%), a new formulation is required to consider an entirely different microstructure.

Deriving the new formulation starts by defining the void ratio e_{sand} (for pure sand) and e_{silt} (for pure silt) and call them host void ratio (e_h):

$$e_h = \frac{V_v}{V_h} \tag{3}$$

where V_v is the volume of voids and V_h is the volume of solids, which can be either of a

host sand (V_{sand}) or a host silt (V_{silt}) (Fig. 3a). By adding silt to the host sand, or sand to the host silt, the original packing structure may alter, and it changes the volume of the voids to $V_v + \Delta V_v$ (Fig. 3b).

For the case of mixtures with low fines contents (f_c <25%), the change of volume of voids (ΔV_v) was assumed to be proportional to the amount of silt (V_{silt}) added to the host sand:

$$\Delta V_v = a \cdot V_{silt} \tag{4}$$

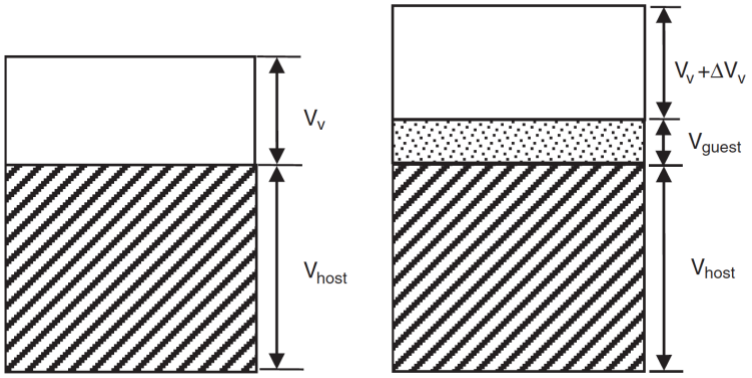

Figure 5- Left: Two phase diagram for host sand; right: three-phase diagram for a mixture of sand and silt (host and guest).

In general, the volume of voids is reduced when silt grains are added to the host sand. An ideal condition is that all silt particles fill into the voids between sand grains without disturbing the original fabric of the host sand, which means that the volume reduction of voids is equal to the solid volume of added silt particles (i.e., a = -1). This ideal condition seems to be the limit for void volume reduction as shown later for different sand-silt mixtures (Fig. 4).

For the case of mixtures with high fines contents (f_c > 35%), when sand grains are added to the host silt (fines content decreases from 100%), the change of the volume of

voids (ΔV_v) can be assumed to be proportional to the volume of sand grains (V_{sand}) added to the host silt:

$$\Delta V_v = b \cdot V_{sand} \tag{5}$$

where V_{sand} is the volume of sand grains added to the host silt and ΔV_v is the change of volume of voids due to the inclusions of coarse grains in the original fine grain packing. In general, the volume of voids increases when sand grains are added to the host silt. An ideal condition is that the volume of voids has zero increase when coarse particles are added to the mixture, which corresponds to $b = 0$. This ideal condition seems to be the limit of void volume increase as shown later for different sand-silt mixtures (Fig. 4).

For sand-silt mixtures the coarse-grain content g_c can be defined simply as:

$$g_c = 1 - f_c = \frac{V_{sand}}{V_{silt} + V_{sand}} \tag{6}$$

where V_{silt} is the original volume of fines (same as V_h in Eq. 3), and V_{sand} is the volume of added sand. The following equation can be obtained for the void ratio of the mixture:

$$e = \frac{V_{voids}}{V_{solids}} = \frac{V_v + bV_{sand}}{V_{silt} + V_{sand}} \tag{7}$$

By replacing V_{sand} from Eq. 6 into Eq. 7 and after simplifications, the following relationship is obtained for the void ratio of the mixtures with high fines content:

$$e = e_{silt} f_c + b(1 - f_c) \qquad \text{or} \qquad e_{silt} = \frac{e - b}{f_c} + b \tag{8}$$

Eq. 8 defines the void ratio (e) of a mixture with f_c>35% as a function of e_{silt} (void ratio of the 100% silt sample) and fines content. For the ideal condition, where b=0, Eq. 8 reduces to $e = e_{silt} f_c$. This is in the same form as that of the inter-fine void ratio in Eq. 2 provided by Thevanayagam and Mohan (2000).

For the mixtures with small amount of fines (f_c<25%), the void ratio of the soil mixture has been calculated by Chang and Yin (2011) and given as:

$$e = e_{sand}\left(1-f_c\right)+af_c \quad \text{or} \quad e_{sand}=\frac{e-af_c}{1-f_c} \tag{9}$$

The relationships in Eqs. 8 and 9 are derived based on the assumption that the void ratios e, e_{sand}, and e_{silt} are produced by the same sample preparation method and effort.

Eqs. 8 and 9 can be used to predict the void ratio of the mixtures with various amounts of fines, prepared to their minimum void ratio (e_{min}) by the same mechanical process and effort. We replace e, e_{sand}, and e_{silt} with e_{min}, $(e_{sand})_{min}$, and $(e_{silt})_{min}$, respectively in Eqs. 9 and 8:

$$e_{\min}=\left(e_{sand}\right)_{\min}+\left[a-\left(e_{sand}\right)_{\min}\right]f_c \quad \text{for low fines contents} \tag{10}$$

$$e_{\min}=\left(e_{silt}\right)_{\min}f_c+b\left(1-f_c\right) \quad \text{for high fines contents} \tag{11}$$

Eqs. 10 and 11 are used to fit the minimum void ratios of six different sand-silt mixtures (Figs. 4a to 4f). The sand and silt types, particles sizes and the respective *"a"* and *"b"* values are given in Table 2 (particle shapes are also given if known).

As discussed in Chang and Yin (2011), the value of *"a"* depends on the size and shape of the particles in the soil mixture, and the mechanical process and effort used to produce the specimen. The value of *"a"* is in the range of -0.6 to 0.4 for different mixtures that are shown in Figure 6. Similar to *"a"*, the value of *"b"* in Eq. 5 depends on the size and shape of fine and coarse particles as well as the sample preparation method and effort. The value of *"b"* is in the range of 0.0 to 0.5 for the mixtures shown in Figure 6. A small value of b indicates that, given the same amount of compaction effort, a denser state can

be achieved for the same mixture. In other words, the soil mixture is more *compactable* when *b* has lower values.

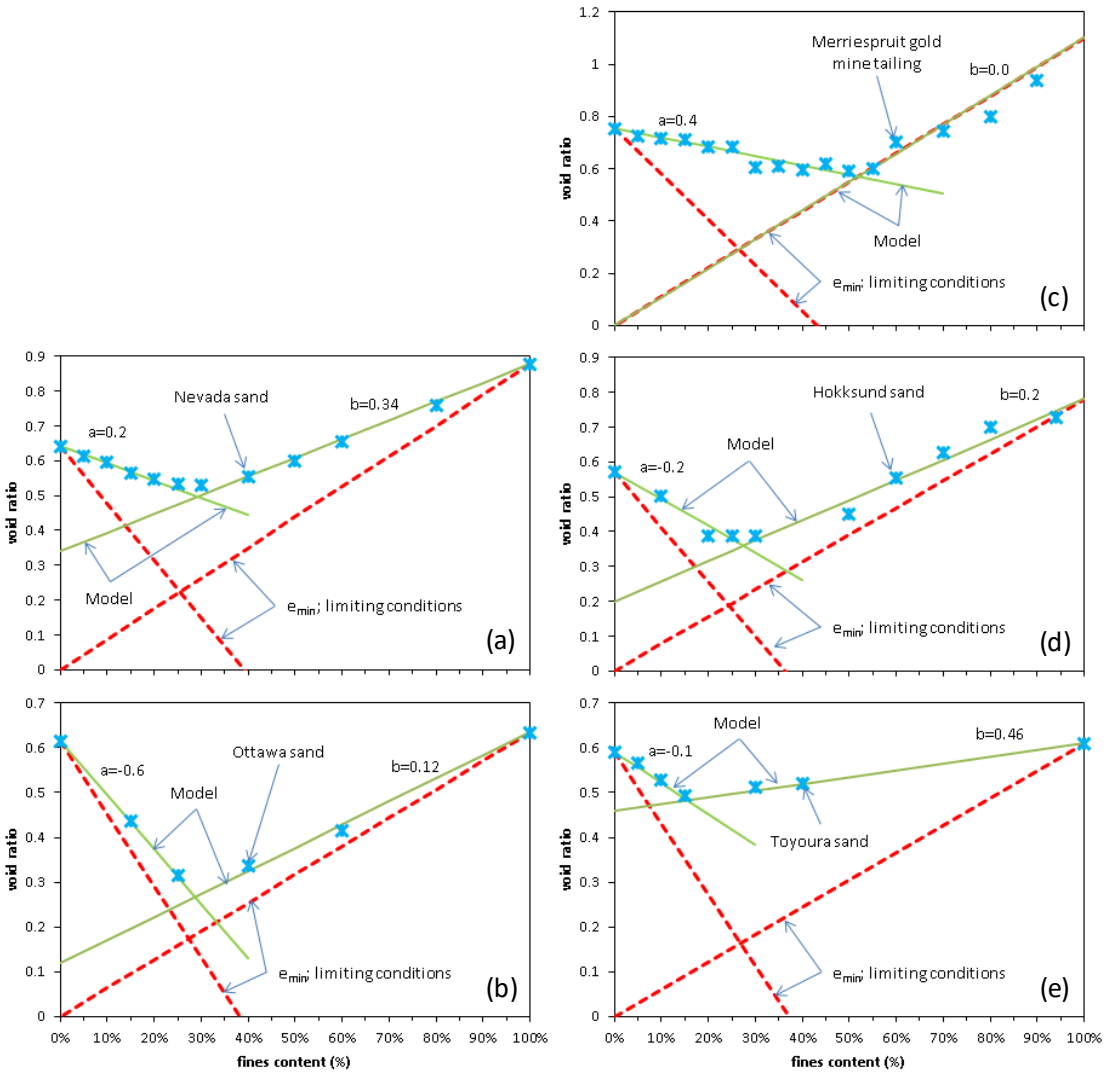

Figure 6- Minimum void ratio for five types of sand with various amounts of fines [Chang and Meidani, 2013].

The parameters *"a"* and *"b"* will be used in section 2.4.2.2 to calculate the "critical void ratio" (or density state) for packings with different sand and silt proportions. The density state will be used in a hardening rule for estimating the magnitude of particle sliding.

Table 1. Some of the reported experimental studies on the monotonic undrained behavior of sand–silt mixtures.

Sand type	Silt type	Fines contents	Confining pressures (kPa)	Sample preparation method	Reference
Brenda mine tailing	Kamloops	0, 4, 7.5, 14, 22%	350	SD[1]	Kuerbis et al. [57]
Ticino	Ticino (milled)	0, 30, 50, 67, 85, 92%	100	WS[1]	Zlatovic [58]
Ottawa C109	Crushed quartz	0, 10, 20, 30, 40%	350	MP[1]	Pitman et al. [59]
Toyoura	Toyoura (milled)	0, 5, 10, 15, 25, 30, 40, 100%	400	DD, MP, WS[1]	Zlatovic & Ishihara [56]
Nevada	Nevada fines	50/80: 0, 10, 20, 30, 50% 50/200: 0, 10, 20, 30%	25 25, 50, 150, 200, 300, 500	DD	Lade and Yamamuro [60]
Ottawa	Nevada fines	50/200: 0, 10, 20, 30, 50% F-95: 0, 10, 100%	25	DD	Lade and Yamamuro [60]
Lagunillas sandy silt		74%	100, 150, 200, 350, 400, 500	DD, MP, WS	Zlatovic and Ishihara [61]
Silica	Sil-co-Sil #40	0, 2, 12%	100	DD	Thevanayagam [8]
	Kaolin silt	27%	100, 200, 400		
Nevada	Nevada fines	50/200: 6, 20% 50/80: 0, 10, 20, 30, 50%	25, 75, 100, 125, 150, 300, 500 25	DD	Yamamuro and Lade [13]
Nevada 50/200	ATC silt	40%	25, 50, 100, 200, 350, 500	DD	Yamamuro and Covert [2]
Foundry F55	Sil-co-Sil #40	0, 7, 15, 25, 40, 60, 100%	100	DD, MP	Thevanayagam et al. [4]
Juamana	HPF4 silt	0, 1, 2.5, 10, 20, 40%	75 (Anisotropic)	DD	Georgiannou [44]
Ham River		0, 1, 2.5, 5, 10%			
Hokksund	Chengbei	0, 5, 10, 15, 20, 30, 50, 70, 94%	50, 100, 150	MP	Yang et al. [10]
Japanese Silica	Non-plastic marine clay	0, 5, 15, 30, 49, 68, 97%	100, 200, 400	WS	Konishi et al. [15]
Ottawa	Sil-co-Sil #106	0, 5, 10, 15%	100, 200, 400	SD, MP, WS	Murthy et al. [53]
Sydney	Non-plastic silt	10%	30, 100, 300, 400, 600, 1115	MP	Bobei et al. [62]
Chrsitchurch silty sand		0, 1, 10, 20, 25, 30, 100%	100, 200	MP	Rees [63]
Chlef Sand	Chlef	0, 10, 20, 30, 40, 50, 100%	100	MP	Belkhatir et al. [12]
Egyptian desert	Assirou	0, 15, 25%	50, 100, 150, 200, 250	DR[1], MP	Stamatopoulous [64]
Ahmedabad sand	Quarry dust	0, 5, 10, 15, 20, 25, 30, 35, 40, 45, 50, 60, 75, 100%	100	DD	Dash & Sitharam [65]
Nevada	Loch Raven	20%	100		Monkul et al. [66]
Cape Girardeau silty sand		38%	160, 220, 270, 330, 400, 425, 640	DD	Sadrekarimi & Olson [67]

1- DR: Dry rodding; MP: Moist placement; DD: Dry deposition; SD: Slurry deposition; WS: Water sedimentation

Table 2. Information on the sand–silt mixtures used in this paper to fit Eqs. 10 and 11 and the respective model parameters.

Sand type and shape	Silt type and shape	e_{min} sand	e_{min} silt	D_{50} (mm)	d_{50} (mm)	$\frac{D_{50}}{d_{50}}$	a	b	Reference
Hokksund (cubical sharp edged)	Chengbei (angular)	0.570	0.760	0.450	0.035	13	−0.2	0.34	Yang [11]
Merriutspruit gold mining tailings[a]		0.755	1.100	0.116	0.009	13	0.4	0.12	Fourie and Papageorgiou [55]
Nevada 50/200	ATC silt	0.642	0.877	0.140	0.036	4	0.2	0.0	Yamamuro and Covert [2]
Ottawa F55 (round to sub-round)	Crushed Silica (angular)	0.615	0.634	0.250	0.010	25	−0.6	0.2	Thevanayagam [68]
Toyoura (elongated sub-angular)	Milled Toyoura (angular)	0.591	0.609	0.170	0.010	17	−0.1	0.46	Zlatovic and Ishihara [56]

[a]There is no information available on the particles shapes for the Merriespruit gold mining tailing.

CHAPTER 2

DOMINANT GRAINS NETWORK AND BEHAVIOR OF SAND-SILT MIXTURES: STRESS-STRAIN MICROMECHANICAL MODELING[1]

2.1. Contact density in granular material

Contact density is a necessary parameter in micromechanical modeling of granular materials. Contact density, *N/V*, is defined as the number of contacts between particles in a unit volume of packing. Contact density has been estimated and correlated from the void ratio, since direct measurement of this parameter is impractical. For example, Oda (1977) and Chang et al. (1989) used void ratio to estimate the contact density of sands. This method of estimating the contact density for sands is not applicable to sand-silt mixtures, because of the significant difference between the sizes of existing particles in such packings.

To estimate the contact density of the mixtures with low fines contents (f_c<25%), Chang and Yin (2011) suggested a method based on an equivalent void ratio for coarse particles skeleton. The equivalent void ratio was proposed by Chang and Yin (2011) for sand-silt mixtures with fines contents less than 25% and is repeated here:

$$e_{sand} = \frac{e - af_c}{1 - f_c} \qquad \text{(9 repeated)}$$

[1] This chapter and a part of chapter one were published as a standalone paper in the International Journal of Numerical and Analytical Methods in Geomechanics (2013). doi:10.1002/nag.2152

This equation is based on the void ratio change characteristics of coarse-grain dominated mixtures. This equivalent void ratio represents the void ratio of an imaginary pure coarse-grain assembly that is assumed to have the same contact density as that of the silty sand with void ratio of e and fines content of f_c.

This equivalent void ratio also reduces to the apparent inter-granular void ratio defined by Vaid (1994) and Thevanayagam (1998) for the ideal conditions (a=-1):

$$e_g = \frac{e + f_c}{1 - f_c} \tag{12}$$

For the case of mixtures with high amount of fines (f_c>35%), the contact density could be estimated based on the same concept, but considering the fine grains network. Eq. 8 is used to define an equivalent void ratio (e_{silt}) for the sandy silt:

$$e_{silt} = \frac{e - b}{f_c} + b \tag{8 repeated}$$

For the mixtures with high fines contents, when b=0, the equivalent void ratio reduces to the apparent inter-fine void ratio as defined by Vaid (1994) and Thevanayagam (1998):

$$e_f = \frac{e}{f_c} \tag{13}$$

Eqs. 12 and 13 represent the void ratios of the dominant (host) grains networks in the absence of guest particles.

Now, these equivalent void ratios can be used in the following empirical equation to estimate the equivalent coordination number of coarse-grain or fine-grain dominated networks:

$$C_n = 13.28 - 8e_{host} \tag{14}$$

where $e_{host}=e_{sand}$ for the mixtures with f_c<25% (see Eq. 9), and $e_{host}=e_{silt}$ for the mixtures

with f_c >35% (see Eq. 8). This relationship was originally proposed for sands by Chang et al. (1989). The contact density, which is the total number of inter-particle contacts per unit volume (*N/V*), can be estimated from the equivalent coordination number (C_n), and the equivalent void ratio of the host material. (either e_{sand} or e_{silt}):

$$\left(\frac{N}{V}\right)_0 = \frac{3C_n}{\pi d^3\left(1+e_{h_0}\right)} \tag{15}$$

where *d* is the mean grain size of the host material and e_{h_0} is the initial void ratio of the host material (the host material is sand in case of f_c<25% and is silt in case of f_c>35%). The evolution of *N/V* due to the change of void ratio from initial (e_{h_0}) to current (e_h) follows:

$$\frac{N}{V} = \frac{3\left(13.28-8e_h\right)}{\pi d^3\left(1+e_h\right)} \tag{16}$$

where e_h is the void ratio of the host material (e_{sand} or e_{silt}).

So, the proposed equivalent void ratios are used merely for calculating the contact densities (*N/V*) of coarse and fine-grain dominated networks to be used in the micromechanics-based model. As mentioned before, similar indices were used by other researchers to correlate various aspects of the mechanical behavior of sand-silt mixtures. (Thevanayagam 1998, 2002; Polito and Martin 2001; Ni et al. 2004; Georgiannou et al. 2006; Rahman et al. 2008).

2.2. Inter-particle contact model for sand-silt mixtures

Recalling the concept of dominant grains network, the behavior of a sand-silt mixture is controlled by a network of the dominant grains. For the mixtures with low fines content the behavior is governed by the coarse-grain network. Thus, the inter-particle model

parameters are defined for an equivalent packing of coarse particles and effect of fines, either filled in the voids or wedged between coarse particles, has been considered in the model parameters. For the mixtures with high fines content, the mechanical behavior of the mixture is dominated by a fine-grain network. Therefore, the inter-particle model parameters are defined for an equivalent packing of fine particles. The effect of floating coarse particles in the fines matrix will be considered in the model parameters. The inter-particle model described below refers to the behavior between dominant grains.

The elastic and plastic parts of the inter-particle contact model are described in the following two sections, respectively.

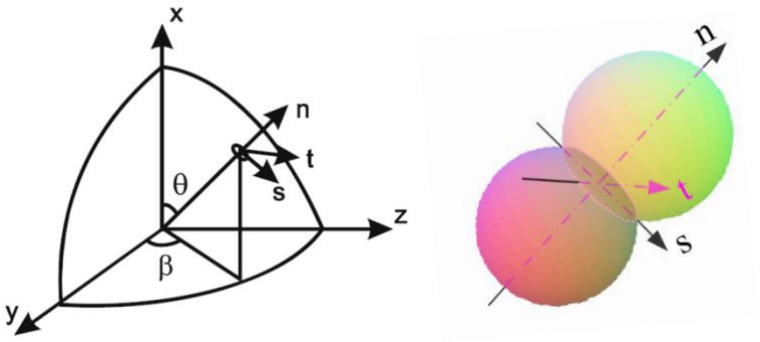

Figure 7- Local coordinate at inter-particle contact.

2.2.1. Elastic inter-particle behavior

In general, the normal (k_n^e) and tangential (k_r^e) elastic stiffness between two particles is assumed to follow a revised Hertz-Mindlin's formulation (Chang et al., 1989):

$$k_n^e = k_{n0}^e \left(\frac{f_n}{f_{ref}} \right)^n \quad ; \quad k_r^e = \varsigma^e k_{n0}^e \left(\frac{f_n}{f_{ref}} \right)^n \tag{17}$$

where k_{n0}^e, ς^e, and n are three material constants in which k_{n0}^e is the reference normal contact stiffness, ς^e is the ratio of shear stiffness to normal stiffness, and n is a constant

exponent. f_n is the normal contact force between two particles, and f_{ref} is the reference value given by $f_{ref} = \frac{3p_{at}}{l_0 (N/V)_0}$; in which p_{at} is the atmospheric pressure equal to 101.3 kPa, $(N/V)_0$ is the initial contact density of the dominant grains network and can be obtained from Eq. 16 using a reference initial void ratio, and l_0 is the initial branch length (defined as the distance between the centroids of the two contact particles).

For a mixture of sand and silt, the three elastic parameters should be functions of the properties of sand and silt particles. However, if the mechanical properties and particle shape of sand and silt grains are similar, ς^e and n can be assumed to be independent of fines content value. This assumption is consistent with that observed by Salgado et al. (2000) for the shear moduli of Ottawa sand samples with various fines contents (5-20%).

The only elastic parameter that seems to be sensitive to fines content is k_{n0}. In the light of mixture theory and postulates by Voigt (1910) and Reuss (1929) the upper and lower bound values for the mean contact stiffness of a mixture comprised of sand and silt particles can be expressed in the following forms, respectively:

$$(k_n)_{equivalent} = (1 - f_c)(k_n)_{sand} + f_c (k_n)_{silt} \tag{18}$$

$$\frac{1}{(k_n)_{equivalent}} = \frac{1 - f_c}{(k_n)_{sand}} + \frac{f_c}{(k_n)_{silt}} \tag{19}$$

In the above formulae, $(k_n)_{equivalent}$ is the average contact stiffness of the mixture, $(k_n)_{sand}$ and $(k_n)_{silt}$ are the contact stiffness values for pure sand and pure silt packings, which are calculated based on Eq. 17 with respective k_{n0} and n for pure sand and pure silt specimens. f_c is the fines content of the mixture.

Based on the concept of dominant grains network, loads are not shared equally between sand and silt particles. Thus, the upper bound solution is not suitable for estimating the average contact stiffness of the mixture. The lower bound solution seems to be more reasonable for estimating the mean contact stiffness for a sand-silt mixture.

2.2.2. Plastic inter-particle behavior

Friction is the main source for dissipation of plastic work between two particles. In our model, a yield function of Mohr-Coulomb type is adopted to determine sliding between two particles. In contrast to the conventional Mohr-Coulomb yield function, which is defined in a stress space, the current yield function is defined in a contact-force space (e.g. f_n, f_s, f_t). In inter-particle force $\left(f_n, f_s, f_t\right)$ and displacement $\left(\delta_n, \delta_s, \delta_t\right)$ nomenclatures, the subscripts *n*, *s*, and *t* are the local coordinates on each contact. The resultant shear force f_r and the resultant plastic sliding δ_r^P can be defined as:

$$f_r = \sqrt{f_s^2 + f_t^2} \quad \text{and} \quad \delta_r^p = \sqrt{\left(\delta_s^p\right)^2 + \left(\delta_t^p\right)^2} \tag{20}$$

The yield surface is given by the following equation:

$$F\left(f_n, f_r, \kappa\right) = \frac{f_r}{f_n} - \kappa\left(\delta_r^p\right) \tag{21}$$

where $\kappa(\delta_r^P)$ is a hardening/softening function. When dF>0, it indicates loading, otherwise unloading.

The hardening function is defined by a hyperbolic curve in $\kappa - \delta_r^p$ plane, which involves two material parameters, ϕ_p and k_r^p:

$$\kappa\left(\delta_r^p\right) = \frac{k_r^p \tan\phi_p \, \delta_r^p}{f_n \tan\phi_p + k_r^p \delta_r^p} \tag{22}$$

The plastic stiffness, k_r^p, is the initial slope of the hyperbolic curve, which is assumed to relate k_n^e by a constant called ς^p:

$$k_r^p = \varsigma^p k_n^e = \varsigma^p k_{n0}^e \left(\frac{f_n}{f_{ref}} \right)^n \tag{23}$$

The value of $\kappa\left(\delta_r^p\right)$ asymptotically approaches the apparent inter-particle friction angle, $\tan\phi_p$. From the physical interpretation, the value of ϕ_p should be equal to the Coulomb friction angle (ϕ_μ). However, due to limitation of the micromechanical model, the value of ϕ_p needs to be modified in order to represent the real behavior. This limitation arises from the static hypothesis used in the micromechanical model. The static hypothesis is necessary to provide the macro-to-micro link (i.e., the inter-particle forces are estimated from the applied stress). Since the detailed geometrical arrangements of each individual particle and its neighboring particles are not required in the model, rather, the orientation distribution of contact number is given. Thus, the forces on each contact orientation predicted from the static hypothesis are only in an average sense and the interaction due to locally varied packing geometry is not considered. As a consequence, the hypothesis may lead to early sliding on contacts in a densely interlocked condition.

To capture the essence of the phenomenon, the Coulomb friction angle is replaced with an apparent inter-particle friction angle. The inter-particle friction angle is no longer a constant material property; instead, the it varies during the loading process, depending on the critical state variables of the packing.

$$\tan\phi_p = \left(\frac{e_{cr}}{e} \right)^m \cdot \tan\bar{\phi}_\mu \tag{24}$$

where *m* is a positive number that is dependent of the type of soil (especially particle shape). In this equation, a reference apparent inter-particle friction ($\bar{\phi}_{\mu}$) is defined, which is assumed to be equal to the critical state friction angle (i.e. $\bar{\phi}_{\mu} = \phi_{cs}$). Similar to the critical state void ratio, the reference apparent inter-particle friction angle ($\bar{\phi}_{\mu}$) is an intrinsic material property for a given type of soil. The type of soil is distinguished by its particle shapes and amount of fines content.

Plastic sliding at an inter-particle contact often occurs with an upward or downward movement. This movement results in a volume change in the soil, which is called shear-induced dilation/contraction, a well-known phenomenon in sand (Taylor 1948, Rowe 1962, Goddard and Bashir 1990). The sliding direction at an inter-particle contact can be derived using an energy hypothesis similar to those proposed by Taylor (1948) and Roscoe and Burland (1968). It was assumed that the plastic work done on a contact plane ($f_n \cdot d\delta_n^p + f_r \cdot d\delta_r^p$) is equal to the hypothesized energy dissipation due to friction ($f_n \cdot \tan\phi_0 \cdot d\delta_r^p$) at the contact. The following form was used for the sliding direction:

$$\frac{d\delta_n^p}{d\delta_r^p} = D\left(\tan\phi_0 - \frac{f_r}{f_n}\right) \tag{25}$$

where *D* is a material constant that controls the intensity of dilation and is typically equal to 1. The value of ϕ_0 in Eq. 25 is typically equal to the reference apparent inter-particle friction angle $\bar{\phi}_{\mu}$. The sliding direction represented by Eq. 25 is not necessarily perpendicular to the yield surface. Treating the particle sliding calculated from Eq. 25 as a flow rule, we note that it has the similar features of macro-scale non-associative flow rule in the conventional plasticity.

At critical state condition, the apparent friction angle is equal to the critical state friction angle, i.e. $\phi_p = \bar{\phi}_\mu = \phi_{cs}$. For a packing at its dense state ($e_{cr}/e > 1$), the apparent inter-particle friction angle (ϕ_p) is greater than the critical state friction angle (ϕ_{cs}). As the dense packing dilates during shear, its density state (e_{cr}/e) decreases and this leads to a reduction of the apparent friction angle and results in strain-softening phenomenon. For a loose packing ($e_{cr}/e < 1$), the apparent friction angle (ϕ_p) is smaller than the critical state friction angle (ϕ_{cs}). As the loose packing contracts during shear, its density state (e_{cr}/e) increases with the apparent friction angle. Eventually, under large shear deformations, the assembly reaches the critical state condition ($e_{cr}/e = 1$) and the apparent friction angle (ϕ_p) becomes equal to ϕ_{cs}. For both dense and loose conditions, the evolution of density state ($\psi = e_{cr}/e$) plays an important role in the plastic behavior at particle level.

To summarize this section, plastic inter-particle model parameters are ς^p, *D*, *m*, and ϕ_{cs} plus e_{cr} to define the density state. These parameters should be functions of the properties of sand and silt particles. The first three of these parameters can be related to the plastic behavior of dominant grains. For the other two parameters (i.e. ϕ_{cs} and e_{cr}), the effect of fines are discussed in the following sections.

2.4.2.1. Critical state friction angle for sand-silt mixtures

Based on the existing experimental results, the critical state friction angle (ϕ_{cs}) change is classified into three ranges of fines content:

ϕ_{cs} for sand-silt mixtures is experimentally found to be insensitive to silt content for fines contents between 0–10% (Bouckovalas et al. 2003). We believe if the ratio between the diameters of coarse and fine particles in a sand-silt mixture varies, the 10% threshold value can also change, since the fines content at which the silt particles start to overfill the coarse matrix voids depends on the d_{silt}/D_{sand}. In this range of fines contents, the value of critical state friction angle for the mixture is dominantly controlled by that of the coarse grains, since almost all of the load carrying contacts in the packing are between coarse particles (Fig. 6a).

ϕ_{cs} for sand-silt mixtures can increase with fines content as shown by Sladen et al. (1985), Salgado et al. (2000), Ni et al. (2004), Konishi et al. (2007), and Murthy et al. (2007), or it can be decreased with the increase of fines content as shown by Yang (2004). The behavior is largely dependent on the critical state friction angle of pure sand, and that of pure silt. For example, the presence of small amounts of angular silt particles wedging between the sand grains can result in an increase of the ϕ_{cs}, whereas adding more fines of round shape will reduce the overall friction angle of the mixture. A simple model is provided in the following to describe this behavior.

For fines contents greater than about 70%, the coarse grains are completely dispersed in the mixture and fine particles contacts play an important role in carrying the load (Fig. 6e); the fine particles dominate the packing behavior including its critical state friction angle. So, ϕ_{cs} will not change with an increase of fine content beyond this threshold (See Fig. 17 for Yang 2004 and Konishi et al. 2007 data).

A simple model is provided here to describe the change of the critical state friction of a mixture as a function of its fines content, and critical state friction angles of pure sand and pure silt packings.

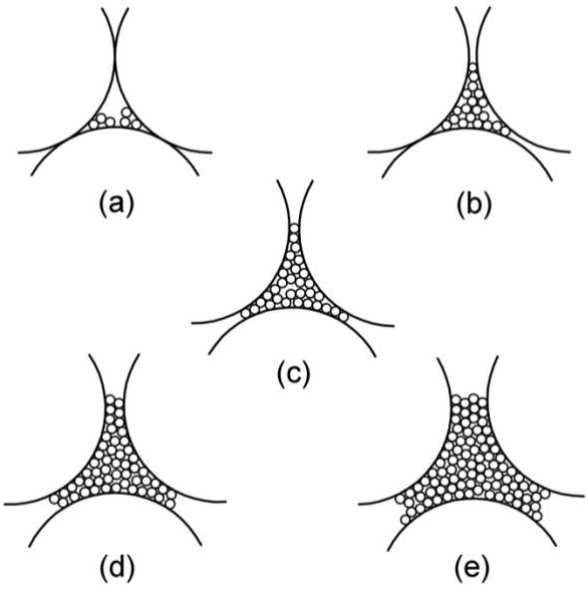

Figure 8- Introduction of fines between coarse particles and separation of coarse grains.

When fines content becomes high enough to occupy all the voids in the coarse grain network, the excessive fines squeeze in between the coarse grains and affect the friction between those larger grains. The change of friction versus the change of fines content is dependent on the number of fine grains that are already sitting between the coarse particles contacts, as well as the thickness of this fine particles layer. The rate of this change is also dependent on the shape of fines. As the number of fines between the coarse particle contacts increases, the friction of packing becomes asymptotic to the friction of fine particles. We assume this change have an exponential rate, since the very first fine particles that squeeze between coarse particle contacts have very high effect on the friction of the packing, whereas at the higher fines contents, there are very few direct

coarse-to-coarse particles contacts left to be separated by the introduction of fine particles. Therefore, inclusion of more fines will not significantly change the friction angle of the whole packing. In other words, by increasing the amount of fines in the mixture, the coarse-to-coarse particles contacts vanish and the friction angle of the mixture is mainly controlled by the friction at fine-to-fine particles contacts.

This phenomenon can be analogized to the change of current in an electric capacitor as the electrons fill between two charging plates. For any capacitor, there is a nominal saturation voltage that limits the number of electrons that can occupy between its plates. Once the voltage is attained, the current becomes zero and can no longer accept electrons. The following formula describes the relationship between current and voltage in a charging capacitor (Floyd and Buchla, 2009):

$$I = \frac{V_b}{R} \cdot e^{-t/RC} \tag{26}$$

where I is the charging current, V_b is the supplying voltage, R is the resistance of the system, t is the time of charging, and C is a constant that describes the capacity of the charging element.

In order to use Eq. 26 to calculate the friction angle of a sand-silt mixture, we need to analogize different parameters of a charging circuit to our sand-silt mixture packing. We take the effect of time on change of current in a capacitor to be similar to the effect of fines content on the change of friction angle in a mixed packing. The time domain of Eq. 26 is $[0,\infty]$. The lower limit of fines content domain in our problem is the amount of fines at which those particles start to squeeze between coarse-to-coarse particles contacts, i.e. $(f_c)_L$=10%, and affect the friction angle of the mixture. The upper limit is the fines

content at which coarse particles start to become totally dispersed in the mixture, i.e. $(f_c)_U$=70%, and inclusion of more fines in the mixture does not affect its friction angle. So, while changing the variable from $t \rightarrow f_c$, a domain transformation from $[0, \infty] \rightarrow$[0.1, 0.7] is needed.

The target domain of Eq. 26 starts from V_b/R at t=0 and reaches 0 as $t \rightarrow \infty$. The target domain of our sand-silt mixture problem should start from the friction angle of sand at $(f_c)_L$=10% and reaches the friction angle of silt at $(f_c)_U$=70%. We normalize the transformed equation with respect to the friction angle of sand and friction angle of silt, while replacing 1/*RC* with a new parameter (α), and the following final form is achieved:

$$\tan\phi_{cs_{mix}} = \left(\left(\tan\phi_{cs}\right)_{sand} - \left(\tan\phi_{cs}\right)_{silt}\right) \cdot e^{-\alpha . x} + \left(\tan\phi_{cs}\right)_{silt}$$
$$x = \frac{f_c - \left(f_c\right)_L}{\left(f_c\right)_U - f_c} \qquad (27)$$

where α is a constant which is dependent on the shape of the fine particles and f_c is the fines content that varies between 0.1 and 0.7. The suitability of this equation to predict the critical state friction angle of sand-silt mixtures will be shown in section 4.2.

2.4.2.2. Critical state void ratio for sand-silt mixtures

The critical state void ratio (e_{cr}) for sand can be calculated as a function of the mean effective stress from the following equation:

$$e_{cr} = e_{ref} - \lambda\left(\frac{p'}{p_{atm}}\right)^{\xi} \qquad (28)$$

where p' is the mean effective stress and p_{atm} is the reference atmospheric pressure. Three parameters are required to define each critical state line (CSL) in void ratio-pressure

space: e_{ref} (zero intercept), λ (CSL slope), and ξ (CSL curvature). The same equation can be used to model the critical state lines of sand-silt mixtures with different amount of fines; however, the shape and location of these lines are not necessarily the same as those of pure sand.

It is generally observed that, for fines contents less than 30%, the critical state lines have the same slope and curvature but shifting downward as the amount of fines increase. For fines content greater than 30%, the critical state lines shift upward from that of the silty sand with almost 30% fines content, and the slope changes. The above mentioned trends in sand- silt mixtures have been observed from triaxial test results on various type of sand; e.g. Ottawa sand (Salgado et al. 2000 and Murthy et al. 2007), Merriespruit gold mining tailings (Fourie and Papageorgiou 2001), Foundry sand (Thevanayagam et al. 2002), Toyoura sand (Zlatovic and Ishihara 1995), Hokksund sand (Yang, 2004), and Japanese Silica sand (Konishi et al. 2007).

We analyzed experimental results from Yang (2004) and Konishi et al. (2007), which are rare data covering full range of silt contents (i.e., 0% - 100%), by fitting Eq. 28 to the critical state data (Figs. 7 and 8) and studied the effect of fines content on the critical void ratio parameters e_{ref}, λ, and ξ.

The analysis of critical state data indicated that the value λ can be regarded as two different constants; one for fines contents less than 30% and another for fines contents higher than 30%, as it is obviously related to the shape characteristics of the dominant grains. The λ value for the high fines contents is almost doubled compared to that for the low fines contents (Table 3). The curvature parameter ξ, however, is found to be

constant for the whole range of fines content for a given type of silty-sand mixture (Table 3).

The change of parameter e_{ref} due to the change of fines content has the same characteristics as that for minimum void ratio. Let the parameters $(e_{sand})_{ref}$ and $(e_{silt})_{ref}$ be the reference void ratios for the host sand and host silt, respectively. Then, by replacing them into Eqs. 7 and 14, we can calculate e_{ref} for different fines contents:

$$e_{ref} = \left(e_{ref}\right)_{sand}\left(1-f_c\right)+af_c \qquad \text{(for low fines contents)} \qquad (29)$$

$$e_{ref} = \left(e_{ref}\right)_{silt} f_c + b(1-f_c) \qquad \text{(for high fines contents)} \qquad (30)$$

The predicted results of e_{min} and e_{ref} from Eqs. 29 and 30 for Yang (2004) data are shown in Fig. 9. Note that the same value of a and b are used to predict minimum and reference critical void ratios. For Konishi et al. (2007) mixtures, there was no data available on the minimum void ratio of mixtures, so we obtained a and b parameters based on the existing e_{ref} values.

The location of the critical state line for different fines contents influences the density state parameter $\left(e_{cr}/e\right)$, which in turn affects the interparticle apparent friction angle $\left(\phi_p\right)$ in Eq. 24. As a result, the amount of plastic sliding between particles would be affected by the fines content in the mixture and changes the stress-strain behavior of the mixture.

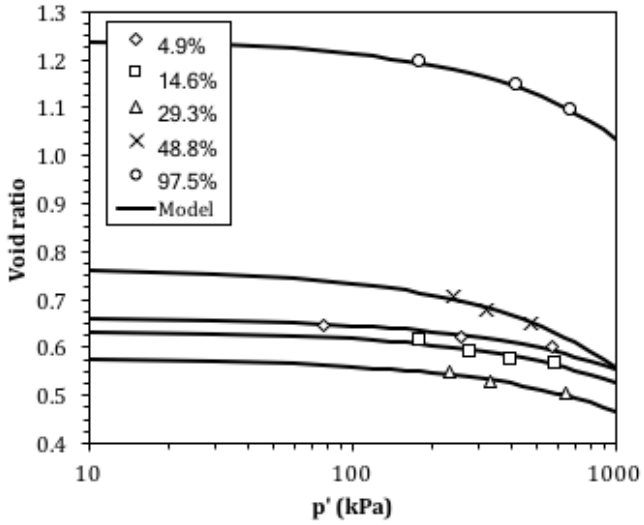

Figure 9- Critical state lines for Japanese silica sand and marine silt mixtures with various fines contents (Konishi et al., 2007).

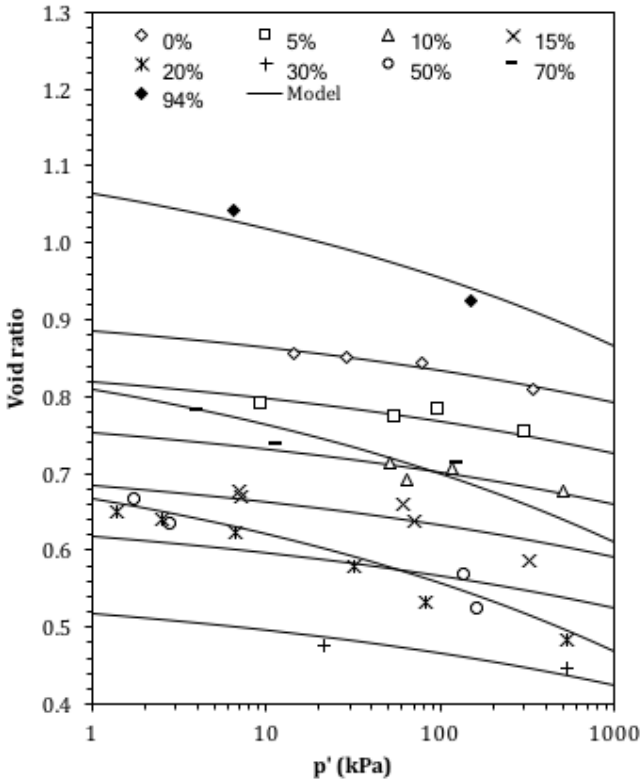

Figure 10- Critical state lines for Hokksund sand and Chengbei silt mixtures with various fines contents (Yang, 2004).

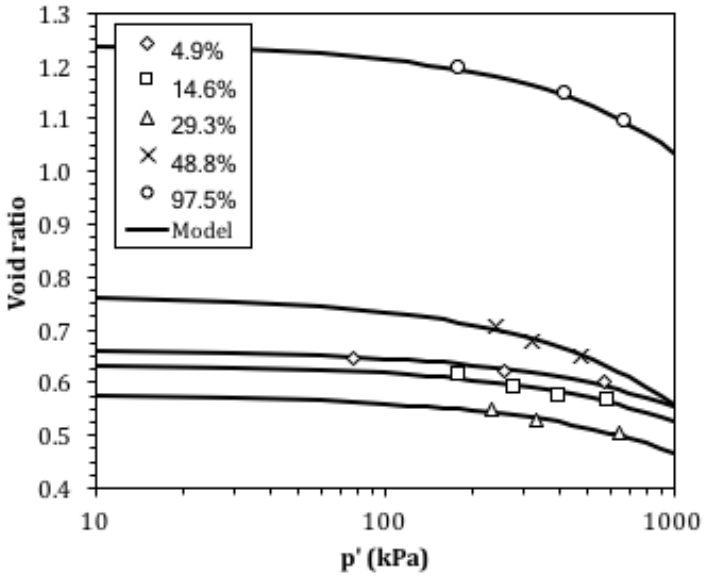

Figure 11- Variation of critical state void ratio with fines content for Konishi et al. (2007) data.

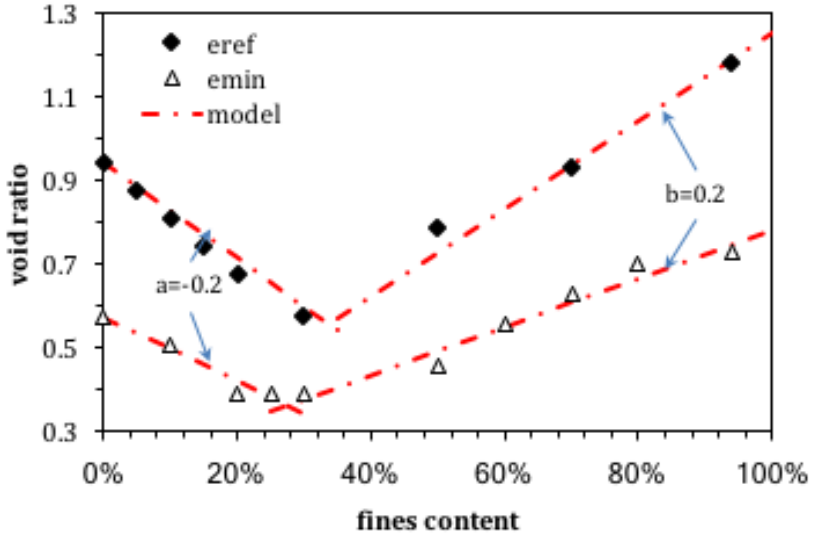

Figure 12- Variation of critical state void ratio and minimum void ratio with fines content for Yang (2004) data.

2.3. Overall stress-strain relationship

With previously described elastic and plastic inter-particle behaviors, a relationship can be established between contact force and relative displacement for two contacting particles based on an elasto-plastic framework. The global stress-strain relationship for a packing will then be obtained by integrating the behavior of inter-particle contacts in all orientations. In the integration process, a micro-macro relationship is required, which is simply based on the concept of force equilibrium in the packing. Using this concept, forces at each inter-particle contact can be calculated based on the stresses on the packing. These forces will be used to calculate the inter-particle deformations at contact level. The detailed process can be found in Chang and Hicher (2005).

There are very few comprehensive experimental studies on the behavior of sand-silt mixtures which cover the full range of fines content from 0 to 100%. Two sets of data are chosen to evaluate the performance of our model: (1) undrained monotonic triaxial tests on Hokksund sand mixed with different amounts of Chengbei silt (Yang, 2004), and (2) undrained monotonic triaxial tests on Japanese silica sand mixed with different amounts of non-plastic marine clay (Konishi et al., 2007). Both data sets cover fines contents from 0 to 100%. Grain size distribution curves for these mixtures are shown in Fig. 11. All of the samples in both sets were isotropically consolidated before shearing.

2.4. Tests selected for model verification

2.4.1. Undrained behavior of Hokksund sand-Chengbei silt mixtures by Yang (2004)

The first set of data includes 27 undrained monotonic triaxial tests on Hokksund sand and Chengbei silt mixtures with 0, 5, 10, 15, 20, 30, 50, 70, and 94% fines content (Yang, 2004). For these tests, Hokksund sand had specific gravity of 2.712 and sharp edged

cubical grains. Particles of Chengbei silt had specific gravity of 2.739 and angular to sub-angular shape. The minimum and maximum void ratios of the sand were 0.572 and 0.949, respectively. The silt had minimum void ratio of 0.731 and maximum void ratio of 1.413. The mean grain size D_{50} is 0.45 mm for the sand and 0.035 mm for the silt (Figure 13). D_{50}/d_{50} is equal to 13. The samples of this set were prepared by moist tamping under-compaction method with a relative density of 21%. Figure 14 shows isotropic compression data points for all the specimens. Undrained triaxial tests were performed on all samples at three different confining pressures: 50, 100, and 150 kPa. The samples were compressed to axial strains of 20% to reach steady state unless they collapsed at lower axial strains due to static liquefaction.

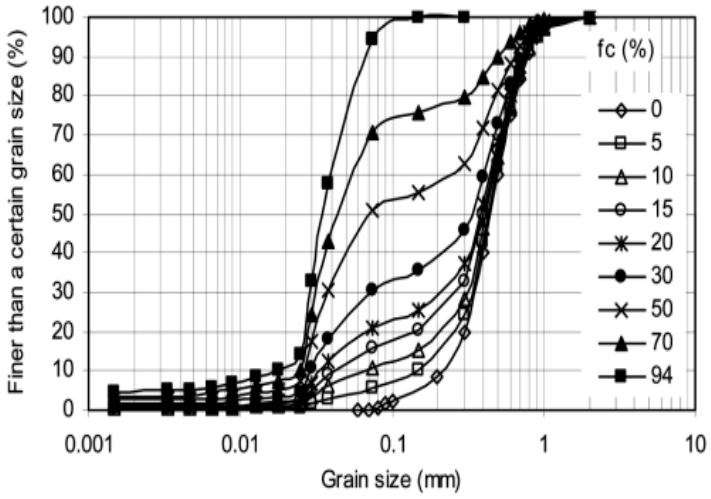

Figure 13- Gradation curves of the selected samples used in this study [Yang, 2004].

In the samples with 0 to 15% fines content (Figure 19), most of the stress-strain behaviors are similar to that of type 2. Large plastic deformation is seen in stress-strain curves after the yield point and samples almost do not gain any shear strength as the axial strain increases.

For the samples with higher fines contents (f_c=20-94%), the stress-strain behavior (Figure 20) can be categorized as type 1. Static liquefaction starts at axial strains around 1% and the samples lose all their shear strengths rapidly due to the increase of axial strain.

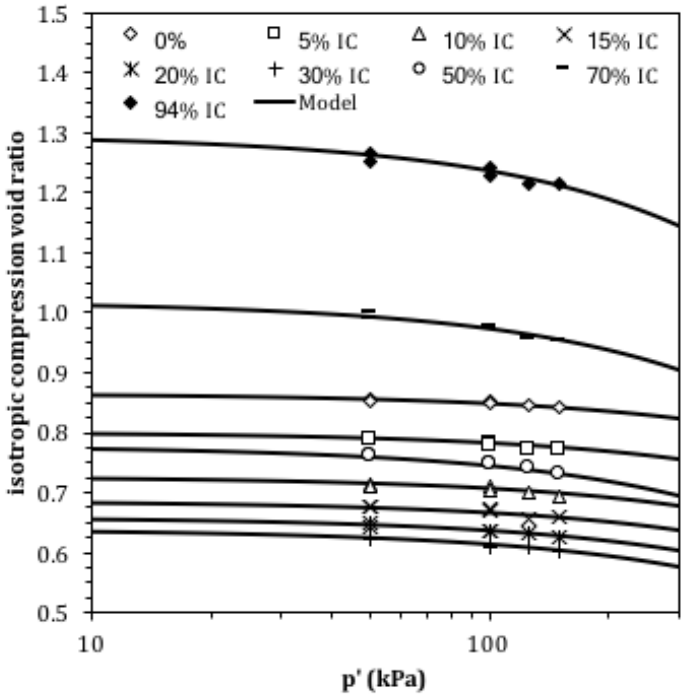

Figure 14- Predicted ICLs (solid lines), and measured values of void ratio (markers) after isotropic compression loading in Yang (2004) tests.

2.4.2. Undrained behavior of Japanese silica sand and marine silt mixtures by Konishi et al. (2007)

The second set (Konishi et al. 2007) includes 16 undrained monotonic triaxial tests on mixtures of Japanese silica sand and marine silt. For these tests, Japanese silica sand and marine silt were mixed in different proportions (0, 5, 15, 30, 50, 70, 97%). The sand and silt specific gravity values are 2.652 and 2.665, respectively. The mean particle size D_{50} for the sand is 0.840 mm and 0.023 mm for the silt, giving a D_{50}/d_{50} of 37 (Figure 15).

The samples of this set were prepared by water sedimentation method at a relative density of 48%.

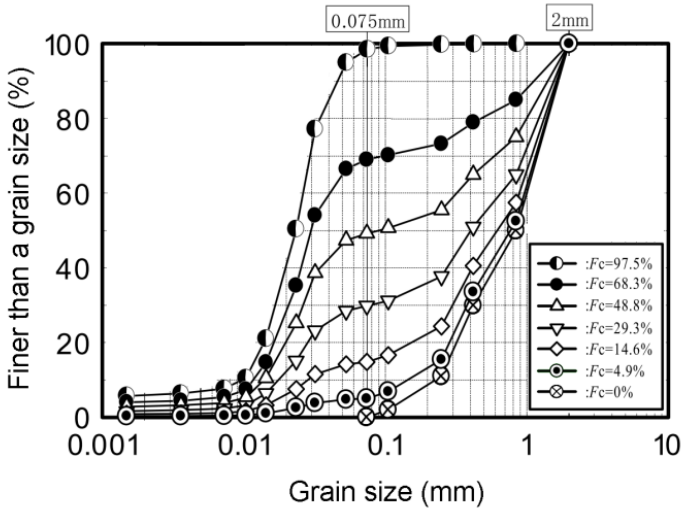

Figure 15- Gradation curves of the selected samples used in this study [Konishi et al., 2007].

Isotropic compression tests data were available for all of the mixtures for confining pressures up to 1600 kPa (Figure 16). For each fines content, three samples were prepared and consolidated under three different confining pressures (i.e. 100, 200, and 400 kPa) and then loaded to large axial strains until steady state condition was reached (Figure 21). None of the samples experienced static liquefaction during shear. The observed behaviors can be categorized as dilative as is shown by type 4.

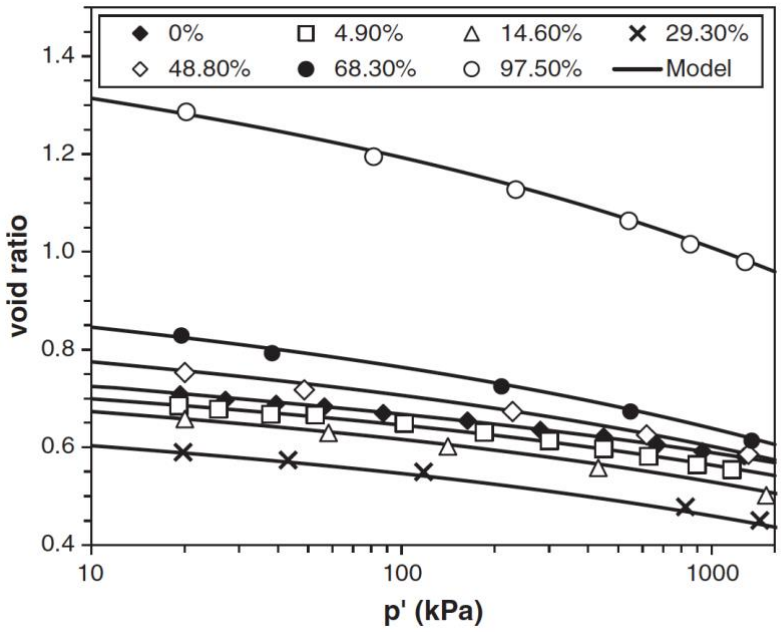

Figure 16- Predicted ICLs (solid lines), and measured values of void ratio (markers) after isotropic compression loading in Konishi et al. (2007) tests.

2.5. Calibration of model parameters

2.5.1. Elastic parameters

A simple lower bound model was proposed earlier to determine the average normal contact stiffness for sand-silt mixtures with various fines contents. According to that model, sand and silt will participate in the average normal stiffness of the mixture based on their fraction in the mixture. For each data set (Yang, 2004; Konishi et al., 2007), the isotropic compression tests data from pure sand and silt specimens are used to find two model parameters, k_{n0} and n. Calculated k_{n0} values, based on the lower bound model (Eq. 19), are shown in Figure 17. These values are then used to simulate the isotropic compression lines by the micromechanical model. Using these values for k_{n0}, the isotropic compression lines are simulated for both data sets and are shown in Figure 14 and Figure 16, respectively. There is a very good agreement between simulated and

measured data. So, the lower bound model is a suitable assumption for normal contact stiffness of sand-silt mixtures. In these simulations, *n* does not change with fines content. However, if the difference between the mechanical properties and shape of coarse and fine particles is significant, *n* could be different for coarse and fine grain dominated mixtures. For our selected data, *n* is found to be 0.15 for Yang (2004) and 0.80 for Konishi et al. (2007) data.

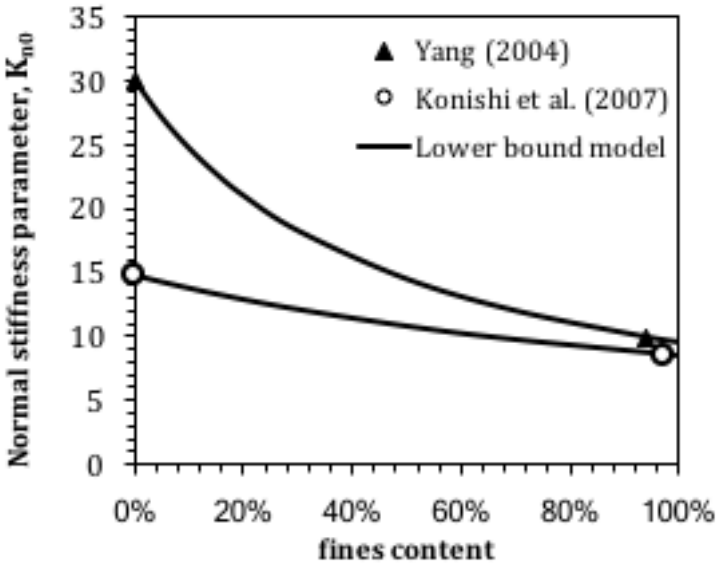

Figure 17- Variation of normal stiffness parameter (k_{n0}) versus fines content for Yang (2004) and Konishi et al. (2007) mixtures.

Parameter ς^e is related to the elastic tangential stiffness between two particles, and is obtained by fitting the initial slope of the simulated stress-strain curve to that of the observed stress-strain curve. ς^e is found to be constant and independent of the amount of fines in the samples. The values for ς^e are shown in Table 3 for both data sets.

2.5.2. Plastic parameters

Parameter ς^p, i.e. initial plastic stiffness (Eq. 23), was determined by fitting the simulation results to the pre-yield data. ς^p has two different values, one value for fines contents less than 25% and another value for fines contents higher than 35%. These values for both data sets are given in Table 3. The change is abrupt; however more tests are needed between 25% and 35% fines contents to see how ς^p changes between these two fines contents.

Parameter *D* is a multiplier for the amount of dilatancy that occurs during plastic flow (Eq. 25). *D* was obtained by fitting the simulation results to the amount of shear strength drop after the peak point. The results show that the samples with fines content more than 35% have higher *D* values than the samples with low fines, which supports the general fact that silts have higher dilation tendency when compared with sands. The ratio between these two values is between 2.2 to 2.4 for both data sets. The values of *D* are shown in Table 3 for both data sets.

Parameter *m*, which controls the magnitude of peak strength, was determined by fitting the simulation results to (1) the stress-strain behavior of the sample after the peak point, and (2) the stress path (*p'*-*q*) results after phase transformation point. A large *m* means it takes more strain for the sample to gain or lose strength after the peak point. The values for *m* are shown in Table 3 for both data sets.

2.5.3. Critical state void ratio parameters

Critical state friction angle (ϕ_{cs}) is an important parameter in modeling stress-strain behavior of soils. Variation of ϕ_{cs} versus fines content for sand-silt mixtures was discussed earlier and a simple phenomenological based model was proposed to predict its

value from the critical state friction angles of sand and silt. The real values of this parameter can be obtained by measuring the slope of stress path curves at critical state condition (M-line in p′-q space). The following relationship describes the relationship between critical state friction angle and M-line slope.

$$M = \frac{6\sin\phi_{cs}}{3-\sin\phi_{cs}} \tag{31}$$

By calculating ϕ_{cs} from the above equation for pure sand and pure silt specimens, ϕ_{cs} for all fines contents can be calculated by Eq. 27. The predicted and observed ϕ_{cs} values for Yang (2004) and Konishi et al. (2007) data are shown in Figure 18.

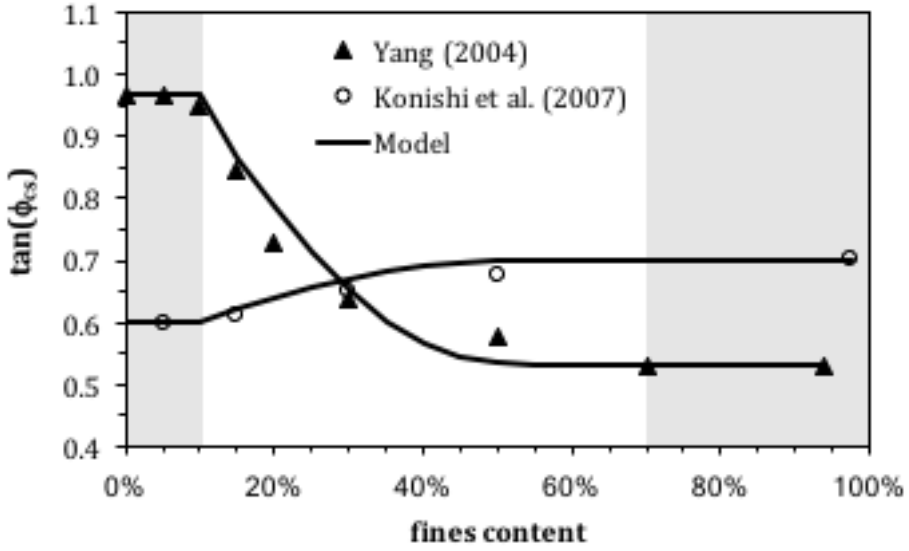

Figure 18- Variation of critical state friction angle versus fines content for Yang (2004) and Konishi et al. (2007) data.

Critical state void ratio parameters for two types of sand-silt mixtures used in this study were already described and are listed in Table 3.

2.6. Simulation results

In order to show the model performance, the simulation results versus tests results for Yang (2004) data are compared in Figure 19 and Figure 20. The behavior of the samples with fines content of 0%-15% is simulated very well for confining stresses of 50 and 100 kPa. However, at this range of fines content, the simulation results do not perfectly match the peak stress for confining stress of 150 kPa. The model shows its capability to simulate types 2 and 3 of behavior for these samples under different confining stresses.

The simulation results and experimental data for Konishi et al. (2007) samples are shown in Figure 21. All of the samples show dilative behavior regardless of the amount of fines in the mixture, and the simulation results match very well with the observed behavior. We can point on four important aspects of stress-strain behavior that is perfectly simulated by our model: (1) initial portion of the stress-strain behavior at small axial strains ($\varepsilon<1\%$), (2) dilative behavior of all mixtures at all confining stresses, (3) the phase transformation point, seen in p'-q graphs, and (4) the behavior of samples at large strains.

The reader could note that the simulation results for Yang (2004) data are not as fit as those for Konishi et al. (2007) data. One important reason is the different correlations between the observed critical state void ratios and the simulated critical state void ratios from Eq. 28. The critical state void ratio plays an important role in the plastic behavior of soils by affecting the density state parameter in Eq. 24. The selected model (Eq. 28) correlated Konishi et al. (2007) data much better than Yang (2004) data.

Overall, the model performance is acceptable in predicting stress-strain behavior of all samples with different fines contents, keeping in mind that we used one set of parameters

for the mixtures with 25% and lower fines content including pure sand, and another set of parameters for the mixtures with 35% and higher fines content including pure silt.

2.6.1. Special case in the simulation of samples with 30% fines content

In the proposed model, if the sample fabric is coarse-grain dominated (f_c<25%), we use the parameter set corresponding to the coarse-grain dominant networks; if the sample fabric is fine grain dominated (f_c>35%), we use the set of parameters corresponding to the fine-grain dominant networks. However, when the samples have fines content between these two values, the soil mixture cannot be clearly categorized as a coarse or fine grain dominant network. This is a gray area for behavior modeling.

Here, the test results for samples with 30% fines content are simulated using both sets of parameters and predict two sets of curves, accordingly. Simulation #1 uses parameter set for coarse-grain dominant networks (f_c<25%), and Simulation #2 uses parameter set for fine-grain dominant networks (f_c>35%) as listed in Table 3. The simulation results along with tests data are shown in Figure 22 for both experiments by Yang (2004) and Konishi et al (2008). It is seen from this figure that the observed behavior in Yang (2004) experiment is better predicted by using the set of parameter for fine-grain dominant networks. The observed behavior in Konishi et al. (2008) experiment is better predicted by using the set of parameters for coarse-grain dominant networks.

We conclude from the above results that for samples with 30% fines content, it is not clear which set of parameters is suitable for predicting the behavior of the mixture. Further study on the stress-strain modeling of mixtures with fines content in this range is needed.

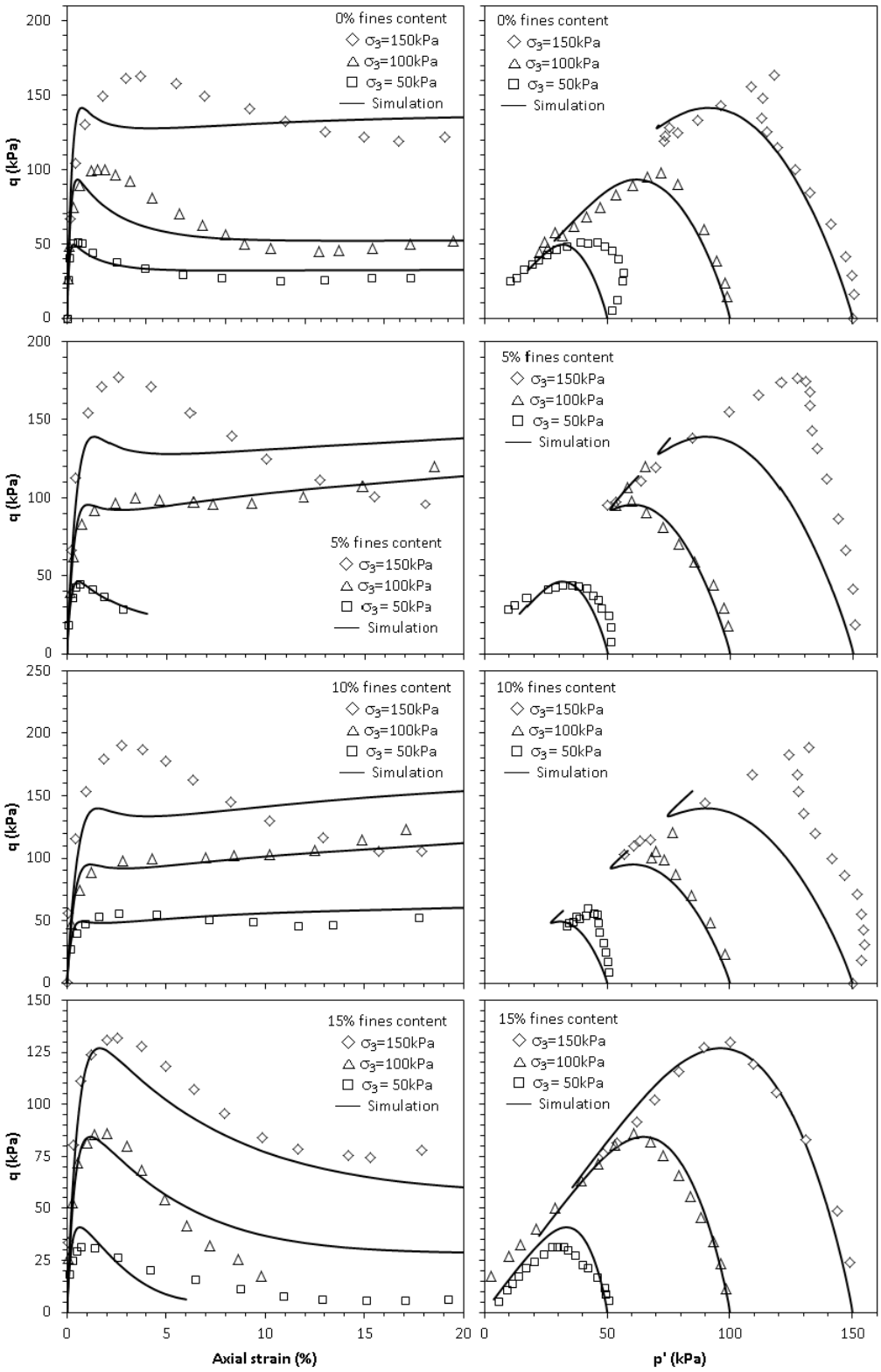

Figure 19- Stress-strain behavior for Yang (2004) tests and model predictions (0% to 15% fines content specimens).

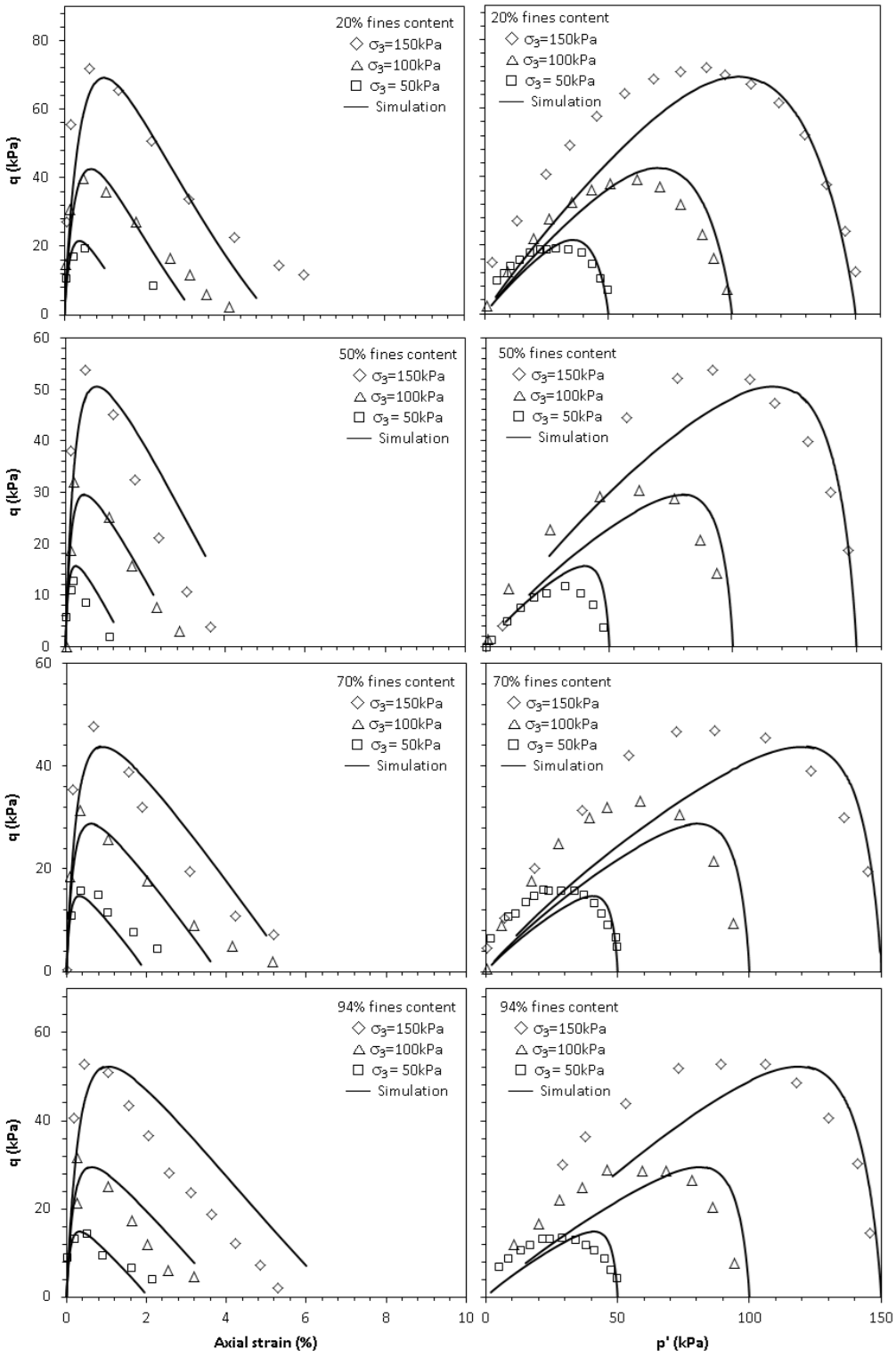

Figure 20- Stress-strain behavior for Yang (2004) tests and model predictions (20% to 94% fines content specimens).

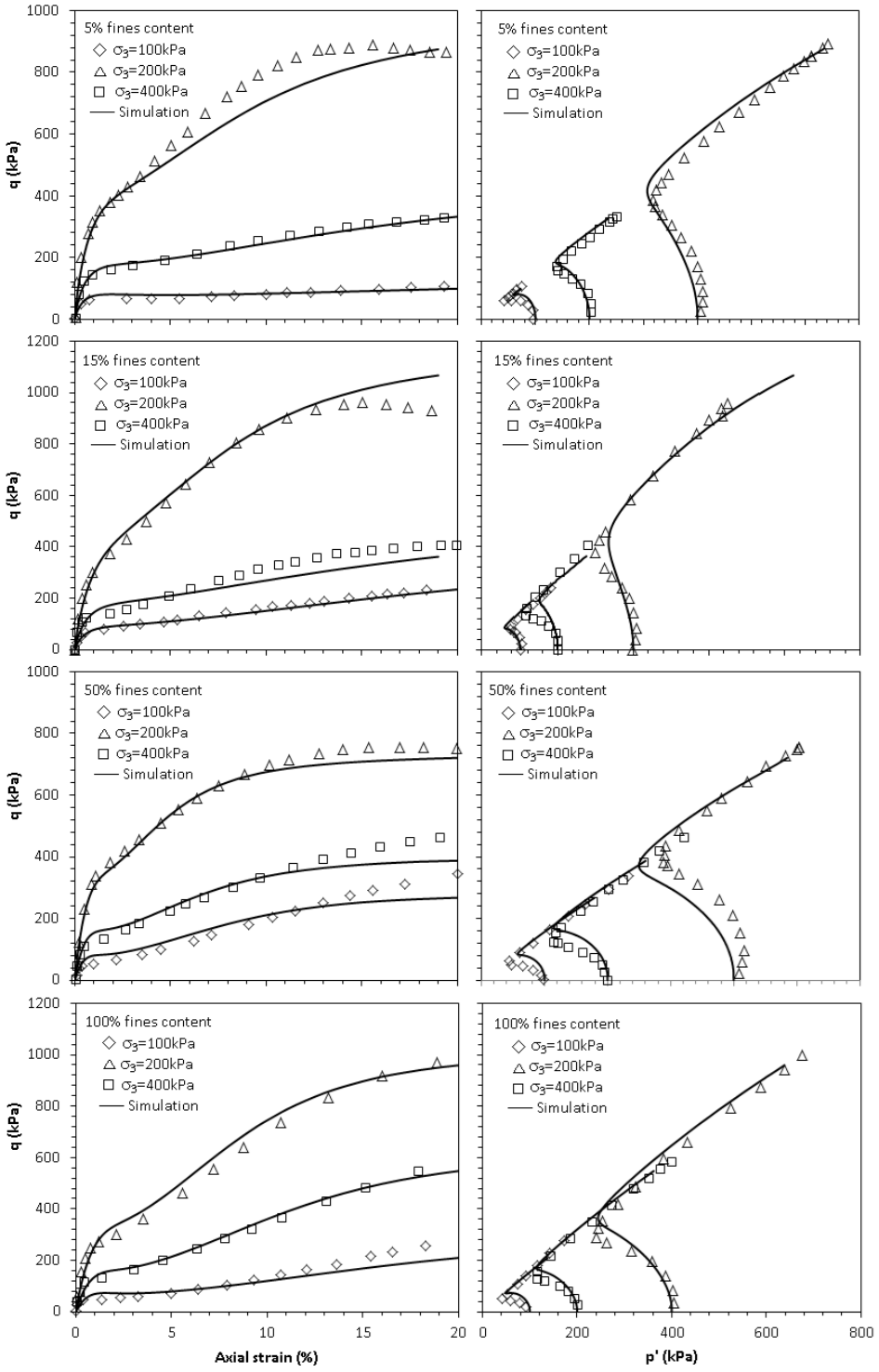

Figure 21- Stress-strain behavior for Konishi et al. (2007) tests and model predictions.

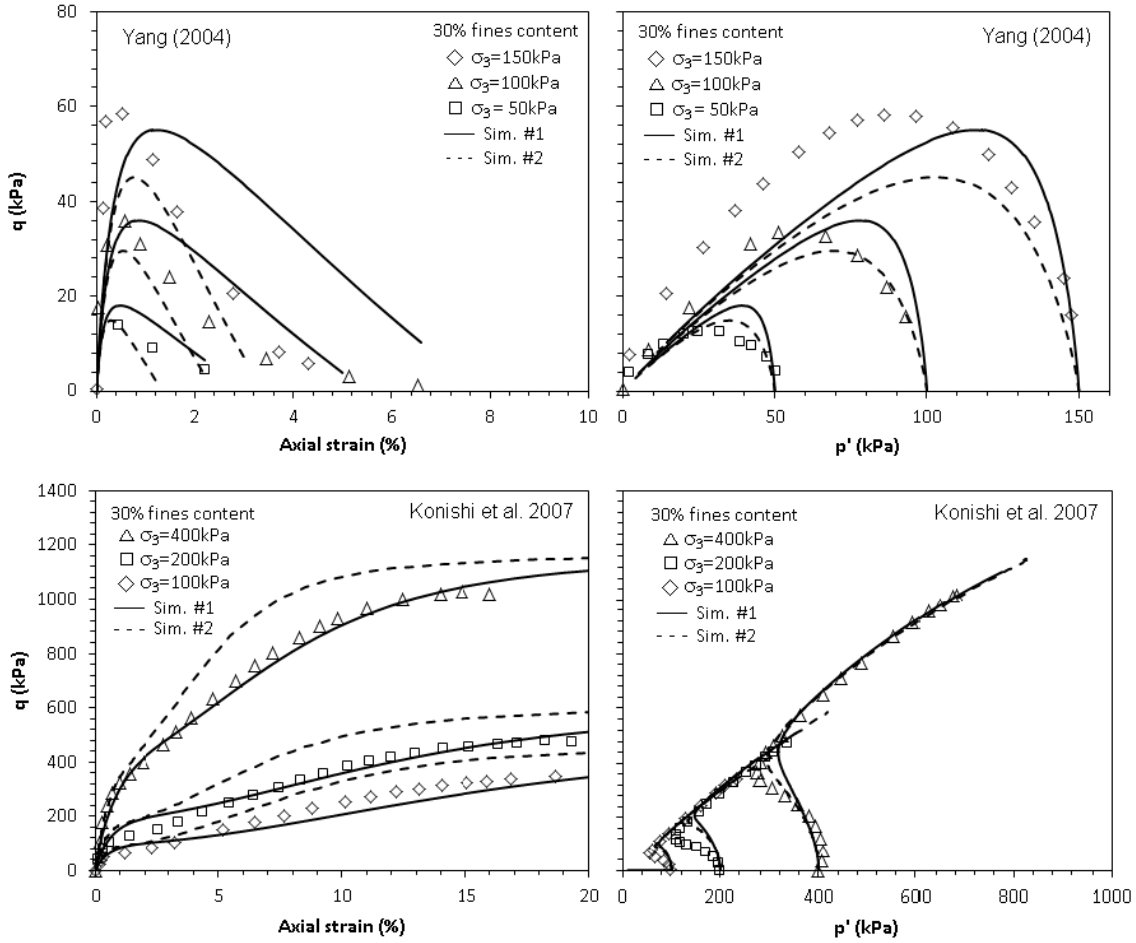

Figure 22- Simulation results based on coarse grain dominated (solid lines) and fine grain dominated (dash lines) set of parameters for the samples with 30% fines content.

2.7. Required developments for the micromechanics model

As was shown in this chapter, in order to predict the deformation behavior and strength characteristics of a sand-silt mixture with any amount of fines, calibration of model parameters is rather complicated and cumbersome. A comprehensive model is needed that can explicitly consider the fines content and eliminated the need for such complicated calibration process. In other words, a model that can get its parameters from the properties of its comprising sand and silt components has a big advantage, because

there are fewer tests are needed for calibration of the model parameters. The first step in developing such model is to have a fundamental relationship between void ratio change, fines content, and stress level. The efforts of this research from this point forward are focused on developing a compression model for granular soils that covers a wide range of stresses. Obviously, a model capable of predicting compressibility at wide ranges of stress should be able to consider the effects of particle crushing as well. In the following chapters, first a hypothesis on dividing the voids in a granular material into two fractions is presented. This hypothesis is used by constructing a compressibility model for sands up to intermediate stress levels. Then the hypothesis is further developed to predict the compressibility of sand-silt mixtures with any amount of fines. Finally, the effects of crushing on compressibility of granular soils is integrated into the model by further developing the concept of active and inactive void ratios and evolution of each with stress.

CHAPTER 3

ACTIVE AND INACTIVE VOIDS AND A COMPRESSION MODEL FOR GRANULAR SOILS[2]

3.1. Introduction

Compressibility models are commonly used in geotechnical engineering for estimating the settlement of foundations (Butterlfield, 1979; Bransby and Randolph, 1998; Lehane and Fahey, 2002), evaluating the subsidence of soil layers as a result of self-weight consolidation (Bartholomeeusen et al., 2002; Stark et al., 2005), or due to fluid extraction, e.g. water, oil or gas (Sherwood and Meeten, 1997). Compressibility models are also used for predicting the foundation settlement in ocean-floor engineering (Houlsby et al., 2005; Krost et al., 2011) or settlement of rockfill structures (Oldecop and Alonso, 2001), studying the propagation of compressive waves in soils (Domenico, 1977), predicting the void ratio and permeability of sands in oil-shale fracturing industry (Chuhan et al., 2002; Zheng and Tannant, 2016), or in conjunction with other constitutive models such as micromechanics models for predicting the stress-strain behavior of granular soil mixtures (Chang and Meidani, 2013).

Geomaterials can be categorized into five groups with respect to their compression properties: (1) granular soils, e.g. non-plastic silt, sand, gravel, and weakly cemented non-cohesive soils, (2) cohesive soils, i.e. plastic silt and clays, (3) rocks, (4) chemically and/or mechanically treated geomaterials, including strongly cemented soils, and (5)

[2] This chapter is published as a standalone paper in the Journal of Engineering Geology (2017) with the same title. doi:10.1016/j.enggeo.2017.03.006

unsaturated soils. In this paper, we focus on modeling the compressibility of the granular soils.

There are two methods to model compressibility of granular soils: (1) discrete element modeling, and (2) analytical modeling. The discrete element modeling (e.g. Minh and Cheng, 2013; de Bono and McDowell, 2015; Cil and Buscarnera, 2016) is a powerful tool to study the displacements and forces at particle level. The advantage of this method is that it can consider the mechanisms of particle rearrangement and crushing in great details. Mineralogy, shape and size of each individual particle can be explicitly considered in the model. Yet, this method has less practical application in engineering analysis and design due to the challenges in defining soil fabric and realistic particle shapes, and computational limitations at the current date.

The analytical modeling is a phenomenological approach and more applicable to the engineering problems. In this approach, the effects of different mechanisms on the compressibility, including particle rearrangement and crushing, are implicitly considered in the model. The method we adopt in this paper falls under the analytical modeling category.

In analytical modeling, mathematical equations are proposed based on experimental data to express compressibility as a function of stress. The three common approaches to express compressibility are: (1) constrained modulus as a function of effective stress in a double-logarithmic space (e.g. Butterfield, 1979; Hardin, 1987, Pestana and Whittle, 1995), (2) compression index as a function of effective stress in a semi-logarithmic space (e.g. Terzaghi and Peck, 1948; Schofield and Wroth, 1968; Vesic and Clough, 1968), and (3) plastic work as a function of stress in a complex form, relating particle rearrangement

and/or crushing to the plastic strains (e.g. Einav, 2007; Xiao et al., 2015; Liu and Gao, 2016; Tengattini et al., 2016).

Compared to these three approaches, the mathematical equation that is developed in this chapter is based on the relationship between compressibility and density state, instead of stress. When the results of compression tests data for various types of granular soil, performed at wide range of stress levels, are plotted on a $\frac{\mathrm{d}e}{\mathrm{d}p'}$ versus e plane (e and p' are the void ratio of the material and applied effective stress, respectively), a linear relationship between these two variables is identified. Based on this linear relationship, a new compression model is derived, which only has two parameters. It should be noted that the linear relationship between $\frac{\mathrm{d}e}{\mathrm{d}p'}$ and e does not mean an elastic behavior in the material, as the linear relationship between $\frac{\mathrm{d}e}{\mathrm{d}p'}$ and p' would imply.

According to Chong and Santamarina (2016), the desirable features for an analytical compression model are: (1) the model should have the minimum number of parameters, (2) the model is in the form of a single continuous mathematical form, (3) the initial formation density should be explicitly included in the model, and (4) the model does not need the yield stress of the material to be identified. It is noted that none of the existing models can simultaneously satisfy these desirable features (Table 3). However, the proposed model in this paper satisfies all these four features simultaneously.

In the following sections, a postulate of dividing the voids into active and inactive fractions is presented, which allows us to incorporate the effects of particle rearrangement and particle crushing into the proposed model. Experimental data is presented to support this postulate.

Based on this postulate, a mathematical equation that expresses void ratio in terms of effective stress and initial void ratio of the material is developed. The performance of the proposed model is verified by comparing the predicted void ratios with the tests data for 20 different types of granular soils with different mineralogy and various initial densities. The comparisons show the suitability of the proposed model for predicting the compressibility of various types of granular soils over wide ranges of stress.

A closed-form solution for the compression index (C_c) is also derived and the predicted results are compared with the measured values at various stress levels for different types of granular soils.

3.2. Active and inactive voids in a granular soil

To study the change of void ratio in a granular soil during loading, the total volume of voids can be divided into two hypothetical fractions: (1) active voids volume, and (2) inactive voids volume.

We define active voids volume as the fraction of voids that can be reduced, and eventually diminished by particles rotation and displacement. In other words, this fraction of voids is reactive to the kinematic process of particle rearrangement. The other fraction, which is not reactive to the kinematic process of particle rearrangement is named inactive voids volume.

The volume of inactive voids is dictated by the densest packing structure of the material. However, due to particle crushing effects, the volume of inactive voids does not remain constant during loading. This inactive volume can be reduced and becomes active due to particle crushing effects. Einav (2007) proposed a similar idea by incorporating his breakage index into constitutive modeling of granular material. The major mechanisms

that change the volume of active and inactive voids in a granular soil during loading are shown in Figure 23.

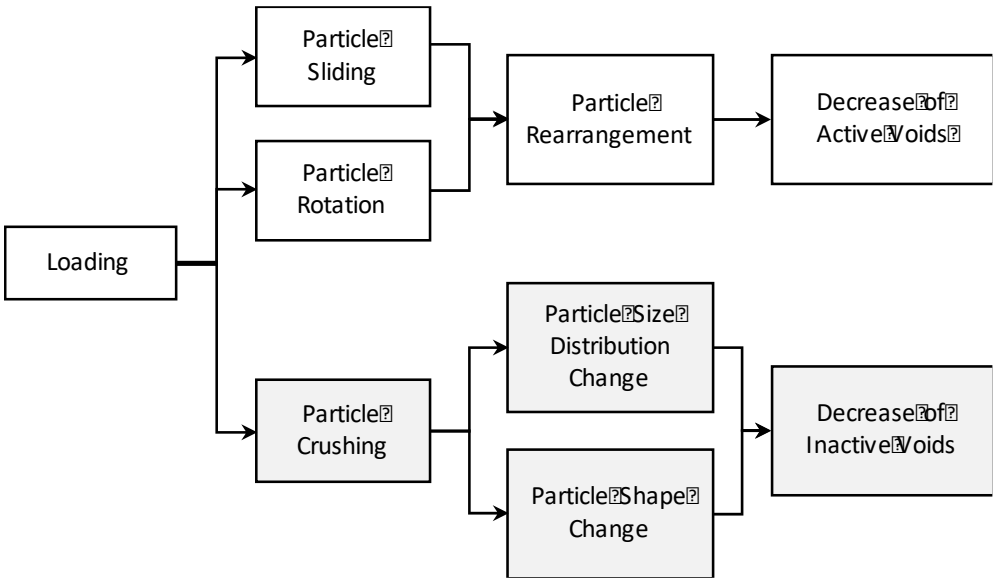

Figure 23. Contribution of different mechanisms to the change of active and inactive voids.

Active and inactive voids can be explained by the example of a random packing of mono-sized spheres. The packing has a random initial void ratio of 0.73. The void ratio of this packing can be reduced to its densest state, due to the kinematic process of particle rearrangement. The densest packing structure for a mono-sized group of spheres corresponds to a rhombohedral structure, with a minimum void ratio of 0.35. This is the absolute minimum void ratio for this mono-sized granular soil. After this point, no matter how much kinematic perturbation is applied to the packing, the absolute minimum void ratio will not decrease. In this case, the available void ratio to the kinematic process (i.e. the active void ratio) is equal to (0.73-0.35=0.38). The unavailable void ratio to the kinematic process (i.e. the inactive void ratio) is 0.35.

Now, if some of the spheres are split or crushed, the resulting smaller particles can occupy some of the existing voids, which were inactive and un-diminishable in the original mono-sized packing. Therefore, particle crushing increases the kinematic degree of freedom of the granular packing and makes some of the previously unavailable voids, available to the particle rearrangement process. This means that the volume of inactive voids is decreased due to particle crushing. Hence, the volume of inactive voids is related to particle crushing, which in turn is a function of the applied effective stress.

In granular mechanics, void ratio is defined as the ratio of the volume of voids by the volume of solids. The active and inactive void ratios are the volumes of active and inactive voids, divided by the volume of solids, respectively. Since the volume of solids does not change during loading (for the stress levels considered in this study), the total void ratio at any stress level can be expressed as the summation of active and inactive void ratios:

$$e(p', e_0) = e_{active}(p', e_0) + e_{\text{inactive}}(p') \quad (1)^3$$

where $e(p', e_0)$ is the total void ratio of sand, and is a function of applied pressure p' and initial void ratio of the soil, e_0.

In the next section, e_{inactive} is shown to be assumed as a constant value throughout the compression loading up to certain stress levels. This constant value is called the representative inactive void ratio or e_r. The simplifying assumption of a constant inactive void ratio during loading does not jeopardize the accuracy of our model in predicting compression lines of granular soils, within the range of validity of the proposed model.

---

[3] To avoid long digits, equation numbers start from 1 for this chapter.

3.3. Derivation of the compression model

Compression tests data are available on Cambria sand and Petroleum Coke on very wide range of stress levels. These granular materials have two different mineralogy: Cambria sand is comprised of quartz particles; Petroleum Coke is comprised of particles ultra-rich in carbon (Table 4). We select these tests data to investigate the rate of change of void ratio ($\mathrm{d}e$) with respect to the change of effective stress ($\mathrm{d}p'$). The variation of $\frac{\mathrm{d}e}{\mathrm{d}p'}$ (i.e. slope of compression line in $e - p'$ space) versus e is shown in Figure 24 and Figure 25 for Cambria sand and Petroleum Coke, respectively. It can be seen that $\frac{\mathrm{d}e}{\mathrm{d}p'}$ has an approximate linear relationship with respect to e up to certain levels of effective stress for these two materials. An $e - \log p'$ child-graph is embedded in these two figures to show the linear correlation between $\frac{\mathrm{d}e}{\mathrm{d}p'}$ and e, shown on the main graph, is still valid beyond the yield point of the material.

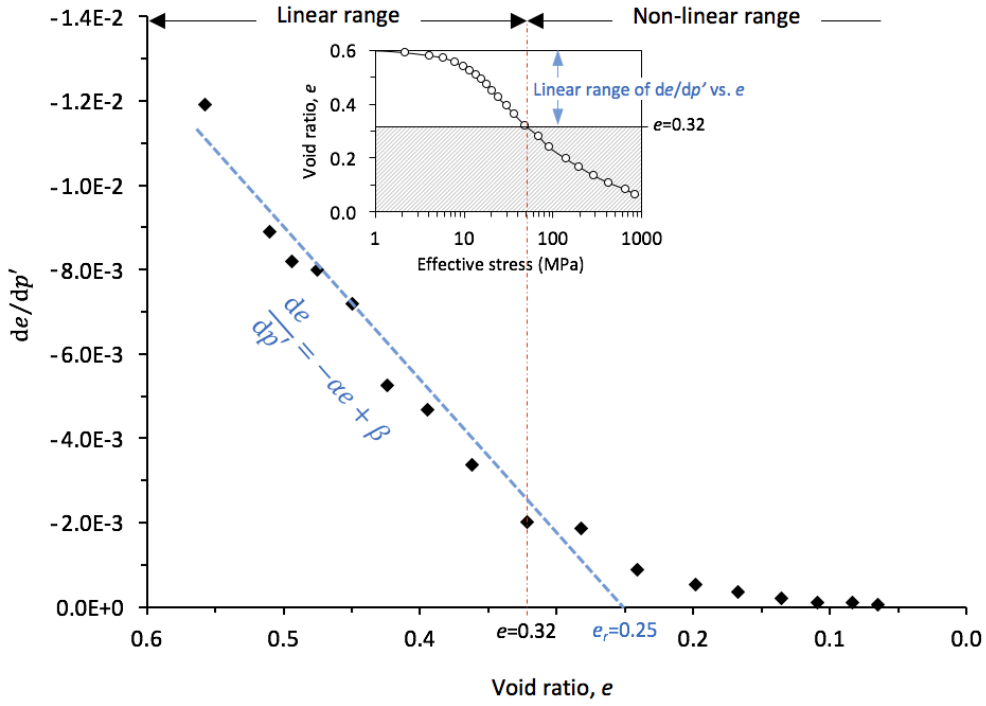

Figure 24. Main graph shows the slope of compression line ($\frac{\mathrm{d}e}{\mathrm{d}p'}$) plotted versus void ratio for Cambria sand, divided into linear and non-linear ranges. The child graph shows the compression line in e-log p' space [tests data from Yamamuro et al. 1996].

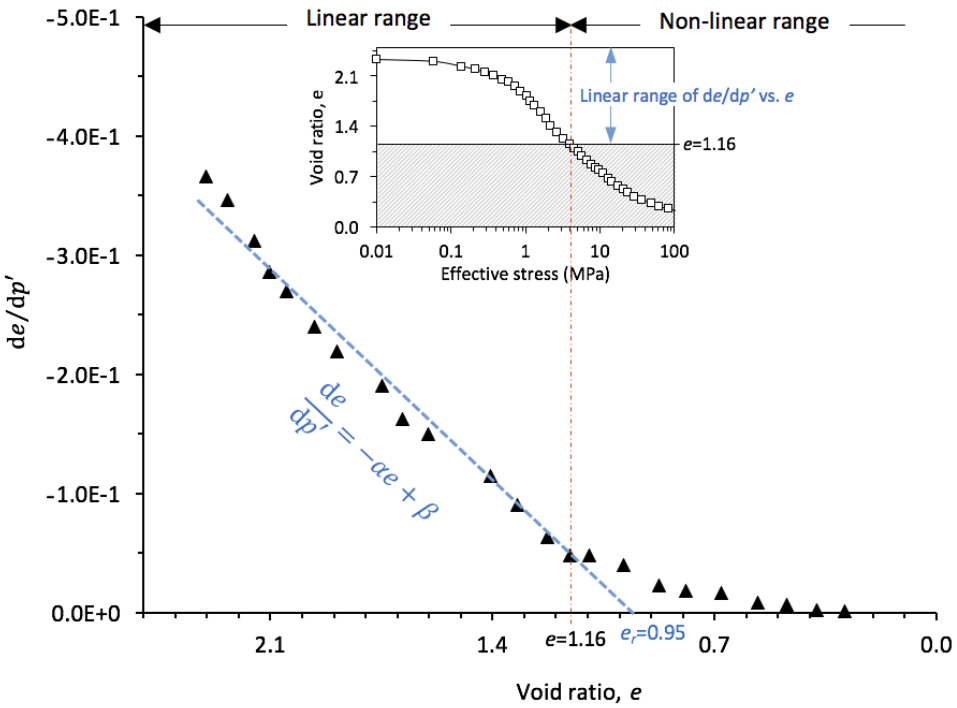

Figure 25. Main graph shows the slope of compression line ($\frac{de}{dp'}$) plotted versus void ratio for Petroleum Coke, divided into linear and non-linear ranges. The child graph shows the compression line in e-log p' space [tests data from Biarez & Hicher, 1994].

To show the validity of this assumption for more granular materials, data selected from compression tests data on eight different granular material are presented in Figure 26: four types of quartz sand tested up to 40 MPa, two calcareous sands tested up to 8 MPa, Petroleum Coke (carbonaceous) tested up to 4 MPa, and Marsala calcarenite tested up to 2.5 MPa. The linear relationship between $\frac{de}{dp'}$ and e is observed for these granular materials up to the aforementioned stress levels.

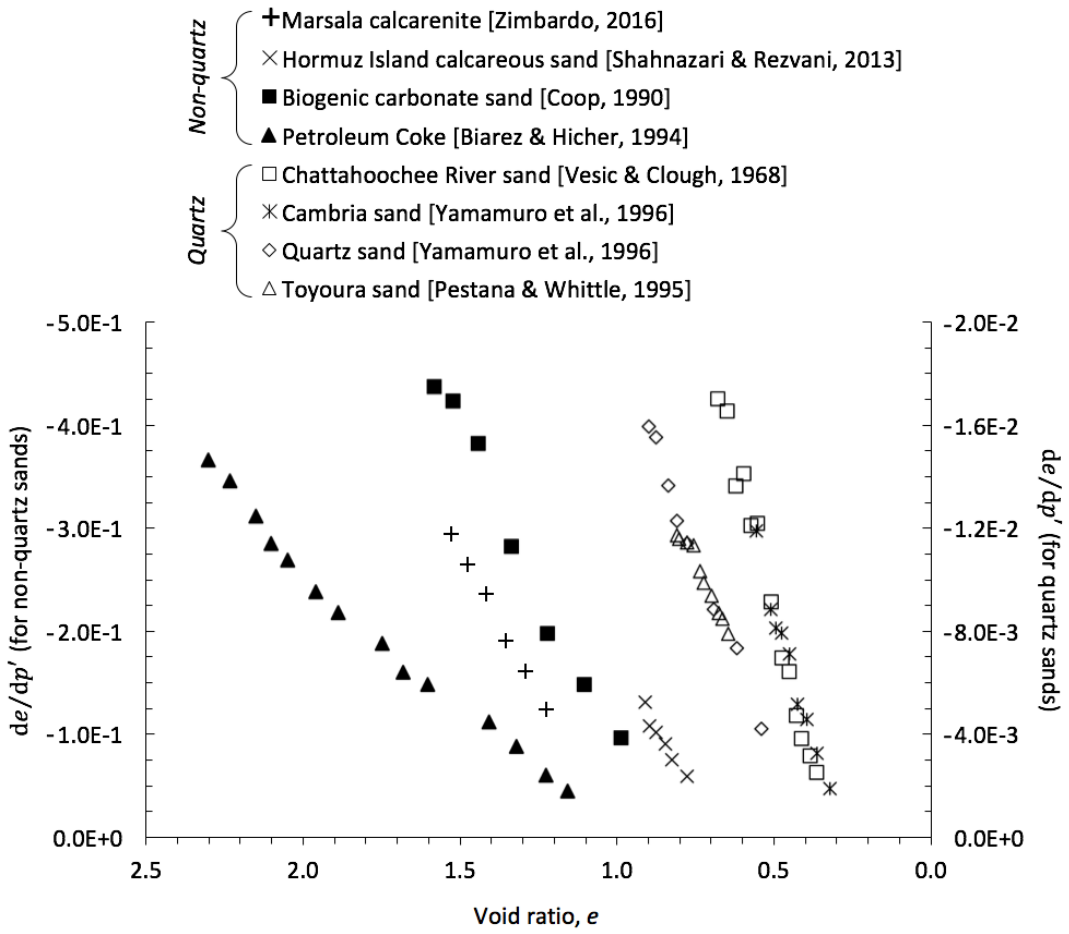

Figure 26. $\frac{de}{dp'}$ vs. e for eight granular material with different particle mineralogy.

According to Figure 24, Figure 25, and Figure 26, we can assume that $\frac{de}{dp'}$ for granular soils has a linear relationship with the current state of void ratio, e, up to certain stress levels. This relationship can be expressed as:

$$\frac{de}{dp'} = -\alpha e + \beta = -\alpha(e - \frac{\beta}{\alpha}) \quad (2)$$

where α and β are the slope and intercept of the fitted line.

When $\frac{de}{dp'} = 0$, the void ratio has reached a limit and does not decrease anymore. This limit is conceptually same as the definition of inactive void ratio defined in the previous section. We call it e_r, standing for representative inactive void ratio:

$$e_r = \frac{\beta}{\alpha} \text{ at } \frac{de}{dp'} = 0 \quad (3)$$

Replacing Eq. 3 into Eq. 2 and integrating Eq. 2 starting from the beginning of the loading ($e = e_0$, $p' = 0$), and up to any arbitrary stress level p', follows:

$$\int_{e_0}^{e} \frac{de}{e - e_r} = -\int_0^{p'} \alpha dp' \quad (4)$$

$$e(p, e_0) = [e_0 - e_r] \exp(-\alpha p') + e_r \quad (5)$$

where e_0 is the initial void ratio of the material, and α and e_r are the model parameters. The model parameters can be obtained for each soil specimen by best-fitting to the compression test data.

Eq. 5 is used to predict the compression behavior of Cambria sand (Figure 27). The prediction is valid up to 40 MPa, at which the linear relationship is valid between $\frac{de}{dp'}$ and e. The model parameters are listed in Table 2. Model prediction fits reasonably well to the actual behavior of Cambria sand up to 40 MPa, then the predicted curve starts to become asymptotic to $e_r = 0.245$, and deviates from the measured data points beyond 40 MPa. This was expected from Figure 24, where the linear relationship between $\frac{de}{dp'}$ and e was valid up to 40 MPa. A phase diagram is presented in Figure 27, with active and representative inactive voids shown next to the compression curve.

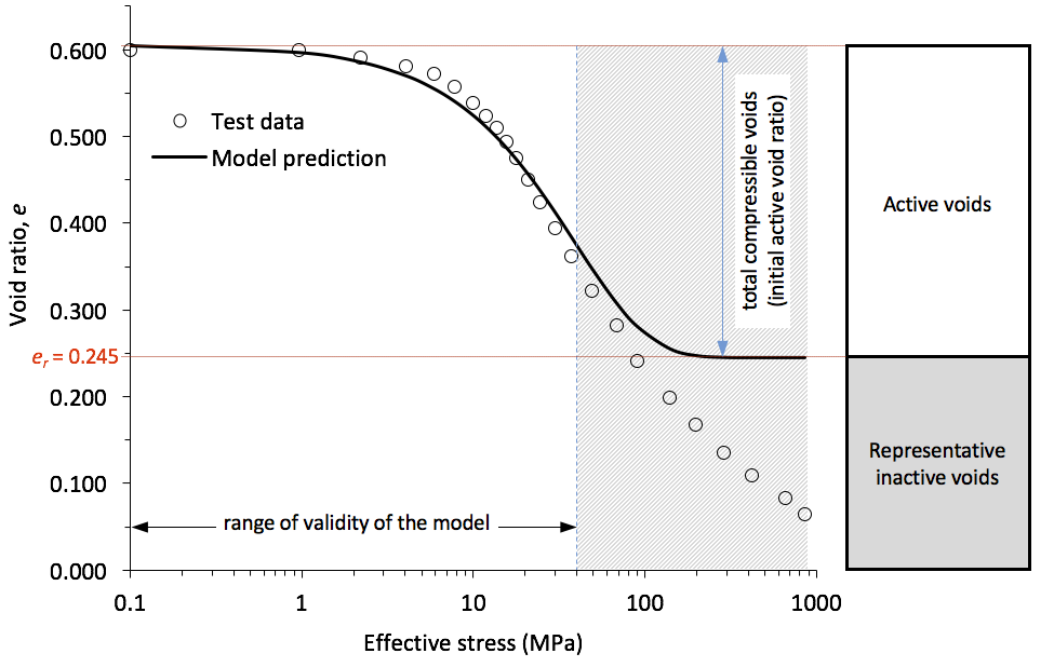

Figure 27. Model prediction and test data for Cambria sand, showing the range of validity of the model [test data from Yamamuro et al., 1996].

For the range of validity of the model, by comparing Eq. 5 to Eq. 1, active and inactive void ratios can be identified as follow:

$$e_{active}(p', e_0) = [e_0 - e_r]\exp(-\alpha p') \quad (6)$$

$$e_{inactive}(p') = e_r \quad (7)$$

According to Eqs. 6 and 7, the change in total voids is only caused by the change in the active voids. Eq. 7 means that inactive void ratio is a constant value for the range of validity of the proposed model.

This seems to disagree with the statement in the previous section about dependence of the inactive void ratio on the effective stress level. But this disagreement can be justified by the following reasons: The conclusion of a constant e_r for the range of validity of this model is directly from the approximation of a linear relationship between $\frac{de}{dp'}$ and e, backed by the experimental evidence as shown in Figures 5, 6, and 7. Therefore, it seems

that within the valid stress range of the model, the effects of particle crushing can be implicitly included in the evolution of active void ratio (Eq. 6). Hence, the inactive void ratio can be approximated by a representative constant value (e_r). However, for the stresses beyond this range, the constant assumption is not applicable anymore. The applicability of assumption of constant e_r will be shown in a later section by comparing the predictions and measured void ratios for the compression lines of 20 different types of granular soils.

To visualize this assumption of constant inactive voids, three different phase diagrams at three stress levels are shown in Figure 28. The inactive void ratio takes a representative value and remains constant during loading, while the active void ratio is being diminished.

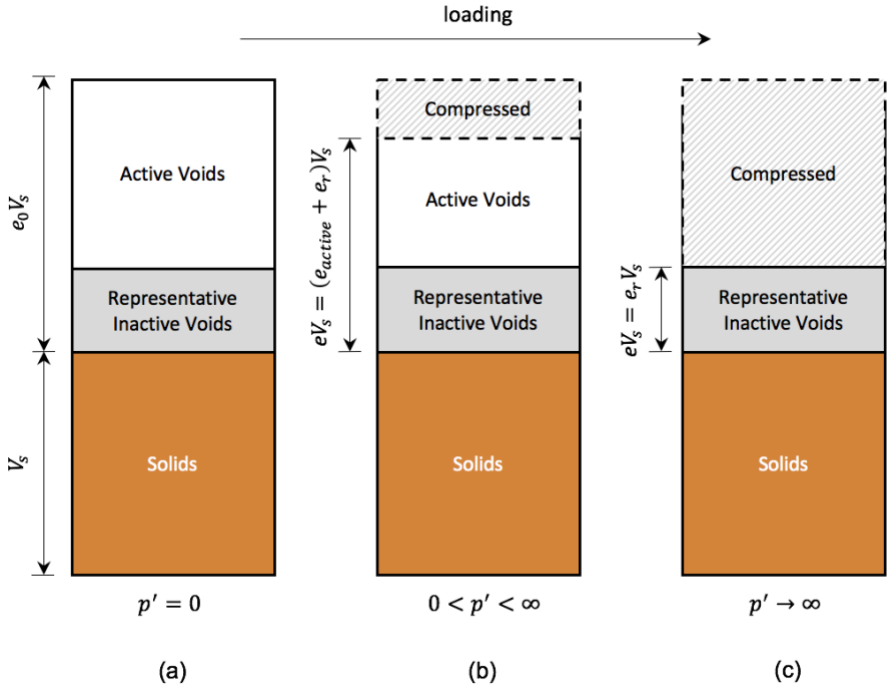

Figure 28. Phase diagrams showing changes in the volume of active voids during loading, assuming a representative constant volume for inactive voids.

3.3.1. Correlation between parameter α and e_0

Eq. 5 is used to predict the compression lines of specimens from four different types of sand. For each sand, several specimens are prepared at wide ranges of initial void ratios (Figure 29). In the calibration process, one parameter α is obtained for each specimen with a given initial void ratio. However, one value for e_r is considered for all the specimens of a certain type of sand, since all the specimens will eventually reach the same void ratio after full compression. The initial void ratio of the specimen loses its relevance on the compression line at higher stress levels (Terzaghi and Peck, 1948; Hong et al., 2012; Chong and Santamarina, 2016).

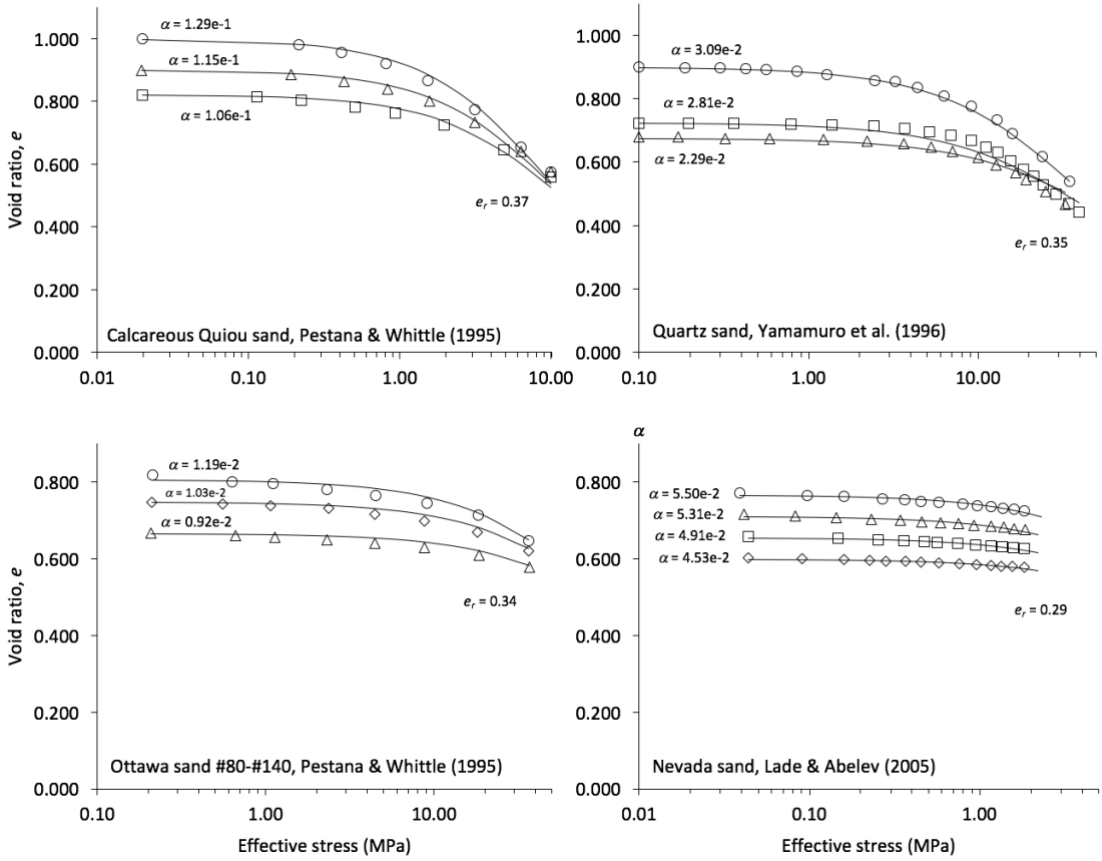

Figure 29. Calculated compression lines using Eq. 6 and tests data for 4 different types of sand with various initial void ratios.

For each sand, the values of parameter α obtained from best-fit process are plotted versus the corresponding initial void ratios in Figure 30. A linear correlation between parameter α and the initial void ratio of the specimen can be identified in this figure. The linear relationship is expressed as $\frac{ae_0}{p_a}$, where a is a unit-less material parameter, and p_a is the reference atmospheric pressure (i.e. 0.101324 MPa).

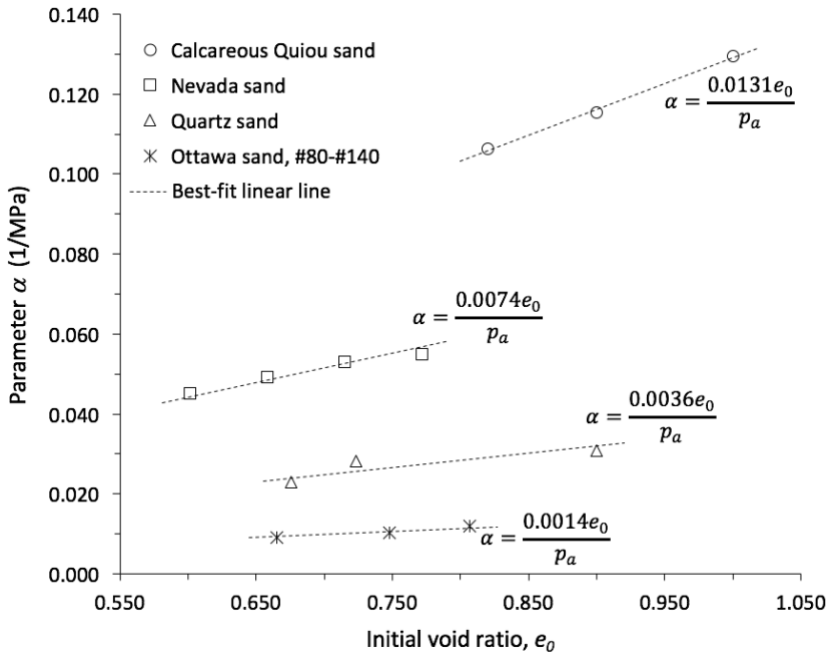

Figure 30. Linear correlation between parameter α and initial void ratio of the specimens, shown for 4 different types of sand.

Using this linear relationship, Eq. 5 becomes:

$$e(p', e_0) = [e_0 - e_r] \exp\left(-\frac{a e_0}{p_a} p'\right) + e_r \qquad (8)$$

For a granular soil, the unit-less model parameters (a and er) can be obtained by best-fitting Eq. 8 to the compression tests data.

3.3.2. Correlation between parameter e_r and minimum void ratio

It is reasonable to assume that the parameter e_r, which is defined as the void ratio after all active voids are diminished, can be correlated to the minimum void ratio of the material, e_{min}. The minimum void ratio of granular soils is determined according to standard tests, such as ASTM D4253-16. The level of particle crushing in these type of tests is not substantial. Most of the densification is due to the particle rotation and rearrangement, eased by vibration or rodding. A general relationship can be suggested between e_r and e_{min} as:

$$e_r = f(e_{min}) \quad (9)$$

To investigate the relationship between the model parameter e_r and the minimum void ratio e_{min}, compression test data for 19 different types of granular soils are selected and the model parameters for each of them is determined using Eq. 8. The determined parameters a and e_r are listed in Table 4 along with the basic physical properties of these materials. The determined values of e_r for these 19 materials are plotted versus the minimum void ratios in Figure 31.

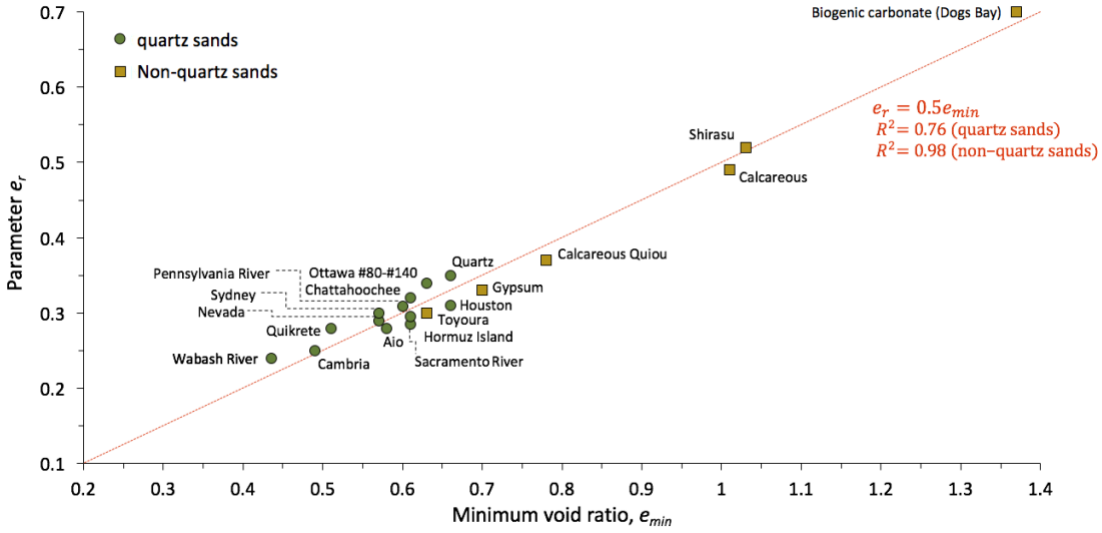

Figure 31. Correlation between parameter e_r and minimum void ratio for 19 granular materials selected in this study.

From regression analysis, a linear relationship is found between e_r and e_{min}:

$$e_r = 0.5e_{min} \tag{10}$$

Replacing e_r by $\frac{e_{min}}{2}$ in Eq. 8, the mathematical relationship can be rewritten as:

$$e(p', e_0) = \left[e_0 - \frac{e_{min}}{2}\right] \exp\left(-\frac{ae_0}{p_a} p'\right) + \frac{e_{min}}{2} \tag{11}$$

This is the final form of the proposed model. The only parameter that needs to be calibrated for each type of sand is "a".

3.4. Calibration of the model parameters

As pointed out by Kolymbas (2012), it is not uncommon to see a new constitutive model is presented, with not much instruction on the calibration process of its parameters. Here, the process of obtaining the model parameters from the compression tests results is described.

If the minimum void ratio of the specimen is known prior, the only parameter that needs to be obtained in Eq. 11 is "a". This parameter is a material constant and does not

depend on the initial void ratio of the soil. Therefore, by obtaining this parameter from the results of the compression tests on a specimen with a given initial void ratio, the user will be able to predict the compression lines for specimens with any other initial void ratio.

Figure 32 shows the compression test data of Sacramento River sand, where the minimum void ratio was already known. To find parameter a for this material, we pick three points from the compression test data on the specimen with e_0 = 0.71. These three points are selected such that the first point is at the beginning of loading, corresponding to a very low effective stress, e.g. 10-35 kPa. The second and third calibration points are on the flatter and steeper parts of the compression line (i.e. before and after the point of maximum curvature), respectively. These three points are shown with solid triangle symbols in Figure 32. After parameter a is obtained by the least-square method using Eq. 11, it is used to predict the compression lines for specimens of Sacramento River sand by adjusting e_0 to 0.87, 0.78, and 0.61, as shown in the same figure. The predicted compression lines match very well with the measured void ratios.

When picking the calibration points, the stress range of validity of the model should be kept in mind. The general stress range of validity of the model can be guessed from the values listed in Table 2 for different particle mineralogy. For example, the upper stress limit for most of the quartz sands is 40 MPa. If one is in doubt, $\frac{\mathrm{d}e}{\mathrm{d}p'}$ can be plotted versus e for the tests data and range of the validity is selected up to the point at which the linear relationship is held between $\frac{\mathrm{d}e}{\mathrm{d}p'}$ and e, with a reasonable approximation.

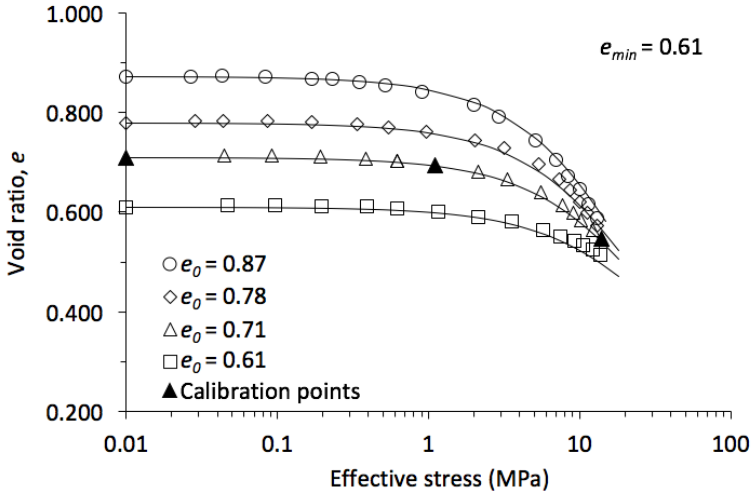

Figure 32. Predicted compression lines for Sacramento river sand specimens with four different initial void ratios [test data from Lee and Seed, 1967].

In case the minimum void ratio of the material is not available, such as for the Petroleum Coke (Table 2), the user can utilize Eq. 8 to obtain parameters a and e_r through the best-fitting process. Both parameters are material constants, and applicable to specimens with various initial void ratios.

Even though parameter a is called a material constant, its value depends on the type of compression test from which it is obtained. If the model is to predict void ratios for a problem that is governed by 1-D loading conditions, parameter a should be obtained from 1-D compression tests with similar loading conditions. The same statement applies to isotropic and K_0 compression tests.

3.5. Morphology of the proposed model

In this section, the effects of variation of e_0, e_{min}, and model parameter a are shown on the characteristics of the calculated compression lines, using Eq. 11.

3.5.1. Variation of initial void ratio

The effect of variation of initial void ratio e_0 on the simulated compression lines of a typical quartz sand, while parameter a and e_{min} are kept constant, is shown in Figure 33. The assumed model parameters for this typical quartz sand are e_{min} = 0.5 and a = 0.05. For a typical quartz sand, the range of validity of the model is 40 MPa (Table 2). It can be seen from Figure 33 that the initial void ratio has an apparent effect on the predicted compression lines: by decreasing e_0 (increasing initial density), the yield stress of the material, which is conventionally considered to be at the point of maximum curvature of compression curve, increases.

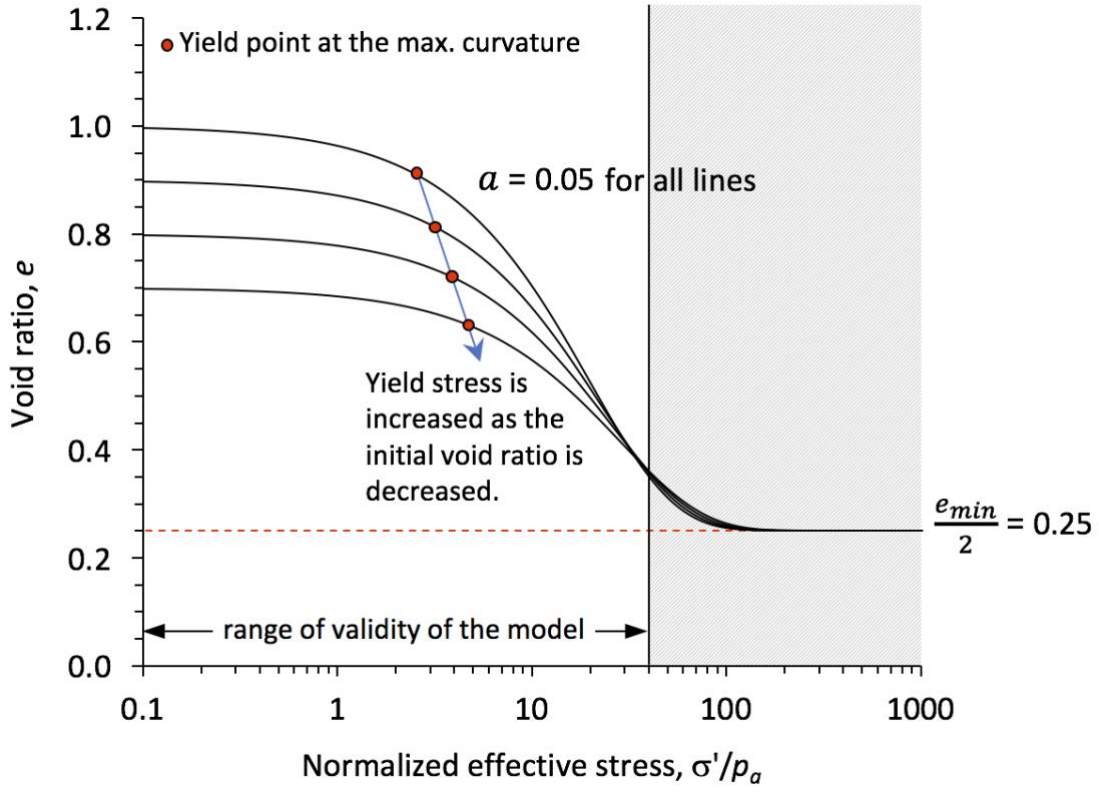

Figure 33. Effect of variation of initial void ratio on the predicted compression lines.

3.5.2. Variation of parameter *a*

In our proposed model, parameter *a* shifts the compression lines on the stress axis. By increasing the value of this parameter, the calculated compression lines move to the left, depicting the behavior of a material comprised of weaker particles, or lower yield stress (Figure 34).

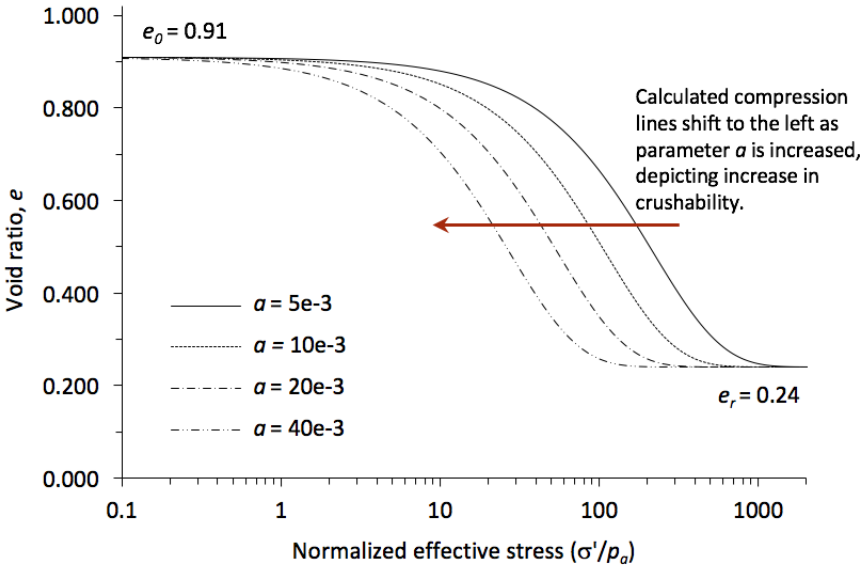

Figure 34. Effect of increasing parameter *a* on the calculated compression lines.

Granular geomaterials are comprised of particles of different origins, e.g. quartz or biological-based. Compressibility of these geomaterials depends on the mechanical properties of the particles as well as their shape and size. Biological-based particles crush at much lower stress levels compared to stronger quartz grains (Coop and Lee, 1993).

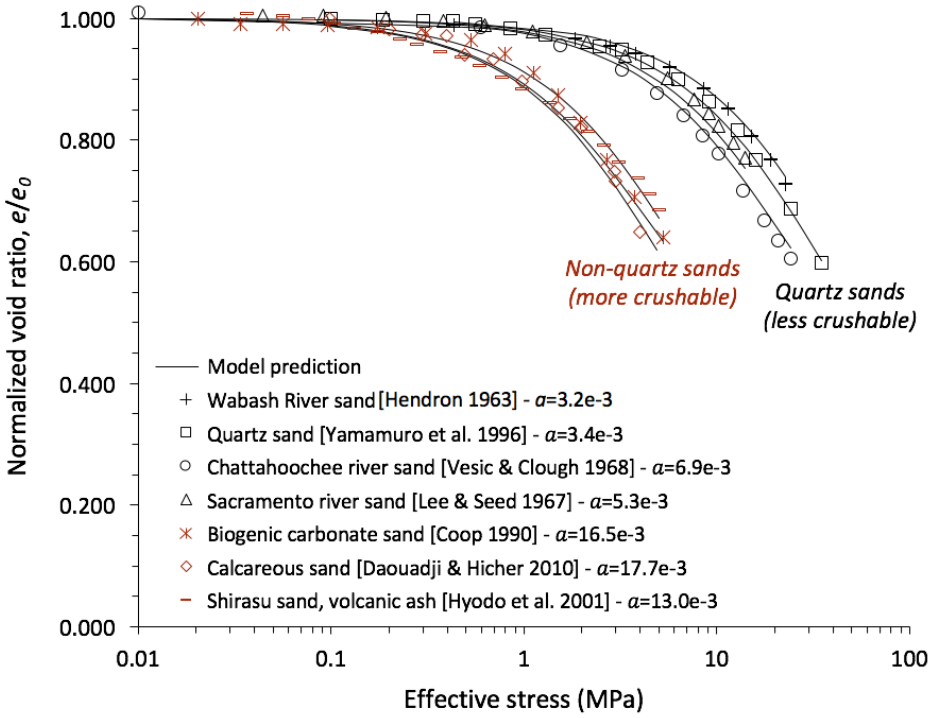

Figure 35. Compression lines of seven types of sand with different particle mineralogy.

For seven different type of sand shown in Figure 35, there is a clear gap between the compression lines of quartz sands, and those of the non-quartz sands. Two of the non-quartz sands shown in Figure 35 are Calcium-based and one of them is volcanic fly ash. The values of parameter *a* shown in Figure 35 indicate larger values for non-quartz sands, compared with those of the quartz sands.

In Figure 36, the values of parameter *a* versus e_{min} for all the sands selected in this study are plotted. SEM images of particles with four different mineralogy are also shown in this figure. The carbonaceous particles found in Petroleum Coke are the weakest among all particles selected in this study. The calcareous particles are usually porous, and have weaker structure (Figure 36c) than the siliceous (quartz) particles (Figure 36e). The

volcanic fly ash particles (Figure 36d) are siliceous, but their structure is very porous, which makes them more crushable than the intact quartz particles found in regular sands.

The parameter *a* for quartz-based sands vary between 0.001 and 0.01. This variation of parameter *a* in quartz sands indicates different crushability in those sands, which is due to the variation of their particles size, particles shape, and surface texture (Mesri and Vardhanabhuti, 2009). More crushable granular materials such as carbonaceous Petroleum Coke, siliceous fly ash (particles are very porous), and calcareous sands have larger parameter *a*. It should be re-noted that larger values for parameter *a* refers to more crushable granular materials (i.e. lower yield stress).

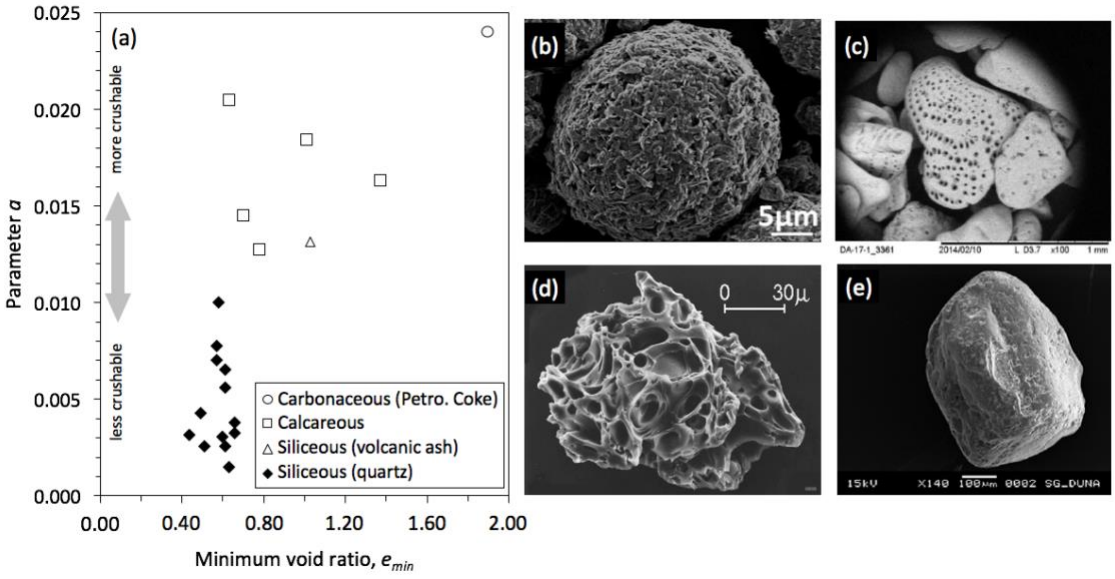

Figure 36. (a) Parameter *a* versus e_{min} for all granular materials used in this study; (b) SEM image of a Petroleum Coke particle [Ren et al., 2015]; (c) SEM image of a calcareous sand particle [Spagnoli et al., 2015]; (d) SEM image of a volcanic ash particle [Wilson et al., 2015]; (e) SEM image of a semi-angular quartz sand particle [Costa et al., 2013]. (Note: e_{min} for Petroleum Coke is not reported in the literature, so we assume $e_{min}=2e_r$ for this material).

3.5.3. Variation of e_{min}

While parameter a is responsible for shifting compression lines on to the stress axis in e-logp' space, different values of e_{min} change the slope of simulated compression lines.

Figure 37 shows the simulated compression lines for 4 different values of e_{min}, while the initial void ratio is equal to 1.0, and parameter a is equal to 0.02 for these simulated compression lines. It can be seen that the specimens with lower minimum void ratio have steeper compression lines. The steeper slope indicates the granular packing is more compressible.

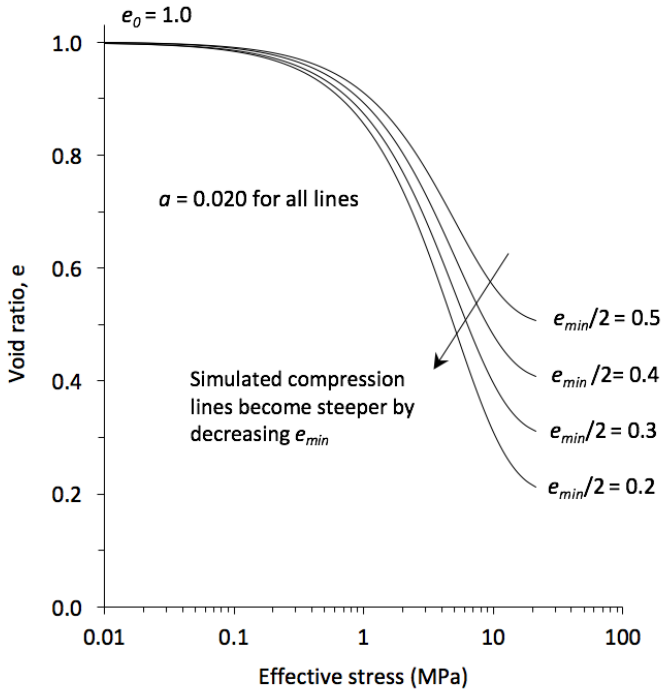

Figure 37. Effect of e_{min} on the calculated compression lines.

3.6. Performance of the proposed model

With prior knowledge of the minimum void ratio for the material as one of the two model parameters, the other material constant, a, can be obtained by best-fitting Eq. 11 to the compression tests data.

Out of 20 granular soils selected for this study (Table 4), the model predictions for 8 sands are already shown in the previous sections (Figures 5, 7, 10, and 13). The predicted compression lines for the remaining 12 materials are shown in Figure 38 for the stress range of validity of the model. It can be seen from this figure that the proposed model is successful in predicting the compression lines of granular soils with different initial void ratios and various particle mineralogy for wide ranges of stress.

For all of the granular soils selected in this study (Table 2), the predicted void ratios are compared with the measured values in Figure 39. The coefficient of determination is 0.997, which proves the suitability of the proposed model to predict the void ratio of different types of granular soils under compression loading.

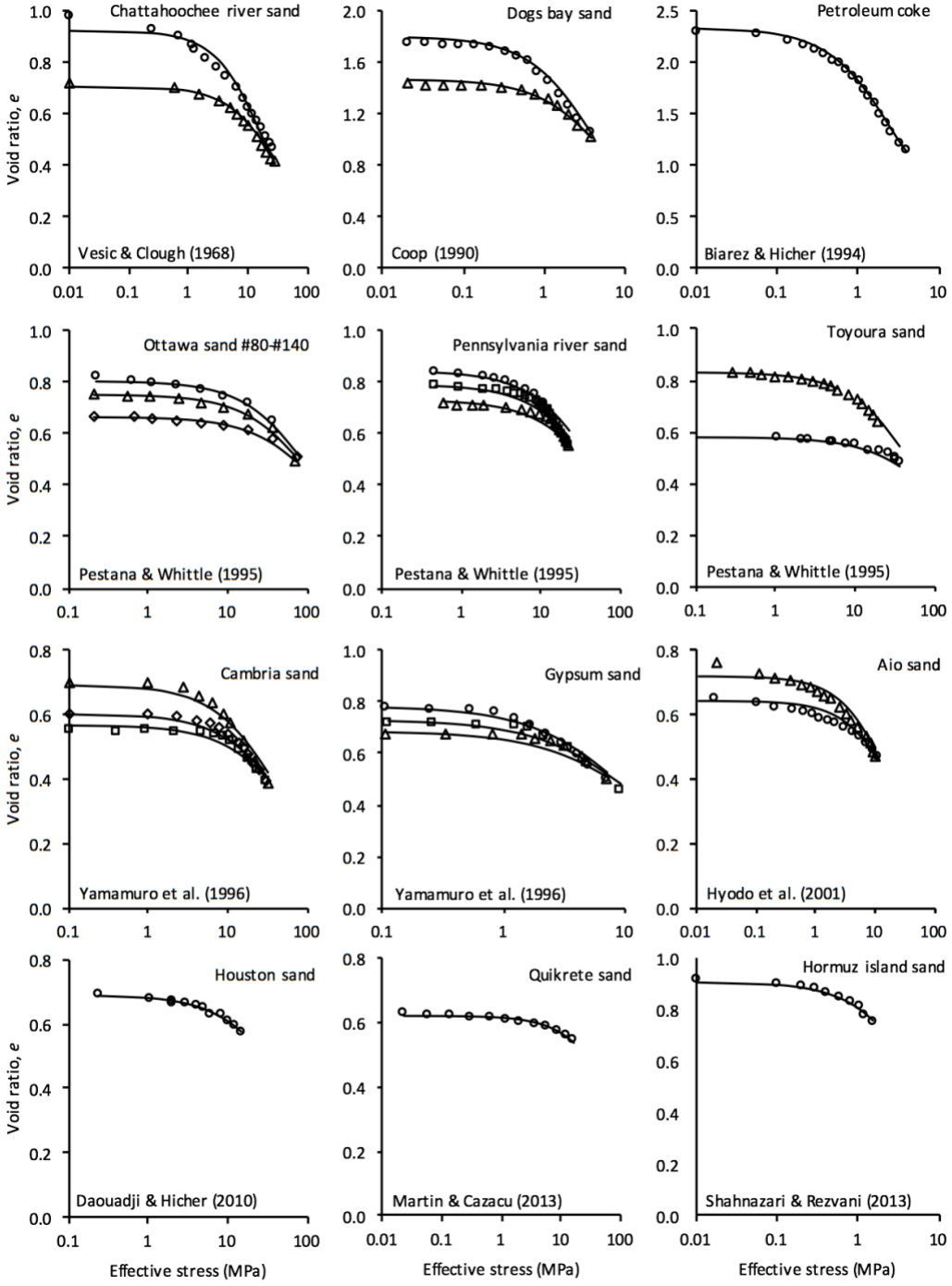

Figure 38. Predicted compression lines using Eq. 11 and the tests data for twelve different types of granular soils [the source of tests data is indicated on each graph].

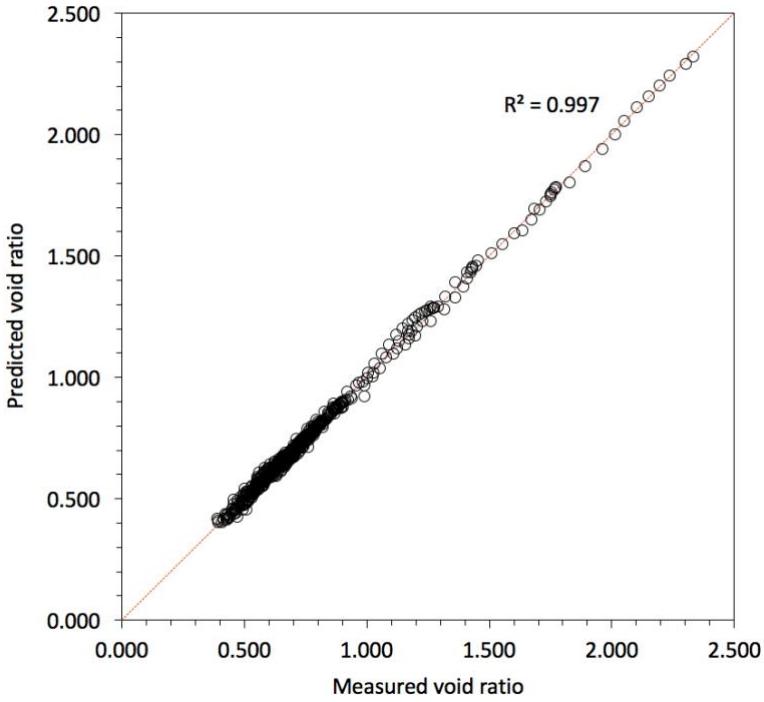

Figure 39. Predicted vs. measured void ratios for all sands used in this study.

3.7. Compression index (Cc)

In this section, a closed-form solution for compression index is derived from Eq. 11. Compression index (C_c) is defined as the tangent slope of the compression curve in $(e, \log_{10} p')$ space. Since the slope of compression curve changes continuously during loading, compression index is defined as a function of stress.

Taking derivative of Eq. 11 with respect to $\log_{10} p'$ gives:

$$C_c(p') = -\frac{\mathrm{d}e(p', e_0)}{\mathrm{d}(\log_{10} p')} = 2.3\left(\frac{ae_0}{p_a}\right)\left[e_0 - \frac{e_{min}}{2}\right] p' \exp\left(-\frac{ae_0}{p_a} p'\right) \quad (12)$$

For the range of validity of the proposed model, the predicted C_c values for five sands are shown in Figure 40 by solid lines, and compared with the slope of compression lines manually determined from the tests data. The general trend shows an increase in the compression index with increasing effective stress. This trend was also shown by Mesri and Vardhanabhuti (2009) and Wu et al. (2016) for several types of sand. The C_c values

calculated from Eq. 12 match the measured values, within the range of validity of the proposed model.

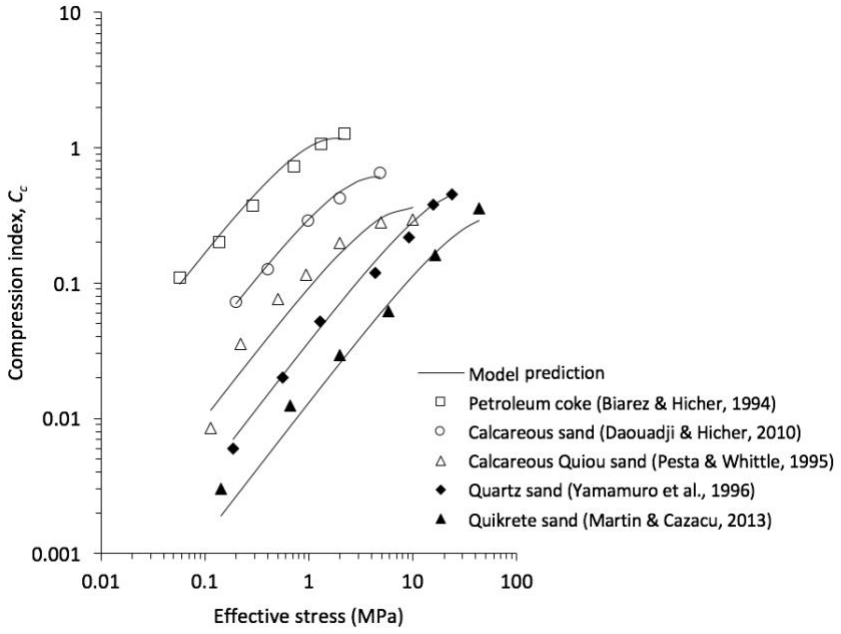

Figure 40. Compression indices predicted by the model compared with the observed values for five different sands.

3.8. Conclusions

Aristotle wrote in his *Posterior Analytics*: "We may assume the superiority of the demonstration which derives from fewer postulates or hypotheses." (McKeon, 1963).

In this chapter, a simple postulate of dividing the voids in a granular material into two hypothetical fractions was examined. This postulate was confirmed by showing that a linear relationship between $\frac{\mathrm{d}e}{\mathrm{d}p'}$ and e exists for several granular soils up to certain stress levels. Based on this postulation, we developed a two-parameter mathematical model to predict the void ratio of granular soils during compression.

The proposed model has these features: (1) it has only two parameters, one of which is the minimum void ratio of the soil, and the other is a material constant determined

from compression tests, (2) the proposed model can predict the compression lines of granular soils with different types of particle mineralogy, (3) the proposed model explicitly considers the initial void ratio of the soil, and (4) the proposed model implicitly considers the effect of particle crushing in its stress range of validity.

For a wide range of stresses (e.g. p'< 40 MPa for quartz-based sands; p'< 8 MPa for Calcium-based sands), we verified the performance of the proposed model by comparing the predicted void ratios with the compression tests data for 20 different types of granular soil. The comparison shows a very good agreement within a wide range of stresses, therefore proves the suitability of our model for predicting the void ratio of different granular soils under isotropic and 1-D compression loading.

Table 3. Comparison of compression models for granular soils (data from Pestana and Whittle, 1995; Vallejos, 2008; Chong and Santamarina,2016)

Explicit mathematical form for void ratio (e) or volumetric strain (ε_v)	Number of parameters	Single continuous form	Unique set of parameters regardless of e_0	Does not need yield stress as an input	Comments	Reference
$e = e_{ref} - C_c \log\left(\frac{p'}{p'_{ref}}\right)$	2	Yes	No	Yes	Void ratio becomes infinitely large at the low stresses, and becomes negative at very high stresses.	Terzaghi and Peck (1948) Schofield and Wroth (1968)
$e = e_H + (e_L - e_H)\left(\frac{p' + p'_c}{p'_c}\right)^{-\beta}$	3	Yes	No	No	p'_c is the characteristics effective stress at which $e = (e_L + e_H)/2$, provided $\beta = 1$.	Butterfield (1979) Juárez-Badillo (1981)
$\frac{1}{e} = \frac{1}{e_0} + \frac{1}{S_{1D}}\left(\frac{p'_v}{p_{atm}}\right)^n$	6-7	No	Yes	No	S_{1D} is a conditional function, based on whether the applied stress is lower or higher than the yield stress.	Hardin (1987)
$e = e_0 - e_0 \exp\left[-C_1 e_o^{C_2} \frac{p'}{p_{atm}}\right] . \exp\left[-C_3\left(\frac{p'}{p_{atm}}\right)^{\alpha}\right]$	4	No	Yes	No	-	Pestana and Whittle (1995)
$\varepsilon_v = \frac{C_1(p/p_r)}{1 + C_2(p/p_r)}$	2	No	No	No	The model parameters need to be calibrated for different stress levels	Qubain et al. (2003)
$e = \left(e_0 - \frac{e_{min}}{2}\right) \exp\left(\frac{-a e_0}{p_{\text{atm}}} p'\right) + \frac{e_{min}}{2}$	1-2*	Yes	Yes	Yes	*If e_{min} is considered an intrinsic material property, then the only parameter needs to be calibrated is *a*.	This paper

Note: The material constants shown by C_1, C_2, C_3 can also be a function containing material constants. p_{atm} is the reference atmospheric pressure.

Table 4. Properties of selected sands for this study to evaluate the performance of the new model.

Granular Material	Test Type*	D_{50} (mm)	D_{60}/D_{10}	Particle Shape†	Mineralogy‡	e_{min}	e_{max}	Model parameters			Reference
								a§ ($\times 10^{-3}$)	e_r§	Range of Validity¶ (MPa)	
Wabash River sand	1-D	0.56	3.0	sR-sA	Q	0.43	0.69	3.2	0.24	25¶	Hendron (1963)
Sacramento River sand	Iso	0.22	1.5	sA-sR	Q	0.61	1.03	5.3	0.28	15¶	Lee and Seed (1967)
Chattahoochee River sand	Iso	0.37	2.5	sA	Q	0.61	1.10	6.9	0.32	40	Vesic and Clough (1968)
Biogenic carbonate sand#	Iso	0.20	2.4	R	Ca	1.37	1.84	16.5	0.70	4	Coop (1990)
Petroleum coke	1-D	-	1.4	R	C	-	-	24.0	0.95	4	Biarez and Hicher (1994)
Toyoura sand	Iso	0.20	1.7	sA	Q	0.61	0.97	2.5	0.29	40	Pestana and Whittle (1995)
Calcareous Quiou sand	1-D	0.70	4.5	A	Ca	0.78	1.20	13.0	0.37	10	ditto
Pennsylvania River sand	1-D	1.28	1.5	A	Q	0.60	0.88	3.1	0.31	24¶	ditto
Ottawa sand No. 80-140	1-D	0.14	1.5	sR	Q	0.63	0.83	1.4	0.34	40	ditto
Quartz sand	1-D	1.15	uniform	A	Q	0.66	1.07	3.6	0.35	40	Yamamuro et al. (1996)
Cambria sand	1-D	1.42	uniform	R	Q	0.49	0.78	4.4	0.25	40	ditto
Gypsum sand	1-D	0.63	uniform	-	Ca	0.70	0.97	14.7	0.33	10	ditto
Shirasu sand	Iso	0.37	3.4	-	V	1.03	1.55	13.1	0.52	5	Hyodo et al. (2001)
Aio sand	Iso	0.41	3.4	sA-A	Q	0.58	0.96	10.0	0.28	10¶	ditto
Nevada sand	Iso	0.18	2.3	sA-sR	Q	0.57	0.86	7.4	0.29	2¶	Lade and Abelev (2005)
Sydney sand	Iso	0.30	1.5	A	Q	0.57	0.86	8.0	0.30	1.2¶	Bobei et al. (2009)
Calcareous sand	Iso	0.17	2.8	R	Ca	1.01	1.67	17.7	0.49	10	Daouadji and Hicher (2009)
Houston sand	Iso	0.32	1.7	A	Q	0.66	1.00	3.6	0.31	15¶	ditto
Quikrete sand	Iso	0.32	-	A	Q	0.51	0.80	2.8	0.28	40	Martin and Cazacu (2013)
Hormuz Island sand	Iso	0.78	4.5	A	Ca	0.63	0.91	20.5	0.30	1.5¶	Shahnazari and Rezvani (2013)

*Iso=isotropic compression test; 1-D=one dimensional compression test
†A=angular; R=round; sA=subangular; sR=subround
‡Q=siliceous (quartz); Ca=calcareous; C=carbonaceous; V=volcanic ash (siliceous)
§Parameter a is dimensionless; Parameter e_r was initially used in the model, and finally replaced by $e_{min}/2$ in Eq. 11.
¶The compression test data was available up to this stress level.
#Also, known as Dogs Bay sand.

CHAPTER 4

A COMPRESSION MODEL FOR SAND-SILT MIXTURES BASED ON THE CONCEPT OF ACTIVE AND INACTIVE VOIDS[4]

4.1. Introduction

Sand-silt mixtures are abundant in Nature as well as in the man-made structures such as levees and embankments. Understanding the mechanical behavior of these materials is essential to the engineers to predict their deformation behavior and strength characteristics under different loading scenarios.

It has been shown by many researchers that the fines content has very important effects on different aspects of the mechanical behavior of sand-silt mixtures (e.g. Benahmed et al., 2015; Chen et al., 2016, Choo and Burns, 2015, Rees, 2010). Several experimental work have shown the effect of fines content on the compression behavior of sand-silt mixtures (e.g. Cabalar, 2010, Dash, 2010, Zlatovich, 1995).

A compression model for sand-silt mixture that accounts for the effect of fines content is needed in different applications of geotechnical engineering, for example in studying the mechanics of internal erosion, as was shown by Chang and Meidani (2012) and Hicher (2013). It is essential to have a compression model for sand-silt mixtures that explicitly considers the amount of fines, to be able to simulate the effects of loss of fines

[4] This chapter is published as a standalone paper in Acta Geotechnica (2017) with the same title. https://doi.org/10.1007/s11440-017-0598-1

on the overall deformation behavior and strength characteristics of the eroded soil.

To date, there is no compression model for sand-silt mixtures that explicitly considers the fines content as a variable in its formulation. The conventional compression models for granular materials consider factors such as initial void ratio, applied effective stress, and particles minerology (e.g. Coop and Atkinson, 1993; Meidani et al., 2017; Pestana and Whittle, 1995; Russel and Khalili, 2004). The material constants in these conventional models need to be calibrated for each mixture with a particular fines content.

In this chapter, a mathematical model is developed to predict the compressibility of sand-silt mixtures by explicitly considering its fines content as an input variable. To do so, the concept of dividing the voids in a granular packing into two hypothetical fractions, named active and inactive voids in further extended. Instead of treating compressibility as a function of stress level, the relationship between compressibility and the density state is studied. Based on the experimental evidence from compression tests on various sand-silt mixtures, a linear relationship between the material compressibility and its density state is identified. It is shown that the linear relationship is valid up to stress levels at which the effect of particle breakage is not prominent, however, there are limited particle crushing effects that are implicitly embedded in this linear relationship.

This linear relationship is expressed in the form of a differential equation. After integration, a mathematical model for the compressibility of sand-silt mixtures is derived. The two hypothetical fractions, i.e. active and inactive void ratios, are identified in the derived mathematical relationship. We show that active void ratio diminishes with an exponential rate with respect to the stress level. It is also shown that the inactive void

ratio can be expressed as an explicit function of fines content. Finally, the proposed model is verified by comparing the predicted void ratios with the measured data for six different types of sand-silt mixtures with various amounts of fines, and different mineralogy.

4.2. Active and inactive voids in granular materials

For convenience in the modeling process, the voids in a granular packing can be divided into two hypothetical fractions: (1) active voids, and (2) inactive voids. The traditional phase diagram for a granular material is shown in Figure 41a. The active and inactive voids are separated in another phase diagram shown in Figure 41b.

The compression of solid particles is negligible for the stress levels considered in this study. Therefore, we can divide the volumes of active and inactive voids by the total volume of solids V_s and define active void ratio e_{active} and inactive void ratio $e_{inactive}$, respectively (Figure 41). The total void ratio (e) of a soil at any stress level is the sum of e_{active} and $e_{inactive}$.

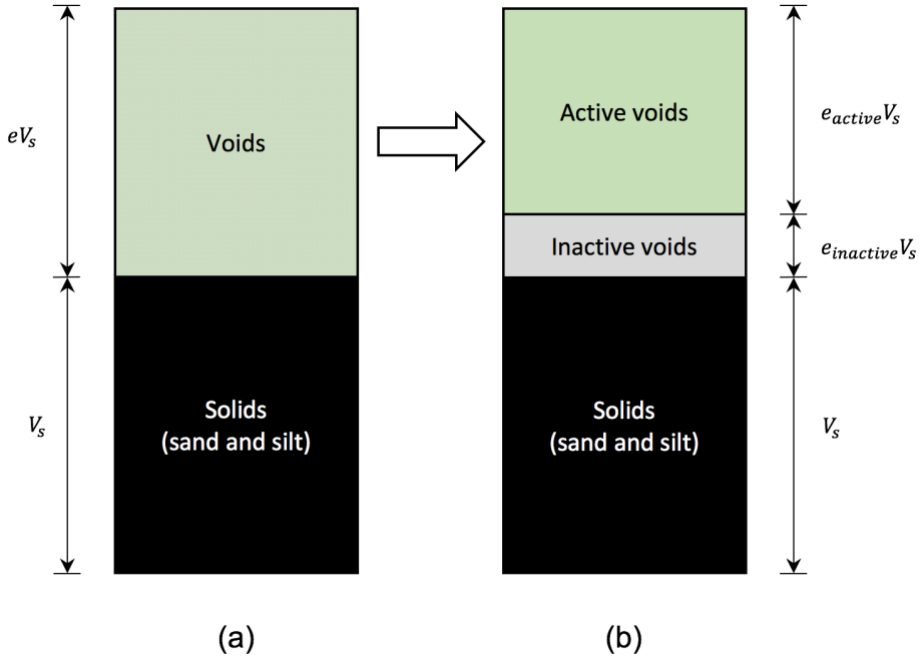

Figure 41. (a) The traditional phase diagram for a granular material; (b) separating the voids into two hypothetical fractions: active voids and inactive voids.

The active voids is defined such that this hypothetical fraction of total voids is kinematically diminishable during compression due to particles rearrangement, i.e. particle sliding and rotation (Figure 42). On the other hand, inactive voids are kinematically unavailable to be diminished by particles rearrangement. The volume of inactive voids is dependent on the particle size distribution (PSD) and particles shapes. These two dictate the densest kinematic limit of a granular packing as described in details by Meidani et al. (2017). PSD and particle shape can be changed by particles breakage, particles bonding, or particles loss (e.g. dissolving or erosion). Varying the fines content in a sand-silt mixture also changes the PSD of the soil (Figure 42).

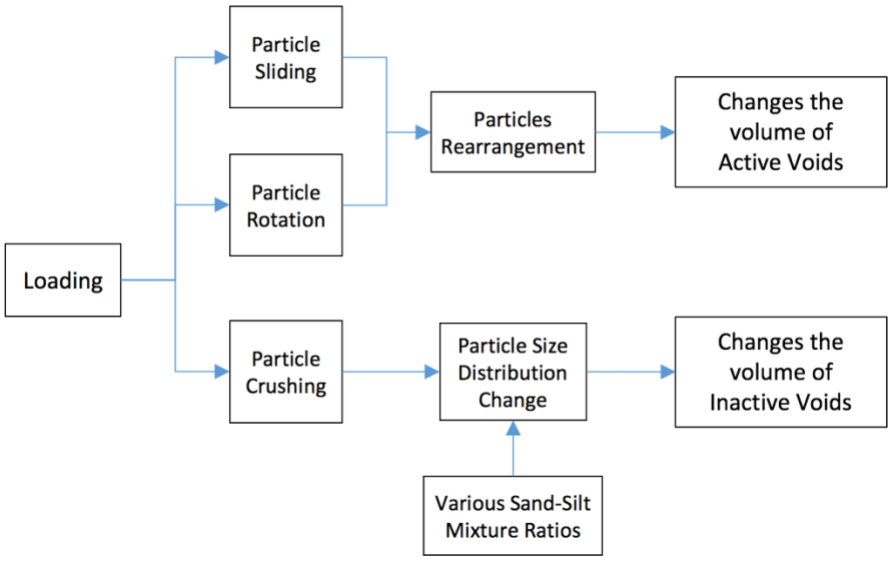

Figure 42. Causes and mechanisms that change the volumes of active and inactive voids in a sand-silt mixture.

A desirable compression model for sand-silt mixtures with a given fines content (f_c) can be written in a following general form as:

$$e(p', e_0, f_c) = e_{active}(p', e_0, f_c) + e_{inactive}(p', f_c) \quad (1)^5$$

where e is the total void ratio of the mixture, p' is the effective stress, and e_0 is the initial void ratio of the mixture. f_c is the fines content in the mixture and defined as the dry mass of fines in the mixture divided by the total dry mass of the mixture. Eq. (1) shows the simple postulate that we want to examine its applicability in this study.

In the next section, a mathematical relationship for the compression of sand-silt mixtures is derived. We show that active voids diminish with an exponential rate with respect to the effective stress and initial density of the mixture. We also show that the

[5] Equation numbers restart from 1 in this chapter to avoid long digits.

inactive void ratio is a function of the fines content, which will be related to the minimum void ratio of the mixture. The inactive void ratio will be shown to be independent of the stress magnitude up to certain levels. We will show that the effects of particle crushing in the range of validity of the proposed model are implicitly carried into the function that defines the evolution of active void ratio.

4.3. Derivation of the compression model

Meidani et al. (2017) showed an approximate linear relationship can be identified between $\frac{\mathrm{d}e}{\mathrm{d}p'}$ and e, based on the compression test data from 20 different types of granular soils. The results of compression tests on a typical quartz sand is shown in Figure 43. Determined from compression test data, it can be seen that the approximate linear relationship is valid up to certain stress level, for example 40 MPa for most quartz sands and 10 MPa for most Calcium-based sands. It is clear that some particle breakage occurs in quartz sand prior to 40 MPa due to compression. Hence, the effects of particle breakage on the change of void ratio are implicitly included in the linear relationship between $\frac{\mathrm{d}e}{\mathrm{d}p'}$ and e up to certain stress levels.

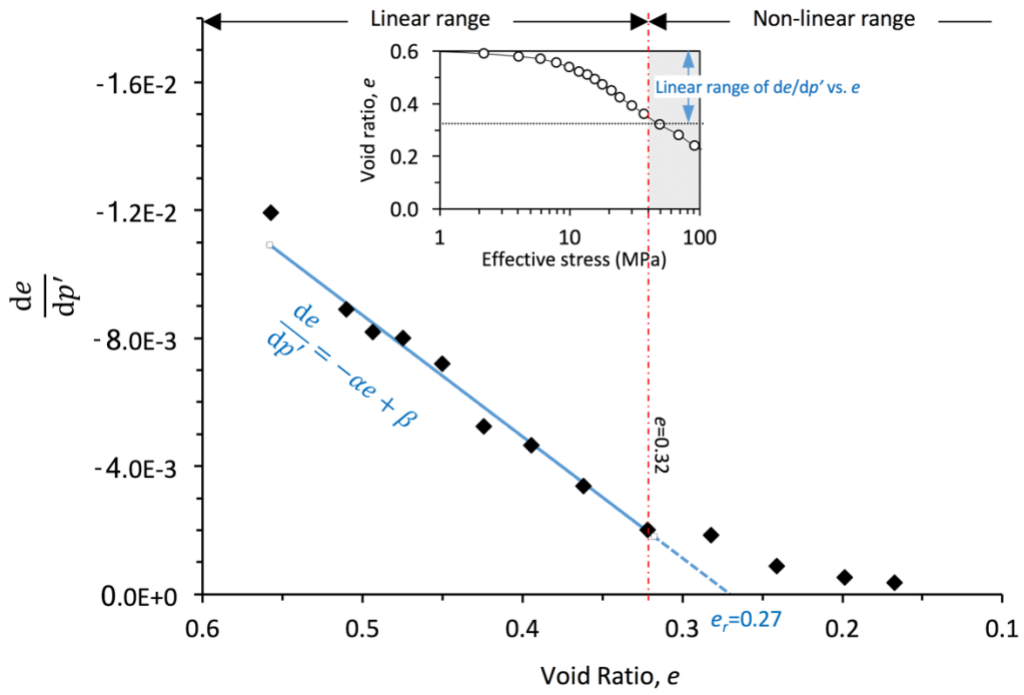

Figure 43. $\frac{\mathrm{d}e}{\mathrm{d}p'}$ plotted versus void ratio e. Data from compression tests on Cambria sand.

We apply the similar concept to the compression of sand-silt mixtures. We select compression tests data on specimens made of Hukksond sand & Chengbei silt with various amounts of fines contents, ranging from 0% to 94% (Table 1) to check the validity of this concept in sand-silt mixtures. After normalizing all applied stresses to the reference atmospheric pressure and defining the normalized effective pressure as $p'_* = p'/p_{\mathrm{atm}}$, where p_{atm}= 0.101325 MPa, the values of $\mathrm{d}e/\mathrm{d}p'_*$ versus e are plotted in Figure 44 for all fines contents.

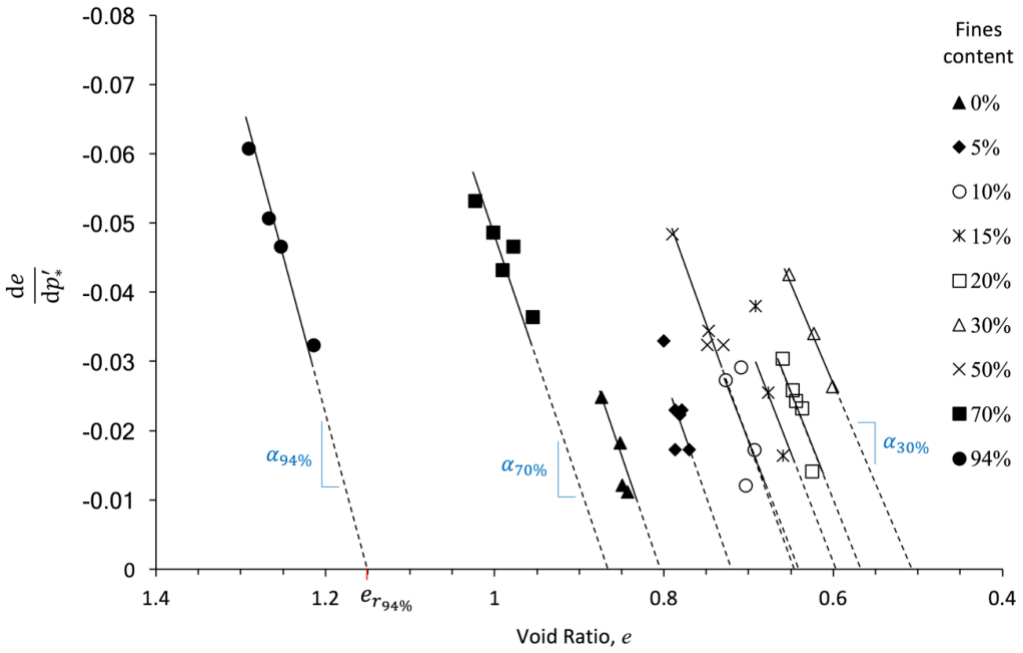

Figure 44. $\frac{de}{dp'_*}$ plotted versus void ratio for mixtures of Hukksond sand & Chengbei silt with various fines contents. The solids lines are the best-fit linear approximation to the tests data with a given fines content. The slopes of three lines from the specimens with 30, 70, and 94% fines content are shown as $\alpha_{30\%}$, $\alpha_{70\%}$, and $\alpha_{94\%}$. The x-intercept of the trend-line for the mixtures with 94% fines content is shown as $e_{r_{94\%}}$.

Linear correlations can be identified among the data points with a given fines content. For instance, the tests results from the mixtures with 70% fines content are shown with solid squares in Figure 44. A line is fitted to these data points. The same procedure is done for all other fines contents. The trend-lines have different slopes and different intercepts. In a general form, these lines can be expressed by the following relationship:

$$\left(\frac{de}{dp'_*}\right)_{f_c} = -\alpha_{f_c} e + \beta_{f_c} \qquad (2)$$

where f_c designates the fines content of the specimen. α_{f_c} and β_{f_c} are the slopes and y-intercepts of the lines, respectively.

Eq. (2) can also be written in the following form:

$$\left(\frac{\mathrm{d}e}{\mathrm{d}p'_*}\right)_{f_c} = -\alpha_{f_c}\left(e - \frac{\beta_{f_c}}{\alpha_{f_c}}\right) = -\alpha_{f_c}\left(e - e_{r_{f_c}}\right) \quad (3)$$

In this equation, $e_{r_{f_c}}$ is equal to β_{f_c}/α_{f_c}, which is the x-intercept of the trend-line for specimens with fines content f_c, as shown in Figure 44. As the void ratio decreases under compression, $\left(\frac{\mathrm{d}e}{\mathrm{d}p'_*}\right)_{f_c}$ decreases linearly. When the void ratio reaches $e_{r_{f_c}}$, $\left(\frac{\mathrm{d}e}{\mathrm{d}p'_*}\right)_{f_c} = 0$, which means that the void ratio will not decrease anymore. According to our postulate, this is when all kinematically available voids are diminished due to particles rearrangement. The remaining voids, $e = e_{r_{f_c}}$, are no longer compressible, as they are kinematically unavailable to the compression process. We name $e_{r_{f_c}}$, representative inactive void ratio. The reason we do not simply call this variable inactive void ratio is that the approximate linear correlation between $\frac{\mathrm{d}e}{\mathrm{d}p'_*}$ and e is only valid up to certain stress levels (Figure 43). So, the x-intercept ($e_{r_{f_c}}$) only represents the compression behavior up to certain stress levels.

Taken from Figure 44, we plot the slopes of the fitted lines α_{f_c} versus the initial void ratios of various specimens made of Hukksond sand and Chengbei silt (Figure 45). A correlation can be found between α_{f_c} and e_0, which is be expressed as:

$$\alpha_{f_c} = \hat{a}_{f_c} e_0 \quad (4)$$

where $\hat{a}_{f_c}$ is a material parameter and e_0 is the initial void ratio of each specimen. As shown in Figure 45, the parameter $\hat{a}_{f_c}$ is approximately 0.4 for all fines contents in this mixture. Therefore, we drop the subscript f_c from $\hat{a}_{f_c}$, and rewrite Eq. 4 as:

$$\alpha_{f_c} = \hat{a} e_0 \quad (5)$$

where $\hat{a}$ is a material parameter. In the case of Hukksond sand and Chengbei silt mixtures, this parameter is 0.4. Even though the proposed linear relationship in Eq. 5 is approximate, we show later that it causes a very small error in void ratio predictions.

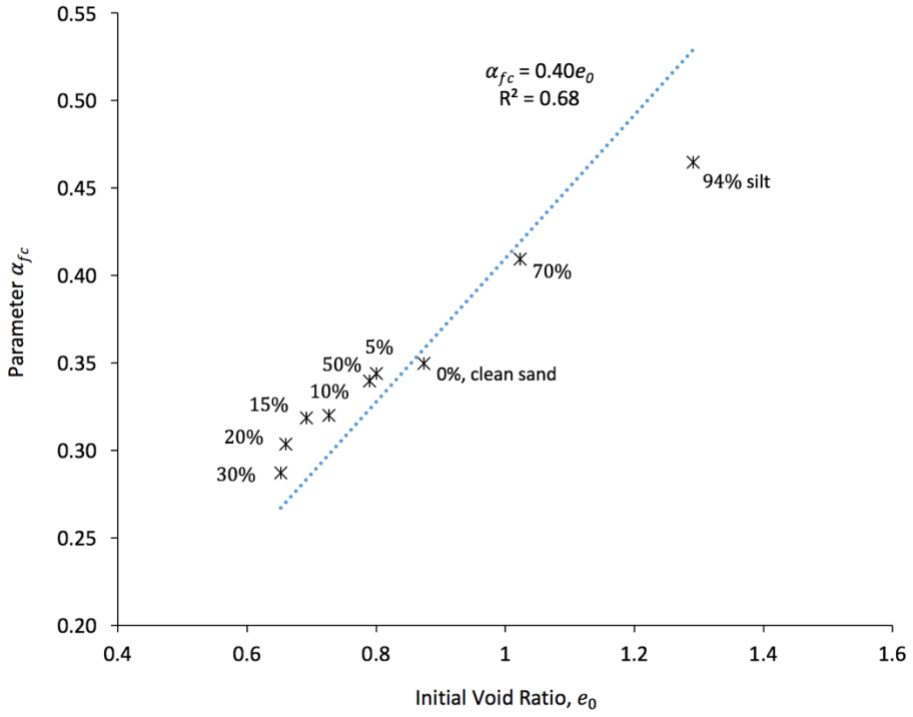

Figure 45. Linear correlation between the slopes of trend-lines (shown in Figure 44) and the initial void ratios of specimens for the mixtures of Hukksond sand & Chengbei silt with various amounts of fines.

Replacing Eq. 5 into Eq. 3 gives:

$$\left(\frac{\mathrm{d}e}{\mathrm{d}p'_*}\right)_{f_c} = -\hat{a}e_0\left(e - e_{r_{f_c}}\right) \tag{6}$$

or, if e_0 is moved to the left side of Eq. 6, we have:

$$\frac{1}{e_0}\left(\frac{\mathrm{d}e}{\mathrm{d}p'_*}\right)_{f_c} = -\hat{a}\left(e - e_{r_{f_c}}\right) \tag{7}$$

which means that if the values of $\mathrm{d}e/\mathrm{d}p'_*$ are divided by the initial void ratio of each specimen, and plotted versus the void ratio, the result will be a group of parallel lines that

has a slope equal to $\hat{a}$ and different x-intercepts equal to $e_{r_{f_c}}$. The intercepts vary with the fines content of the specimen, as shown in Figure 46. The general relationship for these parallel lines is Eq. 7.

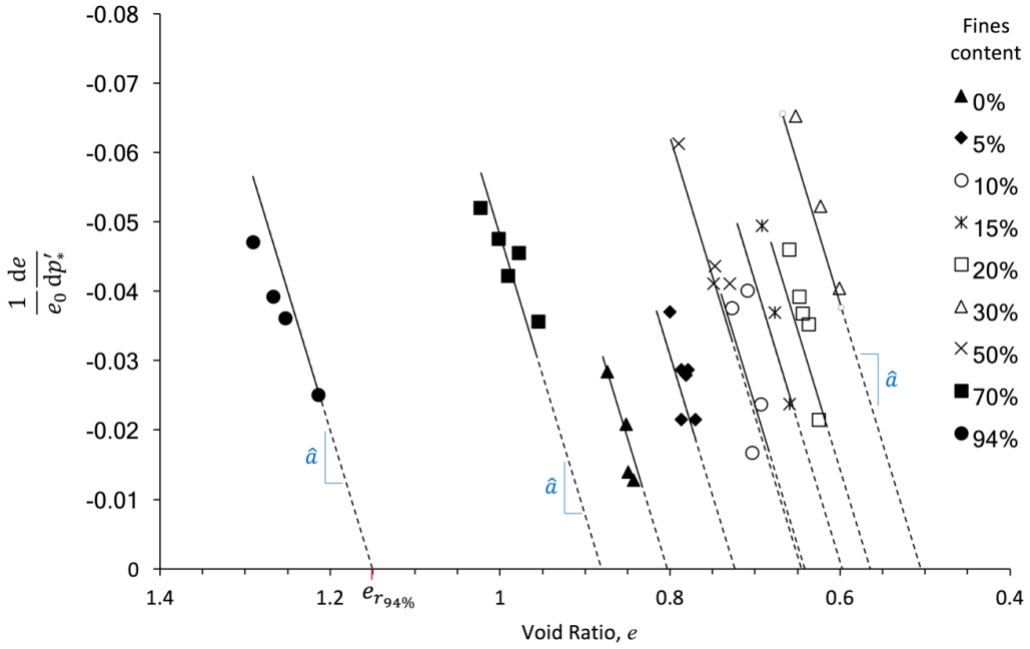

Figure 46. $\frac{1}{e_0}\frac{de}{dp'_*}$ plotted versus void ratio, e for mixtures of Hukksond sand & Chengbei silt with various fines contents. The slopes of three lines from the specimens with 30, 70, and 94% fines content are shown as $\hat{a}$. The x-intercept of the trend-line for the mixtures with 94% fines content is shown as $e_{r_{94\%}}$.

In order to derive the mathematical relationship for the compression model, we reorganize Eq. 7 as:

$$\frac{de}{e-e_{r_{f_c}}} = -\frac{\hat{a}e_0}{p_{\text{atm}}}dp' \tag{8}$$

recalling that $dp'_* = \frac{dp'}{p_{\text{atm}}}$. This relationship can be integrated over the variables e and p' for a constant $e_{r_{f_c}}$ as follows:

$$\int_{e_0}^{e}\left(\frac{\mathrm{d}e}{e-e_{r_{f_c}}}\right)=-\frac{\hat{a}e_0}{p_{\mathrm{atm}}}\int_0^{p'}\mathrm{d}p' \tag{9}$$

where the upper integral limit, e is the void ratio at the target stress p'. For a given fines content, $e_{r_{f_c}}$ is treated as a constant in integration (Figure 46).

Integration of Eq. 9 leads to the following form, which expresses the void ratio as a function of applied stress p', initial void ratio e_0, and representative inactive void ratio $e_{r_{f_c}}$:

$$e(p',e_0,f_c)=\left[e_0-e_{r_{f_c}}\right]\exp\left(-\frac{\hat{a}e_0}{p_{atm}}p'\right)+e_{r_{f_c}} \tag{10}$$

Through analogy of the terms between Eq. 10 and Eq. 1, we can identify the active and inactive void ratios as follows:

$$e_{active}(p',e_0,f_c)=\left[e_0-e_{r_{f_c}}\right]\exp\left(-\frac{\hat{a}e_0}{p_{atm}}p'\right) \tag{11}$$

$$e_{inactive}(p',f_c)=e_{r_{f_c}} \tag{12}$$

The graphical representation of Eq. (9) for a given fines content is shown in Figure 47.

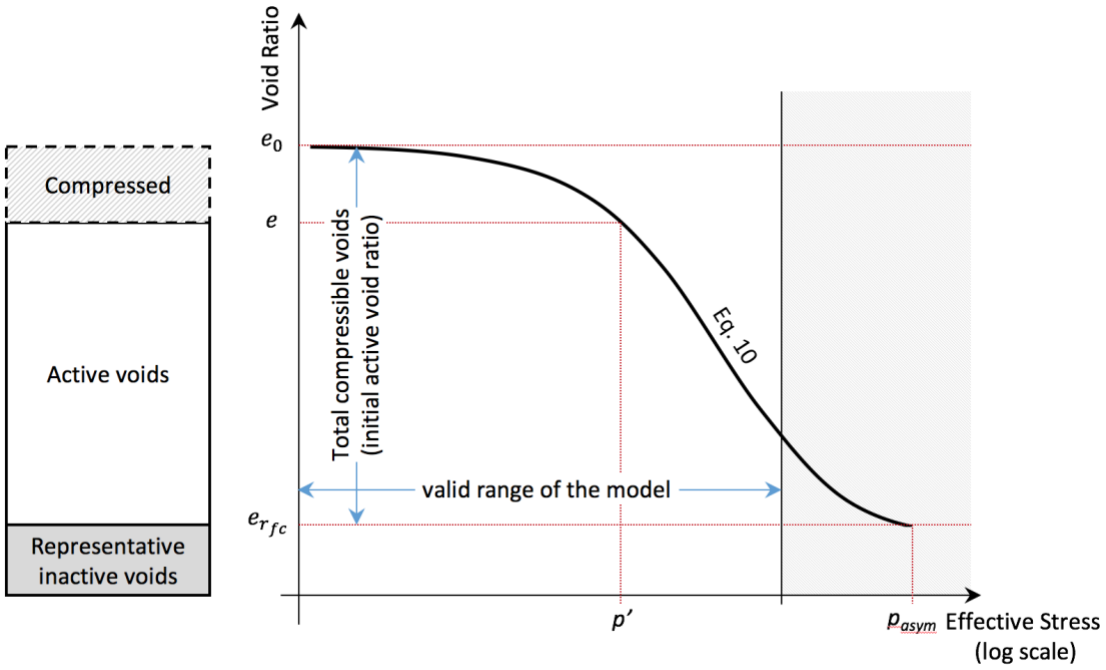

Figure 47. Graphical representation of Eq. 10, showing the evolution of void ratio during compression.

Figure 48 shows the evolution of voids volume during compression in three-phase diagrams for a mixture with a given fines content. Since the volume of the representative inactive voids do not change during loading (Eq. 12) and the volume of solids remains constant, all the volume change is attributed to the change of active voids (Eq. 11).

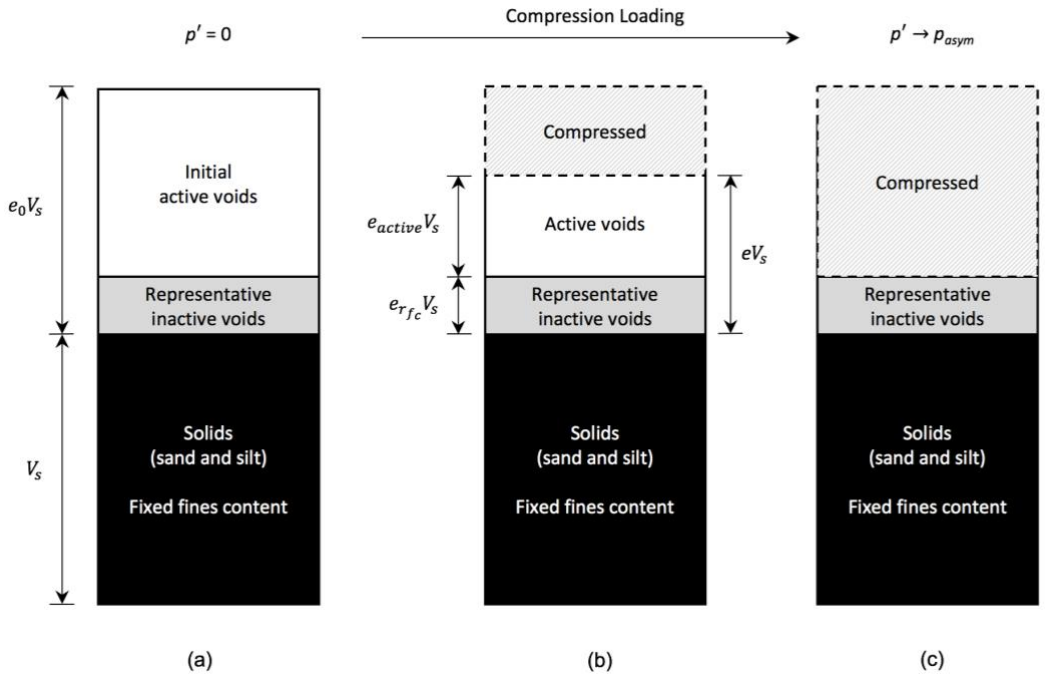

Figure 48. Three phase diagrams showing the evolution of active voids for a sand-silt mixture with a given fines content, while the volume of representative inactive voids and solids remains constant during loading.

4.3.1. Morphology of the model

The effect of variation of model parameters $e_{r_{f_c}}$ and $\hat{a}$ on the calculated compression lines are shown in Figure 49. It can be seen that decreasing parameter $e_{r_{f_c}}$, increases the slope of compression lines, depicting a more compressible material, while increasing $\hat{a}$ does not have a significant effect on the slope of compression lines, but shifts the calculated compression lines to the left, depicting a reduction in the yield stress of the material.

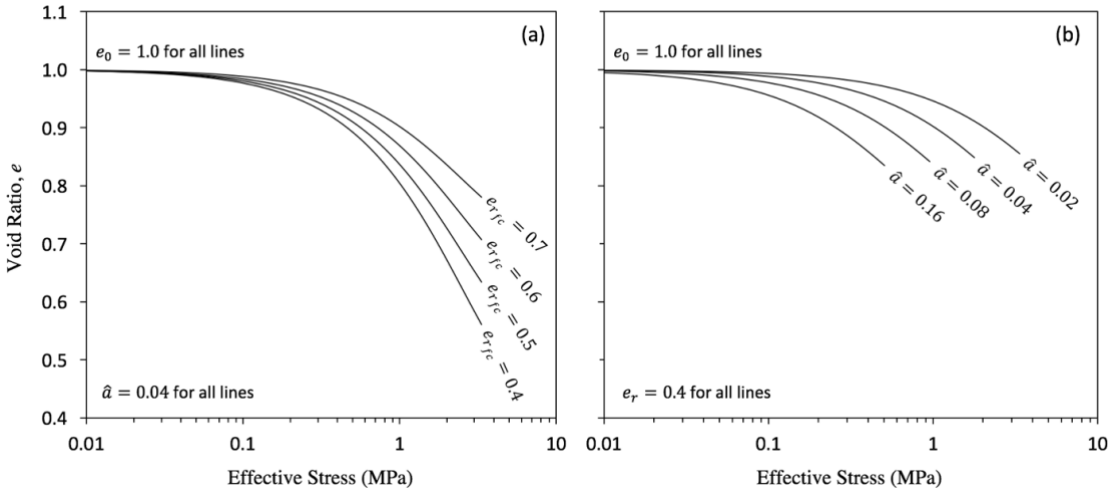

Figure 49. Effect of variation of model parameters (a) $e_{r_{f_c}}$ and (b) $\hat{a}$ on the calculated compression lines from Eq. 10.

4.3.2. Determination of model parameters for the selected sand-silt mixtures

In order to determine the model parameters $\hat{a}$ and $e_{r_{f_c}}$ for the selected sand-silt mixtures (Table 5), we construct $\frac{1}{e_0}\frac{\mathrm{d}e}{\mathrm{d}p'_*}$ versus e graphs similar to Figure 46 for each type of mixture. Five of the mixtures are made from quartz sand and quartz silt with various fines contents. The $\frac{1}{e_0}\frac{\mathrm{d}e}{\mathrm{d}p'_*}$ versus e graphs showed that for each type of mixture, all trend-lines correlated to the compression tests data performed on specimens with various fines contents have the same slope ($\hat{a}$). The determined $\hat{a}$ values for these five types of mixtures are reported in Table 5. The sixth type of mixture, tested by Cabalar (2010), is made of quartz sand and mica fines. When $\frac{1}{e_0}\frac{\mathrm{d}e}{\mathrm{d}p'_*}$ versus e graph for Cabalar's data was constructed, the trend-lines did not seem to be parallel to each other in contrast to the other five types of mixtures. We attribute this difference to the high crushability of mica particles compared with the quartz particles. The determined slopes of trend-lines (i.e. $\hat{a}$) for these mixtures are shown in Figure 50 for various fines contents.

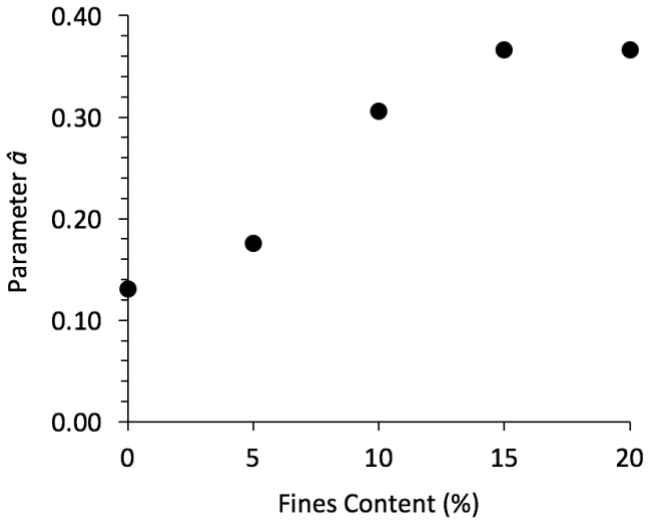

Figure 50. Parameter $\hat{a}$, i.e. slope of trend-lines in $\frac{1}{e_0}\frac{\mathrm{d}e}{\mathrm{d}p'_*}$ versus e space for the mixture of quartz sand and mica fines.

For the six types of mixtures, the determined $e_{r_{f_c}}$ values from $\frac{1}{e_0}\frac{\mathrm{d}e}{\mathrm{d}p'_*}$ versus e graphs are plotted in Figure 51. For all mixtures, and at each fines content, e_0 is also presented in Figure 51. The distance between e_0 and $e_{r_{f_c}}$ represents the range of active void ratio (i.e. compressible voids) for each mixture.

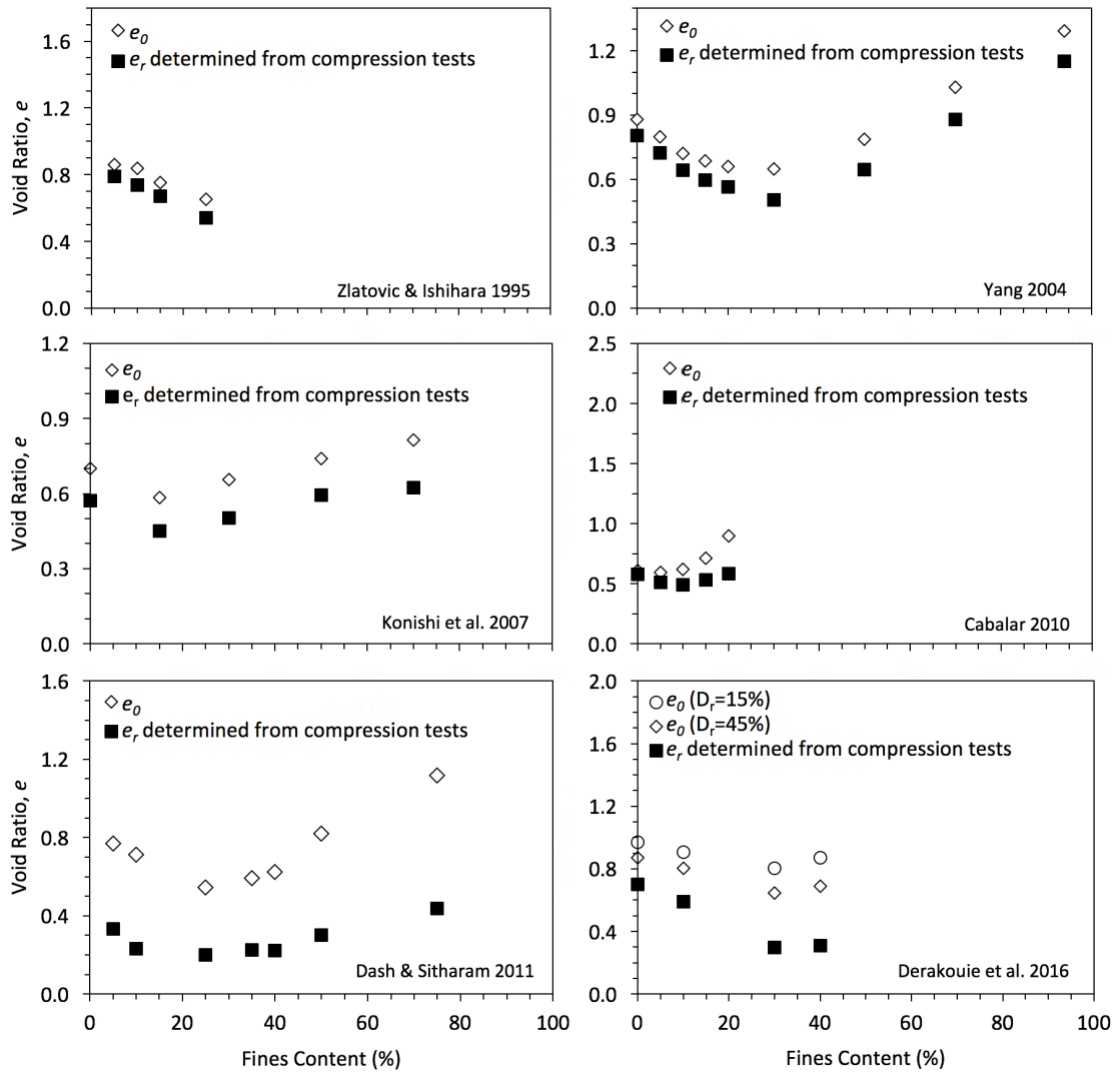

Figure 51. The representative inactive void ratios ($e_{r_{f_c}}$) versus fines content for six different types of sand-silt mixtures. The values of $e_{r_{f_c}}$ are determined from the compression tests data by constructing $\frac{de}{dp'_*}$ vs. e graphs similar to Figure 46.

4.4. Predicting $e_{r_{f_c}}$ as a function of fines content

The schematic trend of $e_{r_{f_c}}$ versus fines content, which is observed in Figure 51 for six different types of sand-silt mixtures is drawn in Figure 52. It can be seen that $e_{r_{f_c}}$ (i.e. kinematically unavailable void ratio) is influenced by the amount of fines in the mixture.

The next step is to find a mathematical relationship between $e_{r_{f_c}}$ and the fines content, so that we can eliminate the need for compression tests at every fines contents and predict $e_{r_{f_c}}$ from fewer experiments.

As the fines content is increased from 0%, $e_{r_{f_c}}$ decreases to a minimum value, then continue to increase after a reversal point. This trend is similar to that observed in the studies for the variation of minimum void ratio of sand-silt mixtures with various amounts of fines. For the minimum void ratio, the specific fines content corresponding to the reversal point is termed threshold fines content by Thevanayagam et al. (2002), transitional fines content by Yang et al. (2006) or limiting fines content by Polito and Martin (2001). This reversal point occurs at transient fine-contents ranging from approximately 20% to 35% for most sand-silt mixtures.

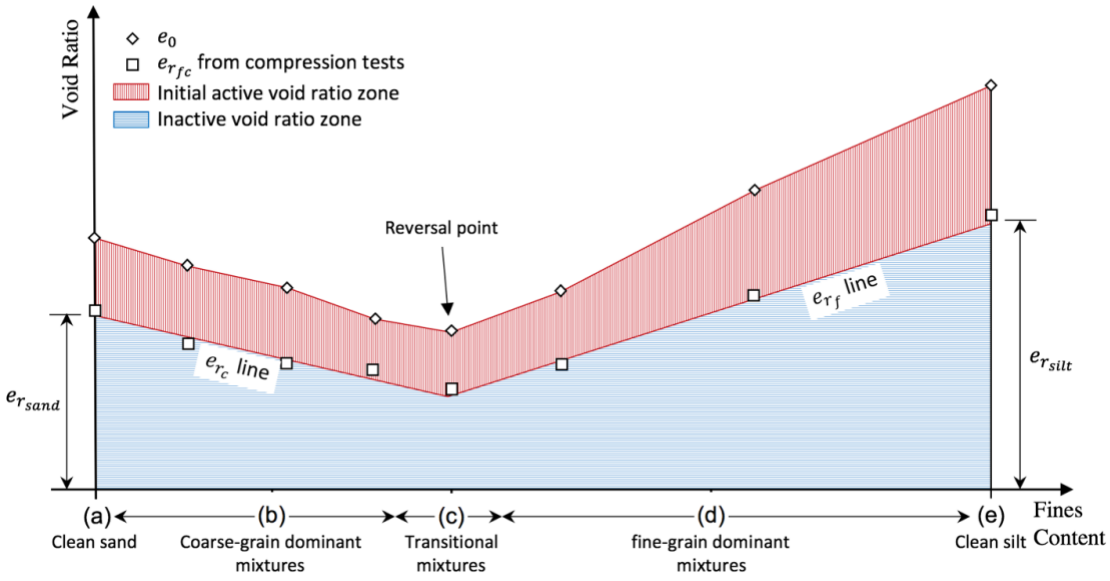

Figure 52. Schematics of variation of active and inactive void ratio for sand-silt mixtures with various amounts of fines.

Intuitively, the theory of mixtures (Bowen, 1976) is the first choice for estimating $e_{r_{f_c}}$ of a mixture from the properties of clean sand and clean silt specimens. We examine the validity of upper and lower bound solutions for predicting the $e_{r_{f_c}}$ from $e_{r_{\text{sand}}}$ and $e_{r_{silt}}$ at various fines contents.

Voigt's upper bound solution for the representative inactive void ratio ($e_{r_{f_c}}$) of a mixture can be expressed as:

$$e_{r_{f_c}} = (1 - f_c) \cdot e_{r_{\text{sand}}} + f_c \cdot e_{r_{silt}} \tag{13}$$

where $e_{r_{sand}}$ and $e_{r_{silt}}$ are the properties of clean sand and clean silt, determined from $\frac{1}{e_0}\frac{\mathrm{d}e}{\mathrm{d}p'_*}$ versus e graphs.

The lower bound solution for $e_{r_{f_c}}$ of a mixture can be calculated from Ruess theory and is given by:

$$\frac{1}{e_{r_{f_c}}} = \frac{(1-f_c)}{e_{r_{sand}}} + \frac{f_c}{e_{r_{silt}}} \tag{14}$$

Figure 53 shows typical measured values of $e_{r_{fc}}$ for sand-silt mixtures with various fines contents (circle symbols). Eqs. 13 and 14 are used to calculate the upper bound (solid line) and lower bound (dashed line) solutions of $e_{r_{fc}}$ for mixtures with $e_{r_{sand}} = 0.5$ and $e_{r_{silt}} = 0.9$. As can be seen in Figure 53, the upper and lower bounds of the mixture theory cannot cover the range of measured $e_{r_{fc}}$ values. The typical measured $e_{r_{fc}}$ values are significantly lower than the Reuss lower bound (Figure 53), although the Voigt's upper bound is not violated in this figure.

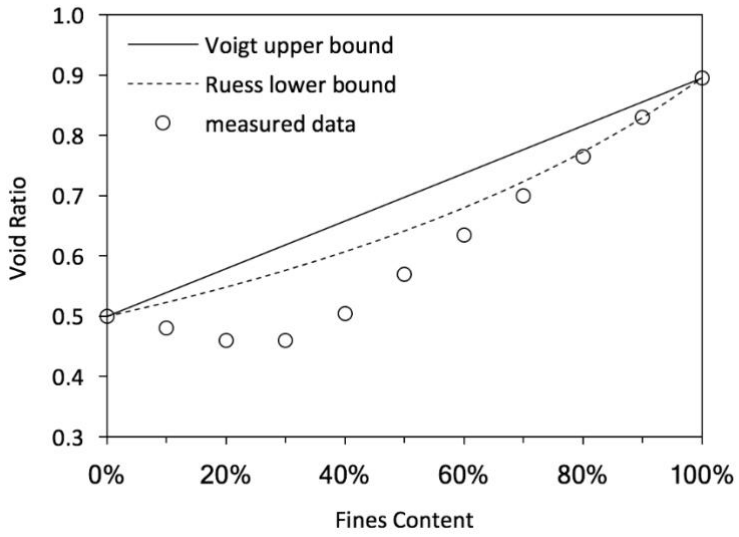

Figure 53. Comparison of the measured data with the upper bound and lower bound from the classic mixture theory.

Previously, Chang and Meidani (2013) showed that the theory of mixtures is not applicable to the variation of minimum void ratio of sand-silt mixtures because this theory does not account for the mixing mechanism of particles; for instance it cannot consider the filling of fines into the voids of the coarse-grains skeleton, or in the other case the embedment of coarse particles into the fine-grains skeleton. Chang and Meidani (2013) proposed a model for the variation of minimum void ratio of sand-silt mixtures, and showed that the same model can also predict the critical state void ratio of such mixture. Chang et al. (2015, 2016) extended the previous model and proposed a new relationship that could predict the minimum and maximum void ratios of such mixtures with a unique set of parameters.

According to Chang et al. (2015), minimum void ratio of sand-silt mixtures can be calculated from the following equations:

$$e_{min_{fc}} = \max\left[e_{min_c}, e_{min_f}\right] \tag{15}$$

where

$$e_{min_c} = e_{min_{sand}}(1 - f_c) + e_{min_{silt}} f_c - \alpha(1 + e_{min_{silt}}) f_c \quad (16)$$

$$e_{min_f} = e_{min_{sand}}(1 - f_c) + e_{min_{silt}} f_c - \beta e_{min_{sand}}(1 - f_c) \quad (17)$$

The subscripts *c* and *f* on the left side of Eqs. 16 and 17 refer to the coarse-grain and fine-grain dominant structures, respectively (Figure 54). The minimum void ratios of clean sand ($e_{min_{sand}}$) and clean silt ($e_{min_{silt}}$) are known a priori. Eqs. 16 and 17 represent the lines on the left and right sides of Figure 54. Out of the two values of minimum void ratio calculated from Eqs. 15 and 16, the higher one is the easier outcome during mixing, because it consumes less energy. Based on Eq. 15, the solid line is the true solution for the minimum void ratio of a mixture.

The range of coefficients α and β is between 0 and 1. These two coefficients are used to include the effects of inclusion and embedment of coarse and fine particles into the dominant-grain structure. The special case of $\alpha = \beta = 0$ corresponds to the Voigt solution (upper bound). The special case of $\alpha = 1$ corresponds to a case where the change of voids volume is equal to the volume of fines particles added to or removed from the mixture. The special case of $\beta = 1$ represents a case where the volume of voids remains the same after removing or adding coarse particles into the mixture. The coefficients α and β are determined by back fitting Eqs. 15 and 16 to the minimum void ratio data.

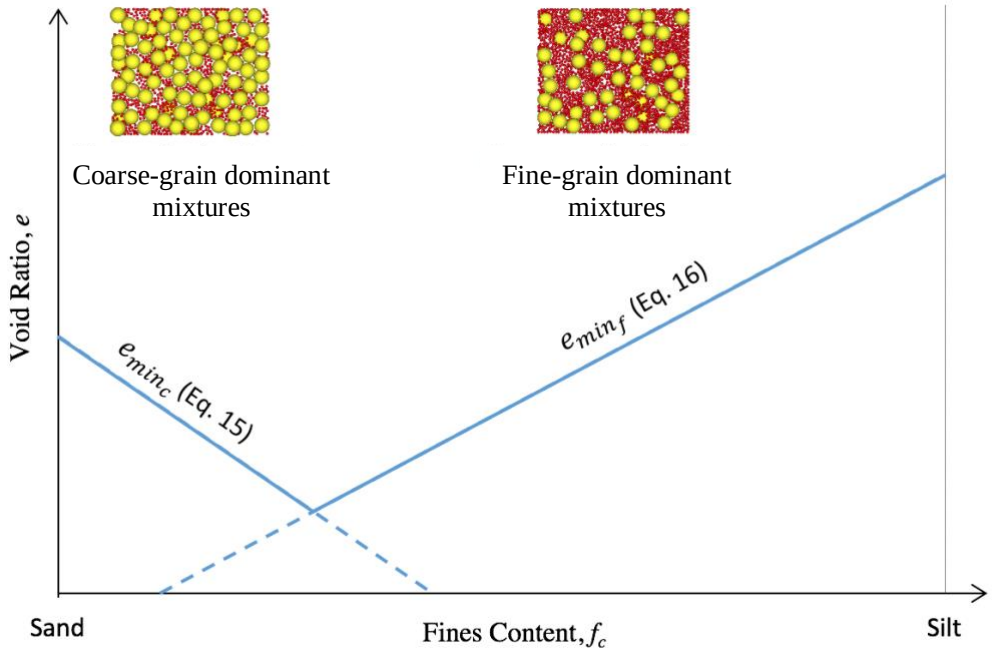

Figure 54. Generic variation of $e_{min_{fc}}$ versus fines content calculated from Eqs. 15 and 16 for coarse-grain and fine-grain dominant mixtures.

In what comes next, the validity of Eq. 15 for prediction of $e_{r_{fc}}$ for sand-silt mixtures with various amount of fines is examined.

Even though the two density state measures $e_{r_{fc}}$ and $e_{min_{fc}}$ are determined from two different loading processes and different degrees of particle crushing occurs in each process, they both bear the same meaning toward the inactive void ratio concept. The loading process to reach the minimum void ratio includes vibration of the specimen under small vertical load. The loading process to reach $e_{r_{fc}}$ is compression (isotropic or 1-D) where all active voids are diminished by particle rearrangement. Therefore, the values of $e_{r_{fc}}$ and $e_{min_{fc}}$ are not expected to be the same as can be seen in Figure 55, where

experimentally measured values of $e_{r_{fc}}$ and $e_{min_{fc}}$ for the six types of sand-silt mixtures are plotted versus fines content.

Despite their difference, the effect of varying fines content in a mixture seems to be similar on the variation of $e_{r_{fc}}$ and $e_{min_{fc}}$ as can be seen in Figure 55. Eqs. 16 and 17 are employed to predict $e_{r_{fc}}$ for sand-silt mixtures by replacing e_{min} with e_r:

$$e_{r_c} = e_{r_{sand}}(1 - f_c) + e_{r_{silt}} f_c - \alpha(1 + e_{r_{silt}}) f_c \quad (18)$$

$$e_{r_f} = e_{r_{sand}}(1 - f_c) + e_{r_{silt}} f_c - \beta e_{r_{sand}}(1 - f_c) \quad (19)$$

where e_{r_c} and e_{r_f} are the reference inactive void ratios for coarse-grain and fine-grain dominant mixtures, respectively. Similar to the case of minimum void ratio, out of the two calculated values from Eqs. 18 and 19, the higher one is the true solution:

$$e_{r_{fc}} = \max\left[e_{r_c}, e_{r_f}\right] \quad (20)$$

The coefficients α and β used in Eqs. 18 and 19 are the same as those used for calculating e_{min} of the same type of mixture.

For six different types of mixtures selected for this study, the coefficients α and β are determined for 5 types of mixtures from the minimum void ratio data. The sixth dataset from Konishi et al. (2007) did not report the values of minimum void ratio, so these two coefficients are determined from $e_{r_{fc}}$ values for this type of mixture. These values are shown in Table 5.

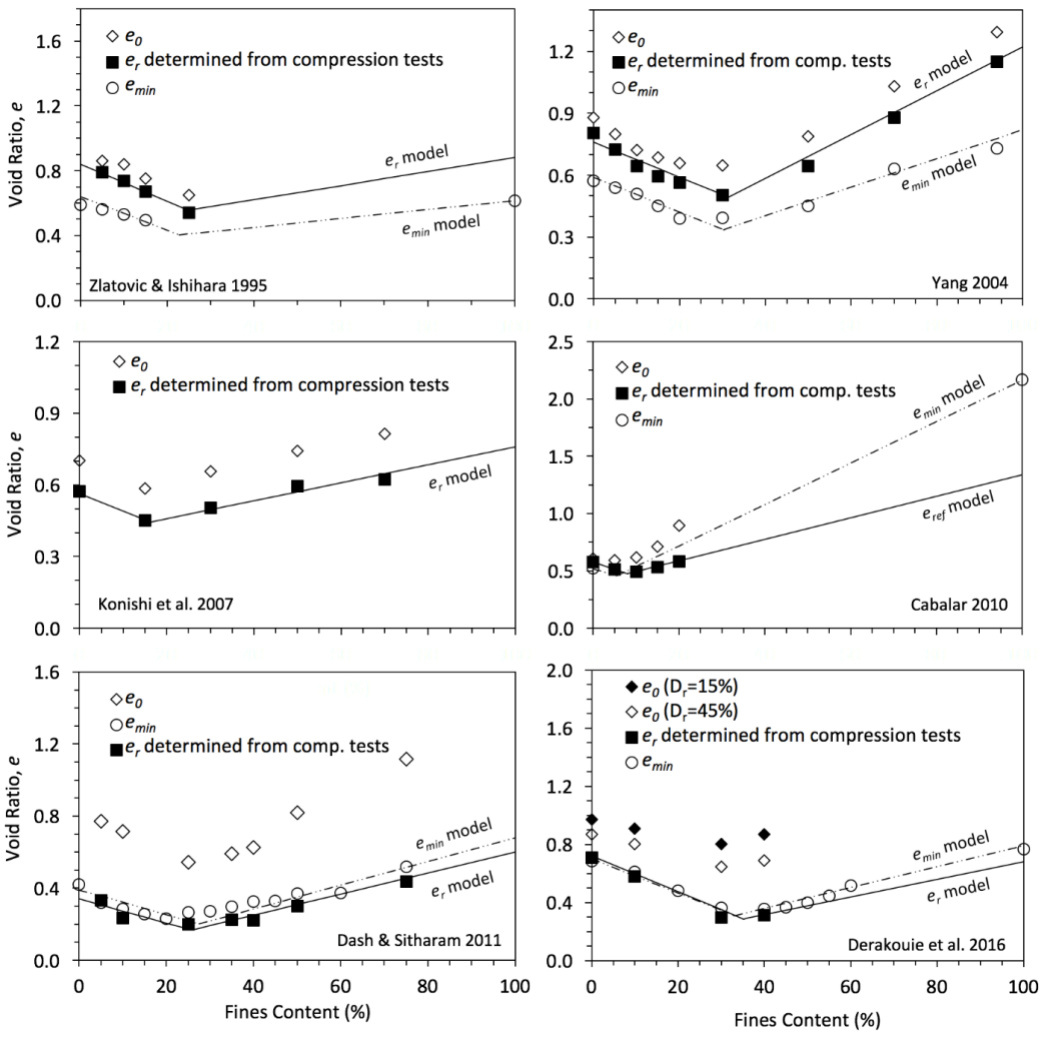

Figure 55. Predicted $e_{r_{f_c}}$ for all fines contents (solid lines), predicted *emin* (dot-dash lines) based on the same sets of α and β coefficients for six different types of sand-silt mixtures. The $e_{r_{f_c}}$ points determined from best-fit analysis, the measured *emin* values, and specimen initial void ratio are shown with square, circle, and diamond symbols, respectively.

4.5. Calibration of the model parameters and instructions on using the proposed model

The proposed model can predict the compression lines of sand-silt mixtures with any amount of fines with a given initial void ratio, using 2 main parameters, i.e. $\hat{a}$ and $e_{r_{fc}}$

(Eq. 10). Parameter $\hat{a}$ is directly determined from a compression test on one mixture with an arbitrary fines content. Parameter $e_{r_{fc}}$ is dependent on the fines content of the mixture, and is predicted by an augmented model expressed by Eq. 20. In order to calculate $e_{r_{fc}}$ from Eq. 20, four parameters are required: $e_{r_{sand}}$, $e_{r_{silt}}$, α and β. These four parameters are determined from compression tests on two specimens with different fines contents, and maximum density tests on four mixtures with different fines contents. Briefly, the model uses 5 parameters to predict the compression lines for a type of sand-silt mixture with any amount of fines and with any initial void ratio. The total number of required tests for calibration of the model parameters are: compression tests on two specimens, and minimum void ratio tests on four mixtures.

The process of calibrating the model parameters is shown in Figure 56 and Figure 57 in detailed steps.

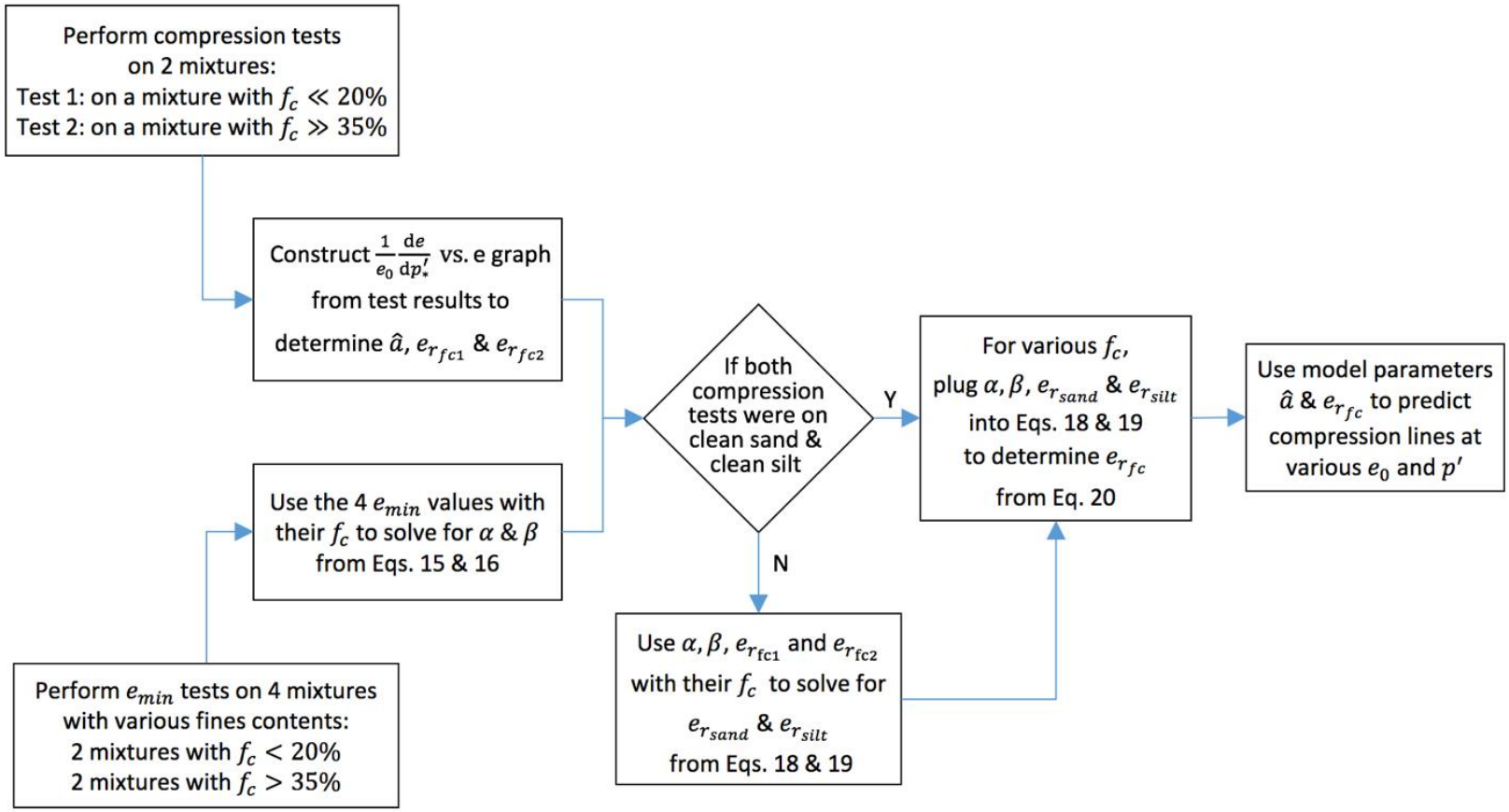

Figure 56. Flowchart showing the calibration process to determining the model parameters from compression tests and minimum void ratio data.

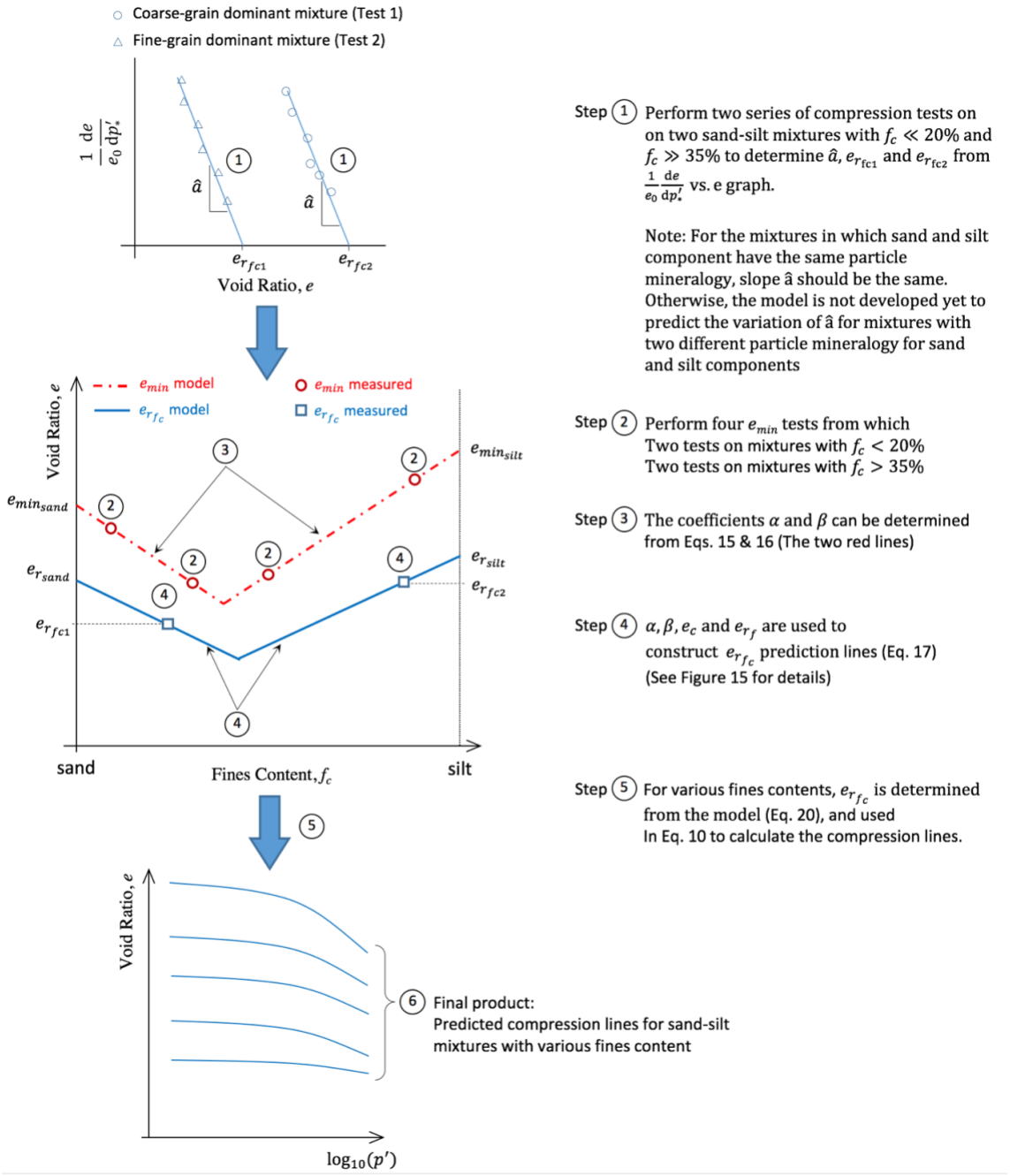

Figure 57. Steps toward calibration of the model parameters and implementing the model for prediction the compression lines of sand-silt mixtures with any amount of fines.

4.6. Performance of the proposed model

Based on the augmented model proposed for $e_{r_{f_c}}$ (Eq. 20), and plugging the predicted values of $e_{r_{f_c}}$ in the proposed model (Eq. 10), the compression lines for the selected sand-silt mixtures are predicted in the stress ranges shown in Table 5. The predicted compression lines are shown in Figure 58 together with the measured void ratios from the experiments.

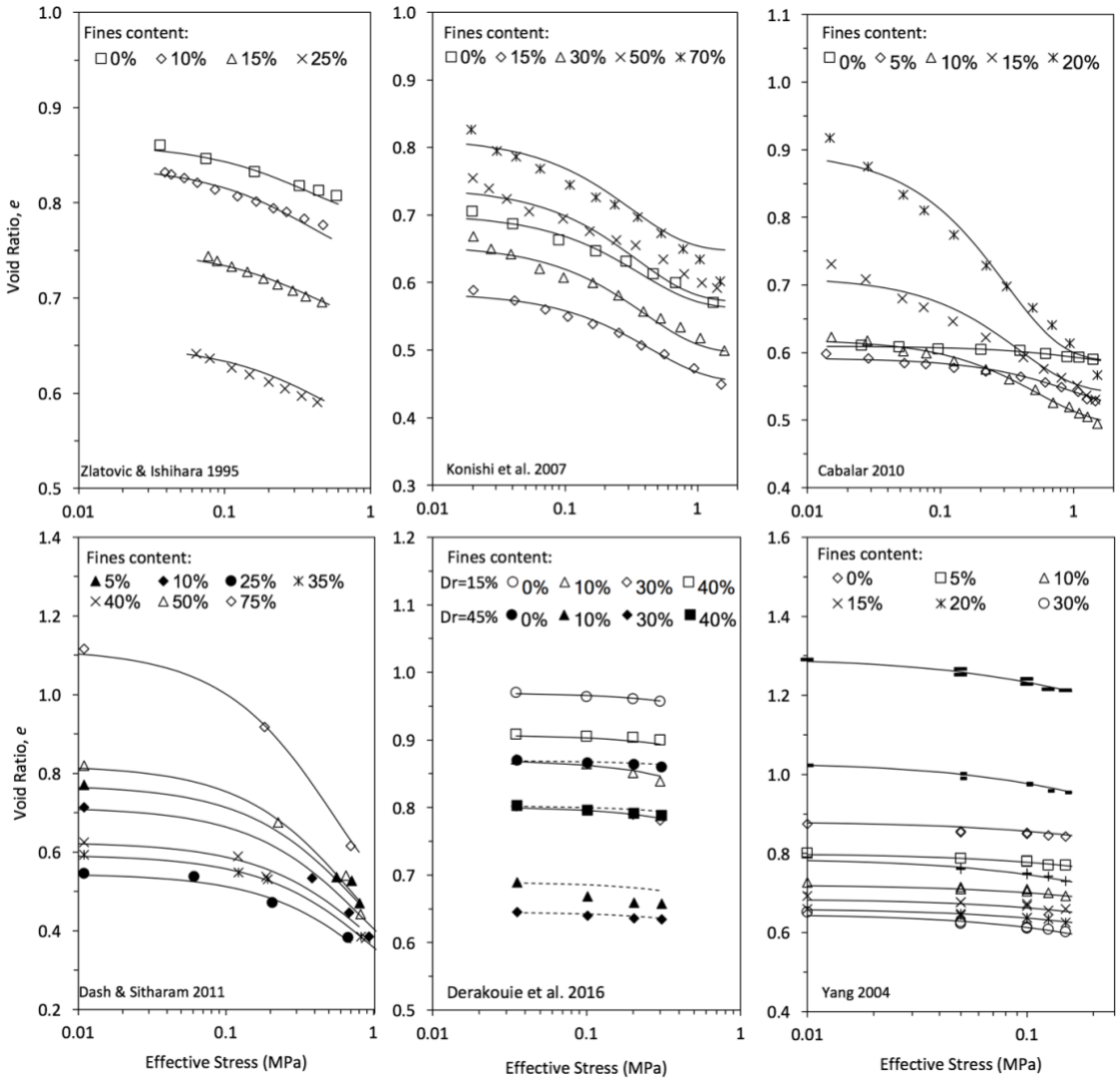

Figure 58. Calculated compression lines for six types of sand-silt mixtures using Eq. 10 with their representative inactive void ratios determined from Eq. 20.

To check the performance of the proposed model, the predicted void ratios are plotted versus the measured void ratios in Figure 59 for the selected six types of mixtures. The coefficient of determination R^2 is equal to 0.97, which proves the suitability of the proposed model to predict the compression lines for different types of sand-silt mixtures with any amount of fines.

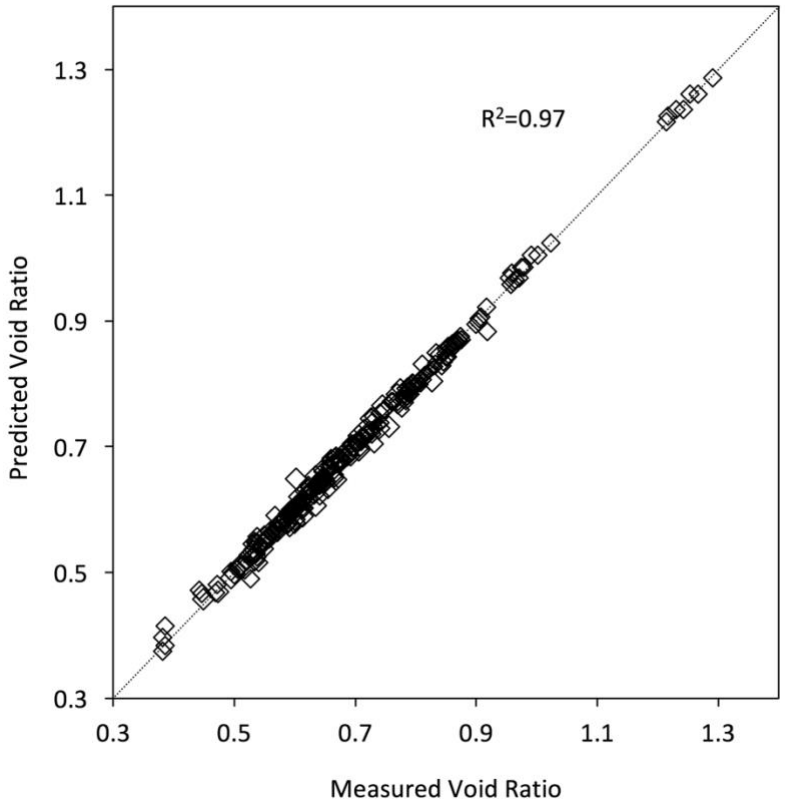

Figure 59. Correlation between the predicted and measured void ratios for the six types of sand-silt mixtures.

4.7. Conclusions

We introduced a postulate to divide the voids in a sand-silt mixture into active and inactive fractions. On the basis of this postulation, we proposed a mathematical expression to predict the void ratio during 1-D and isotropic compression for sand-silt mixtures with various fines contents. This model has two main parameters $\hat{a}$ and $e_{r_{fc}}$. A

method was proposed to predict the model parameter $e_{r_{fc}}$ as a function of fines content, which is based on four coefficients. Two of the coefficients (i.e. α and β) can be determined from the minimum void ratio tests on four different sand-silt mixtures. The other two coefficients $e_{r_{sand}}$ and $e_{r_{silt}}$ are determined from compression tests on two specimens of sand-silt mixture with two different fines contents.

The performance of the proposed model is verified by comparing the measured and predicted compression lines for six types of sand-silt mixtures with various fines contents. The results show a coefficient of determination $R^2 = 0.97$, thus proves the suitability of the proposed model for predicting compressibility of sand-silt mixtures with any fines content under compression loading.

Table 5. Properties of selected sand-silt materials used in this paper.

Materials (coarse & fines)	Tested fines contents (%)	Max. Stress (kPa)	Sand type†	Silt type†	Parameter $\hat{a}$	Sand e_{min} e_r	Silt e_{min} e_r	Coefficient α	β
Hukksond Sand & Chengbei Silt	0, 5, 10, 15, 20, 30, 50, 70, 94	125	Q	Q	0.43	0.59 0.76	0.82 1.22	0.61	0.77
Toyoura sand & milled fines	0, 10, 15, 25	580	Q	Q	0.32	0.64 0.84	0.61 0.88	0.56	0.46
Bird-Picked Sand & nonplastic fines	0,15,30,50,70	1600	Q	Q	0.39	N/A 0.56	N/A 0.76	0.52	0.32
Leighton Buzzard sand & mica fines	0, 5, 10, 15, 20	1500	Q	M	Fig. 10	0.52 0.58	2.16 1.34	0.87	0.30
Ahmedabad sand & Gujarat silt	5, 10, 25, 35, 40, 50, 75	1000	Q	Q	0.17	0.42 0.34	0.65 0.60	0.57	0.87
Terrigenous silica sand & silica silt	0, 10, 30, 40	300	Q/F	Q/F	0.02	0.68 0.72	0.77 0.68	0.71	0.90

† Q: quartz; M: mica; F: feldspar

CHAPTER 5

EXTENDING THE COMPRESSION MODEL TO CONSIDER THE EFFECTS OF PARTICLE CRUSHING ON THE COMPRESSIBILITY OF GRANULAR SOILS

5.1. Introduction

Particle crushing in granular material adds complexity to the material behavior during loading. Examples of real life cases where the effects of particle crushing on the stress-stress behavior of soils cannot be overlooked are particle crushing at the tip of driven piles, particle crushing at large-strain shearing (e.g. landslides), particle crushing due to intense and transient compression waves. Soil friction angle reduces as a result of particle crushing at very high stresses (Marachi et al. 1969). Particle crushing also changes the stress-strain behavior of soil (Miura et al., 1984). The response of soil during liquefaction is affected by particle crushing (Hyodo et al. 2000) as the critical state of the material shifts downward and makes the soil more susceptible to liquefaction at its current density state (Kikumoto et al. 2010).

Modeling compressibility of granular material becomes complicated when the applied stresses are very high and particles start to crush. When substantial particle crushing occurs, the particle size distribution changes and the material no longer has the same mechanical properties as prior to crushing. Even though particle crushing is believed to initiate from low stress levels, where for example particle edge chamfering takes place, the major effects of particle crushing on compressibility start at high stress levels.

Meidani et al. (2017) showed that the compressibility of granular soils can be modeled by a simple linear relationship between change of void ratio with respect to stress (de/dp') and void ratio (e). However, this linear relationship is only valid up to certain stress levels, for example 40 MPa for most quartz sands. According to the hypothesis proposed by Meidani et al. (2017) volume of voids in a granular soil can be divided into two hypothetical fractions: (a) active voids, and (b) inactive voids. While active voids are the fraction of total voids volume that can be diminished with particle rearrangement during loading, inactive voids are the volume of voids when the material is backed to its densest state by rearranging its particles. In other words, inactive voids volume is constant unless a change in particle size distribution takes place. That is where particle crushing effects come into play.

Particle crushing continues to change particle size distribution of the material up to ultra high stress levels. However there is an upper stress limit where comminution of particles takes place instead of crushing. The upper-stress limit for particle crushing was studied for synthetic ceramic granulates by Bouville and Studart (2017). Their results showed that when the material is subject to compressive stresses at room temperature the grain size reduction due to particle fragmentation stops at 500 MPa, and most of the deformation beyond this stress level is elastic and reversible. We extend their finding to the granular soils and conclude that for natural granular soils there is an upper stress limit at which particle crushing stops and the deformations beyond this point are elastic. This upper stress limit is dependent on the mineralogy of particles comprising the material.

In this paper, we adopt the previous model for compressibility of granular soils developed by Meidani et al. (2017) and extend it to higher stress levels where the effects

of particle crushing has to be explicitly considered in the model. We show that this new model can be explained by physical measures of particle crushing such as Breakage Index (Einav, 2007). The comparison between measured and predicted void ratios for a number of granular material shows the applicability of this new model for prediction of compressibility over a very wide range of stresses and up to comminution limit of material.

5.2. Active and inactive voids in granular soils

The concept of active and inactive voids in granular materials (Figure 60) is recently developed and used in modeling compressibility of sands by Meidani et al. (2017). Later Chang et al. (2017) showed that this concept can be used in a more general case for modeling compressibility of sand-silt mixtures with any amount of fines. As Meidani et al. (2017) showed the voids volume change during compression can be attributed to the volume change of active void and inactive voids. According to this hypothesis, volume change is solely caused by particle rearrangement, which reduces the active voids volume. Particle crushing changes the kinematics of the system of particles and makes more active voids, ready to be diminished by particle rearrangement. Inactive void ratio defines the densest state of granular packing at its current particle size distribution. However, the magnitude of inactive void ratio is not exactly the same as the minimum void ratio of the material since there are two different mechanisms involved in static compression tests and standardized minimum void ratio vibratory tests. The evolution of active voids volume under applied load is already described in details in the above mentioned papers. In this section, we develop a mathematical model for the evolution of

inactive voids under applied load. This evolution is shown to be primarily related to the extent of particle breakage in the material.

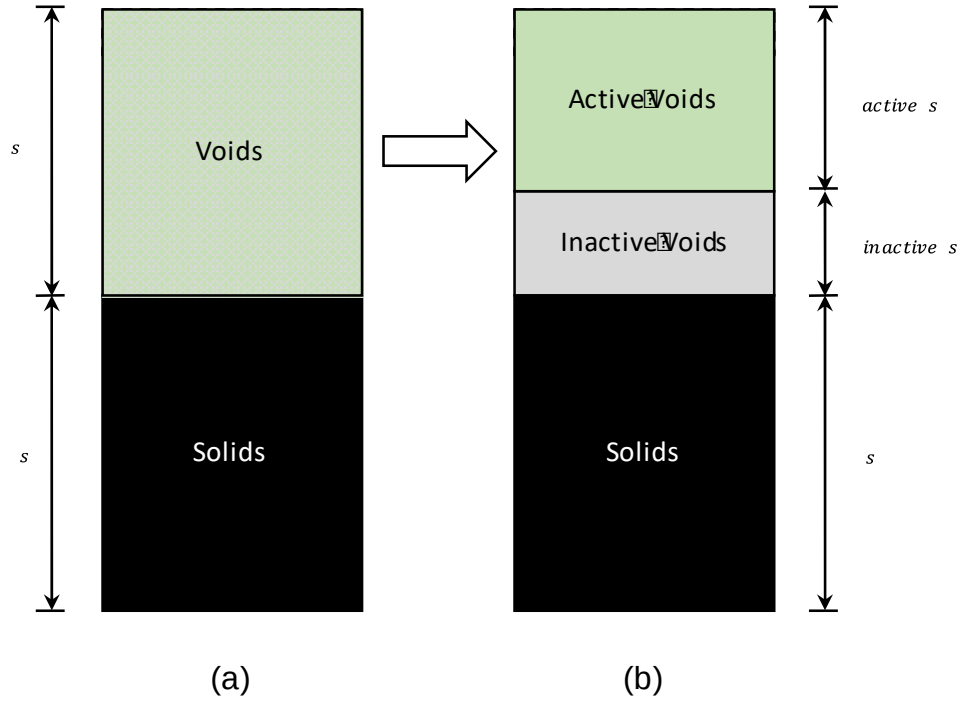

Figure 60. Phase diagrams for a granular material showing voids and solids in (a) traditional way; (b) voids split into active and inactive fractions.

Three stages can be identified during compression of a granular material (Figure 61) with respect to the evolution of active and inactive voids:

Stage 1: at lower stress levels and before particle breakage intensifies, almost all compression is due to reduction of active voids caused by particles rearrangement (Figure 61.b);

Stage 2: At medium to very high stress levels, particle breakage starts to affect volume change of material. Particle breakage is believed to become noticeable from 4 MPa for most quartz sands (Laufer, 2015). During this stage, part of the inactive voids is

mobilized due to crushing and becomes active. Thus, more active voids volume are available for compression (Figure 61.c);

Stage (3): at ultra-high stress levels, particle breakage effects are diminished, material reaches comminution limit. With no further particle breakage, the volume of inactive voids remain constant (Figure 61.d). Further compression is due to elastic deformation of material. Briefly, granular material under low stress to ultra-high stress compression goes into three stages of (1) particle rearrangement, (2) particle crushing and particle rearrangement, and (3) acting as a continuum media beyond comminution limit.

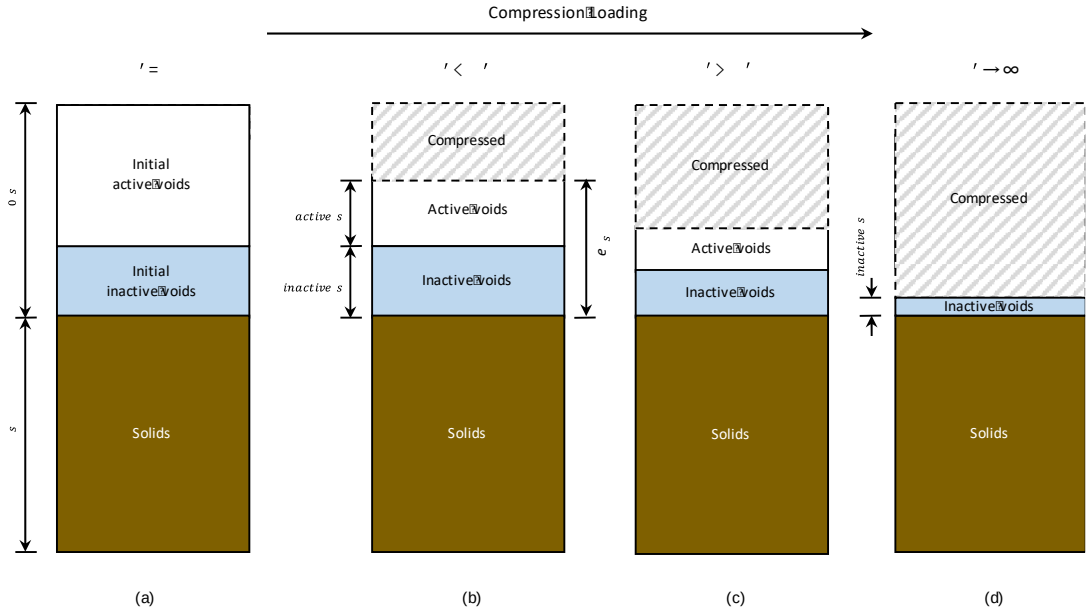

Figure 61. Evolution of active and inactive voids during compression loading.

Comminution, which is the reduction of particle size in a granular material due to mechanical processes such as particle breakage, has been investigated both theoretically and physically by many researchers (e.g. Rumpf and Schönert, 1972; Kendall, 1978a; Boddy, 1943; Puttick, 1979; Kendall, 1978b). In comminution of particles, a critical size is reached from which no further particle breakage is possible (Hagan, 1981). Beyond

this limit, the particles deform in a ductile regime instead of crushing. This point of brittle-ductile transition in a brittle granular material is called comminution limit (Field et al., 2014). The comminution limit for quartz particles is approximately 1-3 micron, according to different models.

5.3. The proposed model

The compressibility model proposed here has two main components: (a) evolution of active voids with stress, and (b) evolution of inactive voids with stress. The first component was discussed in detail in the previous model by Meidani et al. (2017). In the previous model the total void ratio change was only attributed to the change of active void ratio. Inactive voids ratio was assumed to be constant throughout loading. Because of this assumption, range of validity of the previous model was limited. In this chapter, this limitation is removed by developing a mathematical relationship for the evolution of inactive voids with loading. This evolution is caused by crushing of particles as discussed earlier.

Dependency of inactive void ratio on the particle size distribution of material was identified in the previous models (Meidani et al. 2017; Chang et al., 2017) but no mathematical model was developed to explicitly consider the evolution of inactive voids with stress.

When compression test data is plotted in de/dp' versus e space (Figure 62) a linear trend can be identified among the data points up to certain stress levels. This linear trend was the benchmark of the models developed in the previous chapters. The predicted compression line constructed on this trend line can be seen in Figure 63. As expected, this model cannot cover the behavior at very high stress levels and beyond.

There are different ways to extend the existing model to include the behavior at higher stress levels. The simplest way is to fit a continuous function to all of the data point in d*e*/d*p'* vs. *e* space as shown in Figure 64. This method will guaranty the best fit to the measured data. However, not only this approach of blindly trying to fit every data point is philosophically wrong in modelling but also there is no physical explanation to the model. While there are countless ways that the data shown in Figure 64 can be predicted, only the methods that can be explained by the known physical mechanism are legitimate as sharply mentioned by Drucker (1988):

- "We should be sure to include in the framework of any model, the well known qualitative aspects of behavior that are clearly important. Also, do not be overly impressed with the ability to match any given set of data no matter how extensive that set appears to be."
-

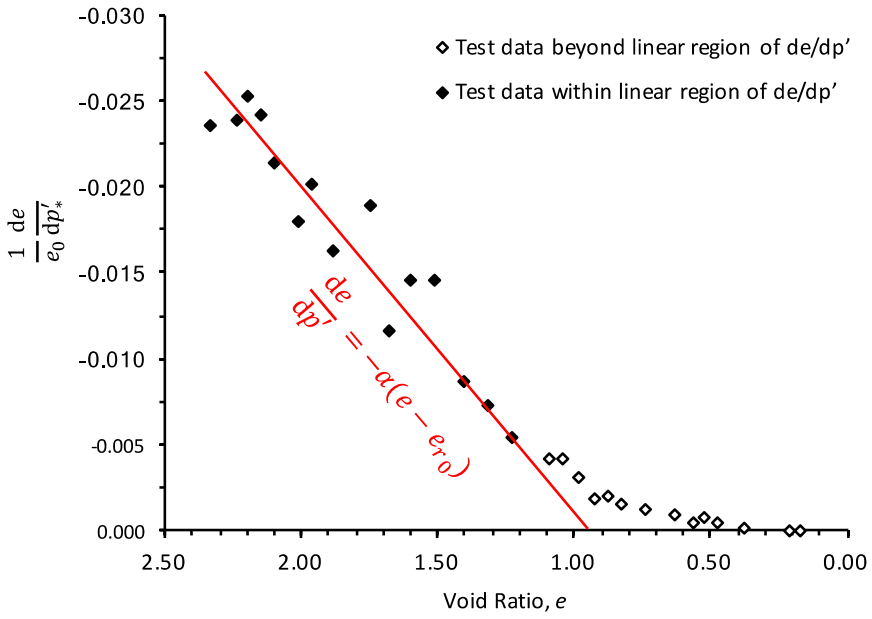

Figure 62. Compression test data on Petroleum Coke plotted in d*e*/d*p*' versus *e* space. [Test data from McDowell, 1996]

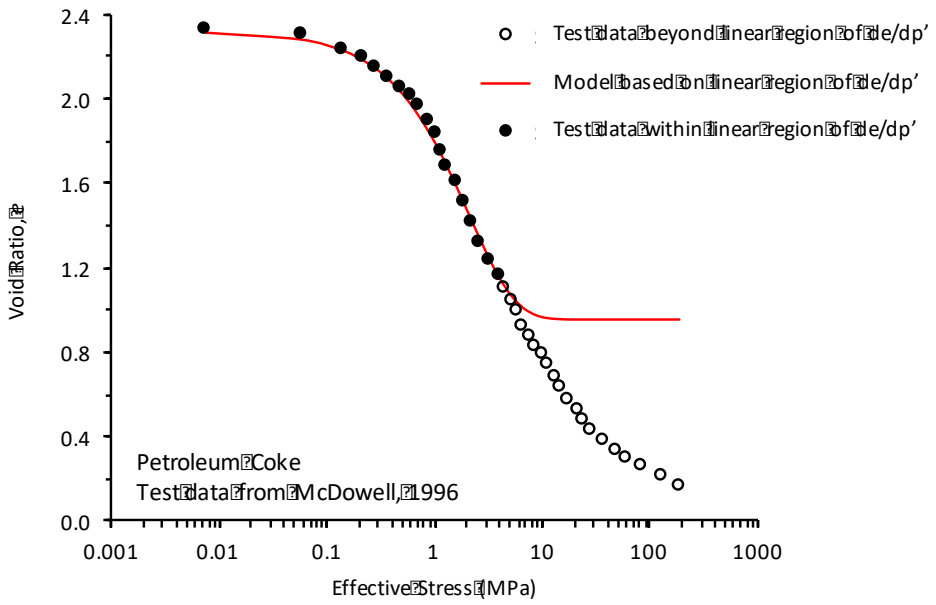

Figure 63. Compression test data on Petroleum Coke and prediction from the previous model. [Test data from McDowell, 1996]

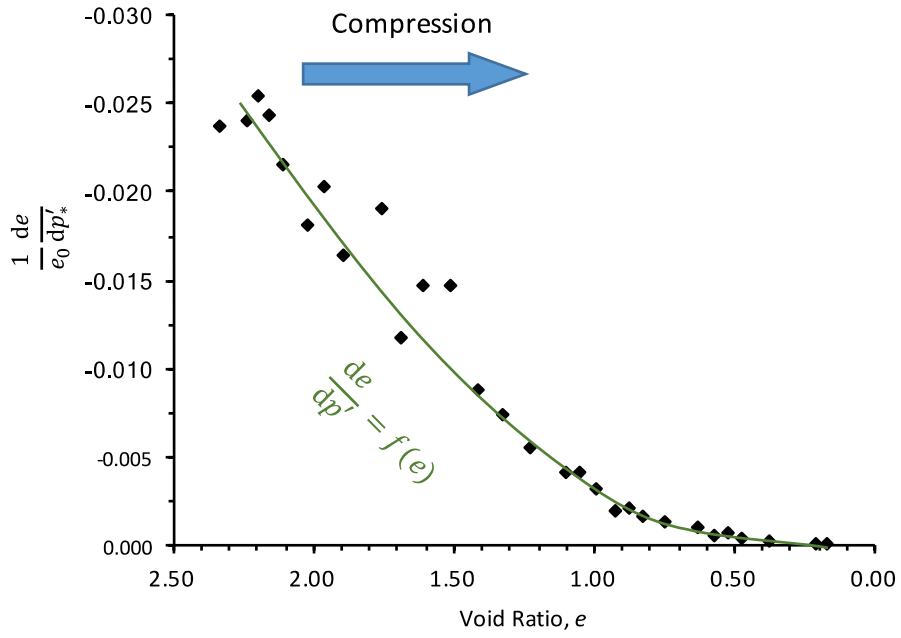

Figure 64. A general mathematical function that may be able to fit all compression test data point, but lacks a physical meaning with respect to the elastoplastic compression mechanism.

Another approach to predict data points shown in Figure 62 is to fit a straight line to the initial linear portion, then build parallel lines in a way that other data points are captured with a similarly sloped line but different e_r values as shown in Figure 65.

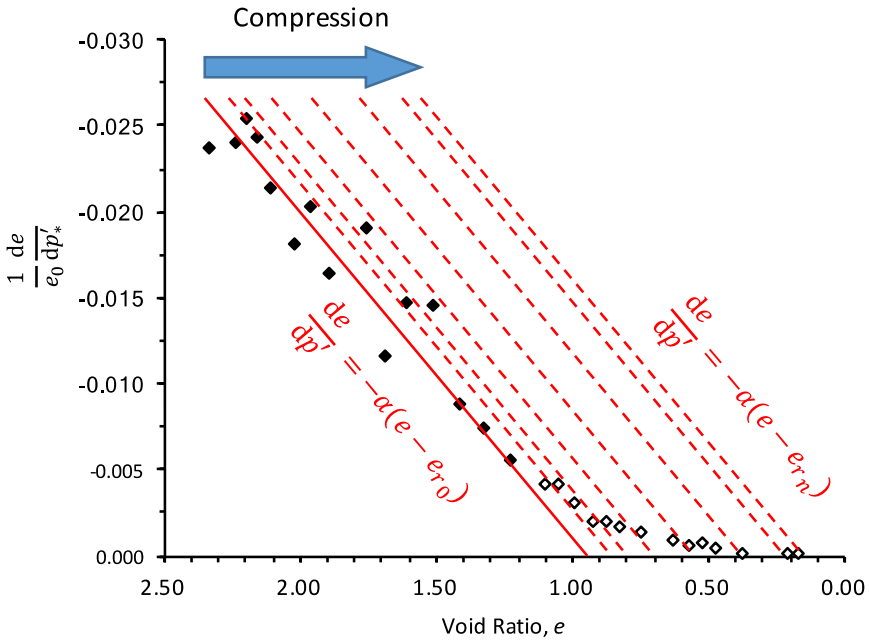

Figure 65. Using parallel lines to model data points beyond the initial linear range for compression test data plotted in d*e*/d*p'* versus *e* space.

For each data point beyond the initial linear range, one line is drawn so it captures the data point. The e_r of this line is measured and another parallel line is drawn to catch the next data point. The determined e_r values for all data points in Figure 65 are plotted in Figure 66, which shows the evolution of inactive void ratio with stress. The shape of Figure 66 remarkably resembles compression curve. When the data points in Figure 66 are plotted in a de_r/dp' vs. e_r space (see Figure 67), similar to what was done for the total void ratio data, a linear trend can also be identified between almost all e_r (inactive void ratios). The only few points that this line cannot fit are from compression tests at ultra-high stresses, which are beyond comminution limit of the material.

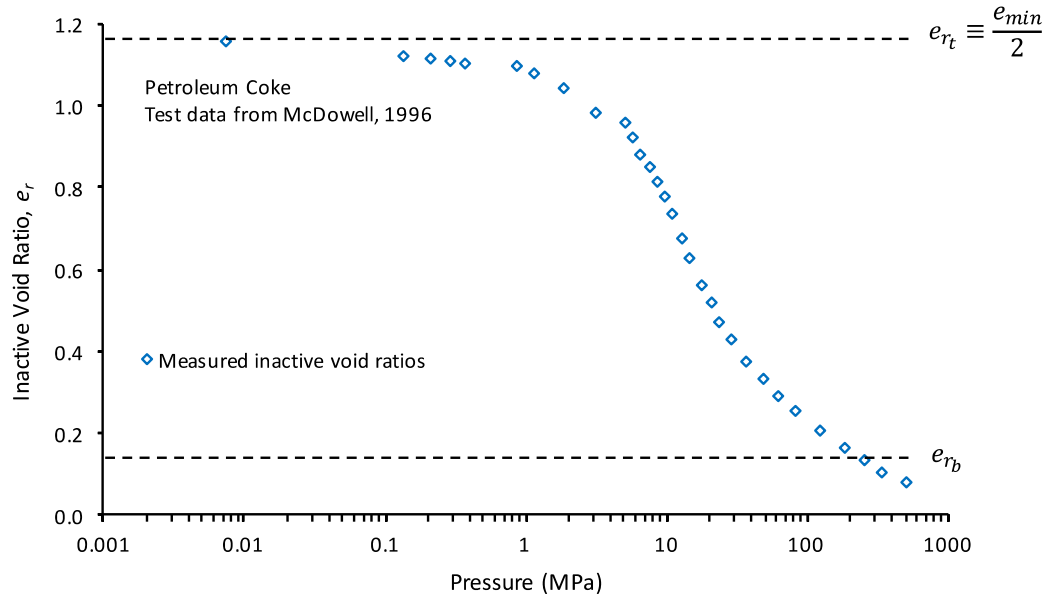

Figure 66. Evolution of inactive void ratio with effective stress during 1-D compression test on Petroleum Coke. Data point determined after constructing Figure 64.

The linear portion of data in de_r/dp' vs. e_r space, as shown in Figure 67, can be modeled as:

$$\frac{de_r}{dp'} = -\beta(e_r - e_{r_b}) \qquad (1)^6$$

where e_{r_b} can be called the absolute minimum void ratio of the material, or void ratio at comminution limit (Kendall, 1978). Comminution limit is the stress at which granular material reaches a fractal limit in its grain size distribution and no further particle crushing occurs in the material. This is the lowest void ratio that a material can reach through particle rearrangement and particle crushing. The volume changes that occur in the material beyond this point is considered to be in a different regime that cannot be

[6] Equation numbers restart from 1 in this chapter to avoid long digits in the text.

explained by particle rearrangement or particle crushing. For most geomaterials, the volume change for stresses above the comminution limit is not considerable. In addition, there are few real-life cases that the material undergoes such intense stresses. More experimental work is needed on the behavior of granular material beyond their comminution limit.

This linear approximation show between de_r/dp' vs. e_r in Figure 67 captures many data points from low to very high stress levels. But as can be seen in Figure 67, few data points from tests at ultra-high stresses are not predicted by this line.

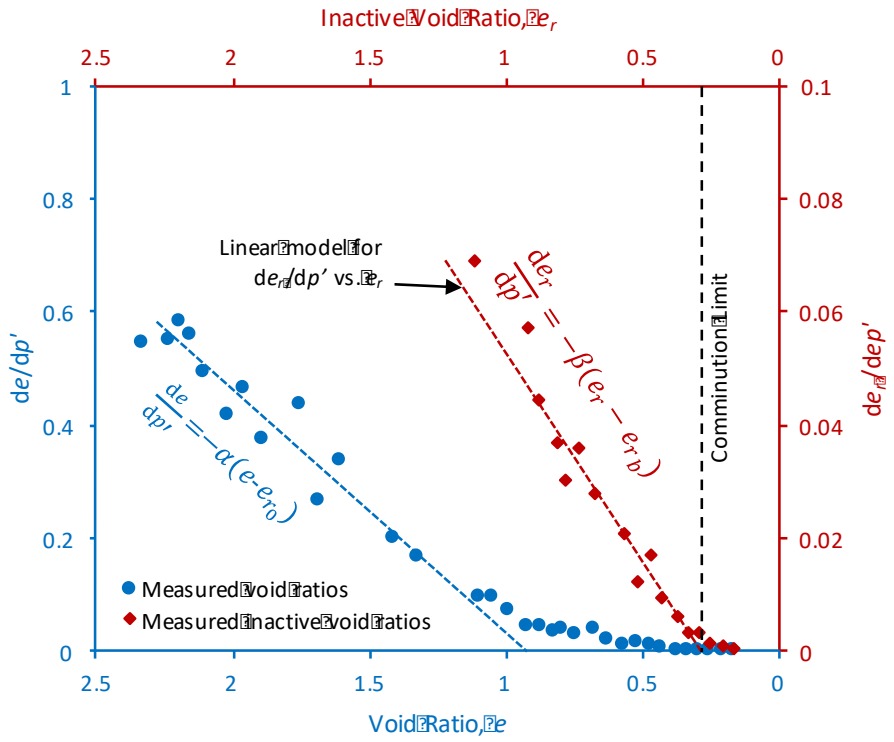

Figure 67. Variation of de/dp' vs. e and der/dp' vs. er for 1-D compression tests on Petroleum Coke.

In order to determine a mathematical relationship for the evolution of inactive void ratio with stress, Eq. 1 is integrated from the start of the compression test, where inactive

void ratio is at its maximum value of e_{rt} (Figure 66), up to an arbitrary inactive void ratio of e_r and stress of p':

$$\int_{e_{r_t}}^{e_r} \frac{\mathrm{d}e_r}{e_r - e_{r_b}} = -\int_0^{p'} \beta \mathrm{d}p' \tag{2}$$

After integration, the following relationship is derived for the evolution of e_r (inactive void ratio) during loading:

$$e_r(p') = \left[e_{r_t} - e_{r_b}\right] \exp(-\beta p') + e_{r_b} \tag{3}$$

This formula can be normalized by dividing effective stress p' by atmospheric pressure p_a. Parameter β is dependent on both material type and its initial void ratio. If the effects of initial void ratio taken out of this parameter, it can be treated as a material parameter only. Our analyses on specimens of granular material with various initial void ratios showed that β can be replaced by $b.e_0$ (similar to what was shown in Chapter 3 for derivation of the simpler model), where b is a material constant and is independent of the initial density of the specimen. Therefore, Eq. 3 can be written in the following form:

$$e_{inactive} = e_r(p', e_0) = \left[e_{r_t} - e_{r_b}\right] \exp\left(-be_0 \frac{p'}{p_a}\right) + e_{r_b} \tag{4}$$

Eq. 4 can be plugged into the following general relationship for the void ratio:

$$e_{total} = e_{active} + e_{inactive} \tag{5}$$

Adopting the model form Meidani et al. (2017):

$$e_{total} = (e_0 - e_{inactive})\exp(-ae_0 \frac{p'}{p_a}) + e_{inactive} \tag{6}$$

where $e_{inactive}$ is defined in Eq. 4. Hence, the total void ratio can be calculated from the following relationship for stresses up to comminution limit:

$$e(p, e_0) = \left[(e_0 - e_{r_b}) - (e_{r_t} - e_{r_b})\, exp\left(-be_0 \frac{p'}{p_a}\right)\right] exp\left(-\alpha e_o \frac{p'}{p_a}\right) + \left[e_{r_t} - e_{r_b}\right] exp\left(-be_o \frac{p'}{p_a}\right) + e_{r_b} \tag{7}$$

Eq. 7 is used to predict the void ratio of Petroleum Coke in 1-D compression up to 200 MPa and the results are shown in Figure 68. As can be seen from this figure, there is good agreement between the measured data and predicted void ratios up to the comminution limit.

Eq. 7 can be further simplified by replacing e_{r_t} with $e_{min}/2$, recalling from the previous chapter that the minimum void ratio was correlated with the representative inactive void ratio in case of no particle crushing. In other words, the active voids can decrease down to $e_{min}/2$ before the effects of crushing need to be included in the model in the evolution of inactive void ratio.

$$e(p, e_0) = \left[(e_0 - e_{r_b}) - \left(\frac{e_{min}}{2} - e_{r_b}\right) exp\left(-be_0 \frac{p'}{p_a}\right)\right] exp\left(-\alpha e_o \frac{p'}{p_a}\right) + \left[\frac{e_{min}}{2} - e_{r_b}\right] exp\left(-be_o \frac{p'}{p_a}\right) + e_{r_b} \quad (8)$$

In this form of the model, there are three material parameters need to be calibrated: *a*, *b*, and e_{r_b}.

5.3.1. Relationship between inactive void ratio and breakage index

Having particle size distribution of Petroleum Coke at different stress levels of 1-D compression tests, the breakage index (Br) for Petroleum coke is calculated at different stress levels according to the definition proposed by Einav (2007). In order to determine the breakage index, the area enclosed between the current PSD and the final PSD curves is divided by the area enclosed between the initial PSD and the final PSD curves as shown in Figure 69. The fractal limit for the PSD is calculated for the material at ultra-high stress levels by the method described in Einav (2007):

$$\%finer = \left(\frac{d}{D_m}\right)^{0.4} \quad \text{- method 1} \quad (9)$$

where d is the diameter of the particle, D_m is the diameter of the largest particle before crushing starts, and $\%\ finer$ is corresponding to the particle with diameter d. For most geomaterials, the smallest particle size that can be reached during crushing is 0.002 mm, therefore the fractal limit GSD curve shown in Figure 70 is truncated at d=0.002 mm.

We also propose a second method for determining the PSD of material at its fractal limit:

$$\%finer = 1 - [\exp(-d^a)]^b \quad \text{- method 2} \quad (10)$$

where d is the particle diameter, and a and b are two constants that are determined by best-fit analysis to the GSD of material at ultra-high stress levels. For Petroleum Coke, fractal GSD calculated by this method is shown in Figure 70. The constants a and b are 0.83 and 0.96, respectively. It seems that the fractal limit PSD determined by our proposed method is a better fit to the measured data (Figure 70). Variation of (1-Br) with stress is shown in Figure 68 next to the inactive void ratio data. It can be seen that the onset of breakage matches the stress at which inactive void ratio starts to dive; both e_r and (1-Br) show similar trend when plotted versus applied pressure. It is noted that the evolution of e_r can be determined from 1-D test alone. There is no need to measure PSD at different stress levels. This comparison is made to show that inactive void ratio is conceptually related to the extent of particle breakage in granular material.

5.4. Model performance

Table 6 shows the properties of five granular materials used to verify the performance of the proposed model. Eq. 8 is used to predict compression lines of these granular material with various initial densities (shown in Figure 68 and Figure 71). Minimum void ratio of the material is taken as one of the material parameters as shown in Eq. 8. The

remaining model parameters, *a*, *b*, and e_{r_b} are determined by best fitting Eq. 8 to the compression data on a specimen with a given initial void ratio. The rest of the compression lines can be then predicted by varying the initial void ratio in Eq. 8 for each material. The predicted compression lines match very well with the measured void ratios for a wide range of stresses. The upper stress range of prediction for each material is listed in Table 6.

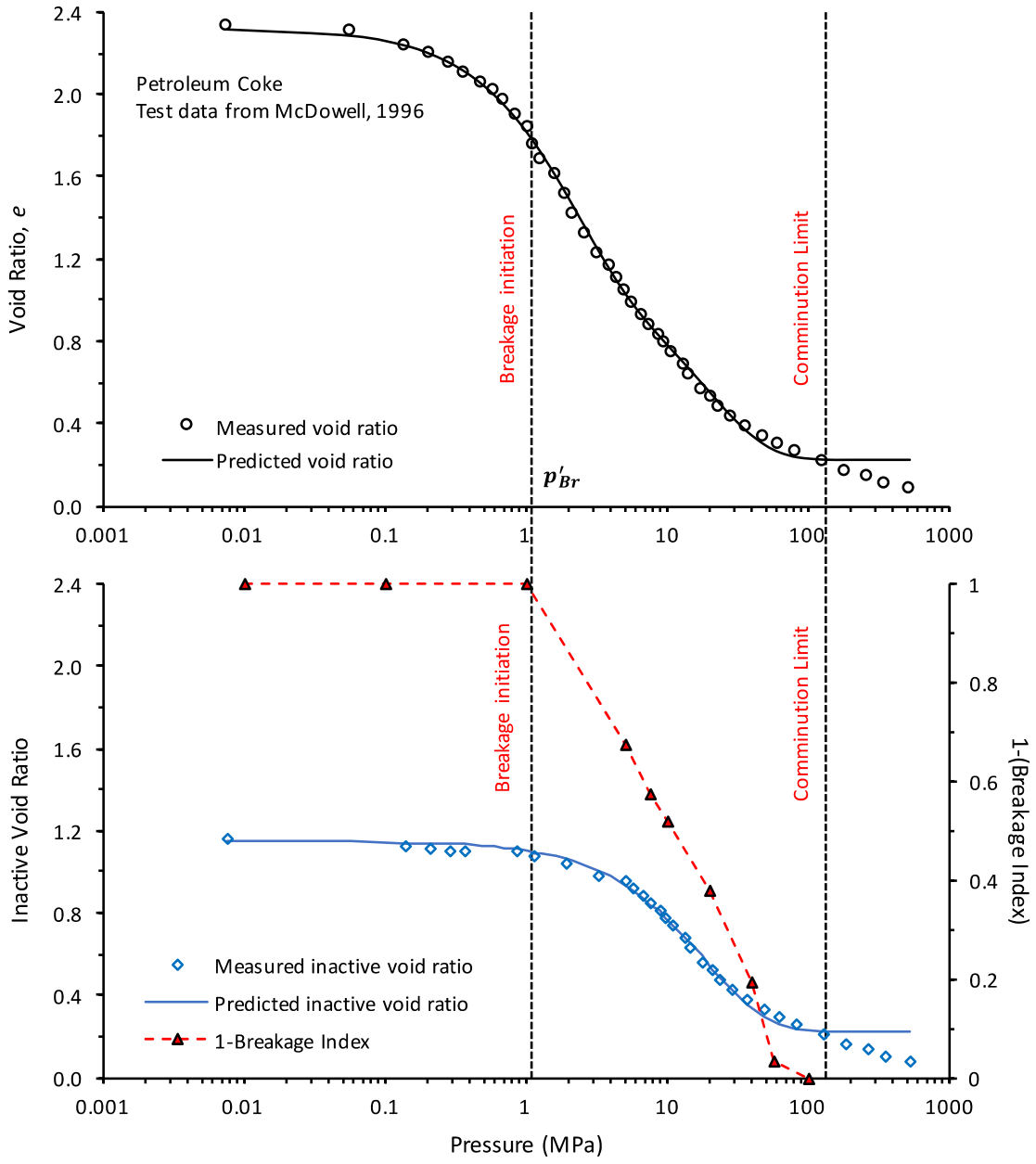

Figure 68. (top) Measured and predicted void ratio from 1-D compression tests on Petroleum Coke; (bottom) Measured and predicted inactive void ratio, together with variation of (1-Breakage Index) determined from the evolution of particle size distribution of Petroleum Coke during 1-D compression tests.

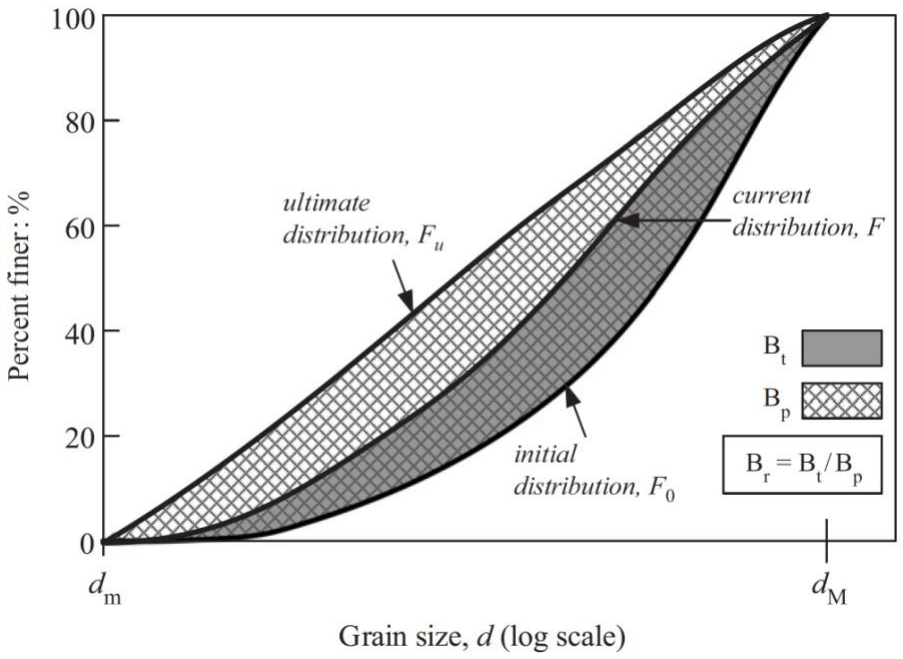

Figure 69. Definition of Breakage Index (Br) by Einav (2007).

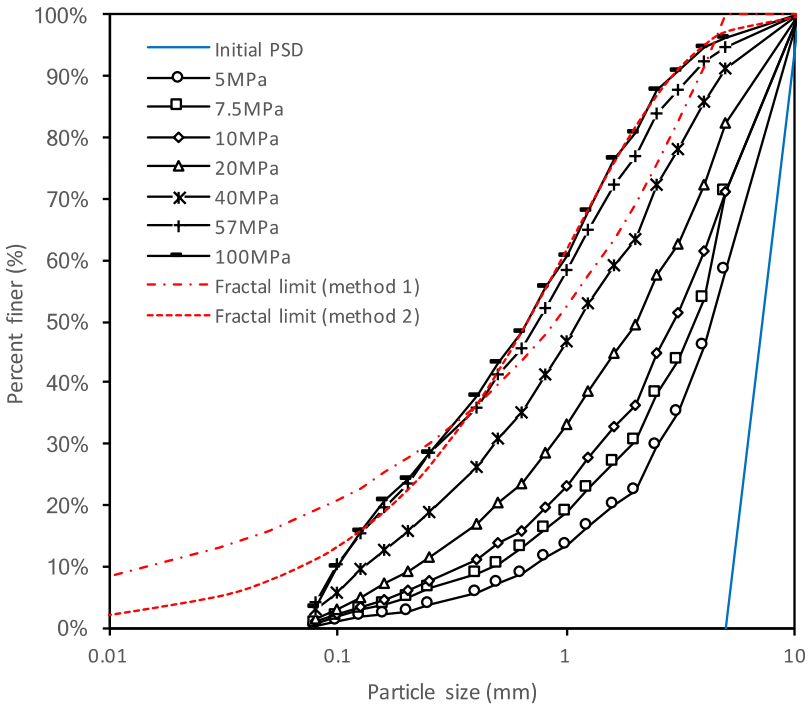

Figure 70. Evolution of particle size distribution for Petroleum Coke during 1-D compression at different stress levels. The ultimate PSD is also calculated by two methods and shown with dashed lines.

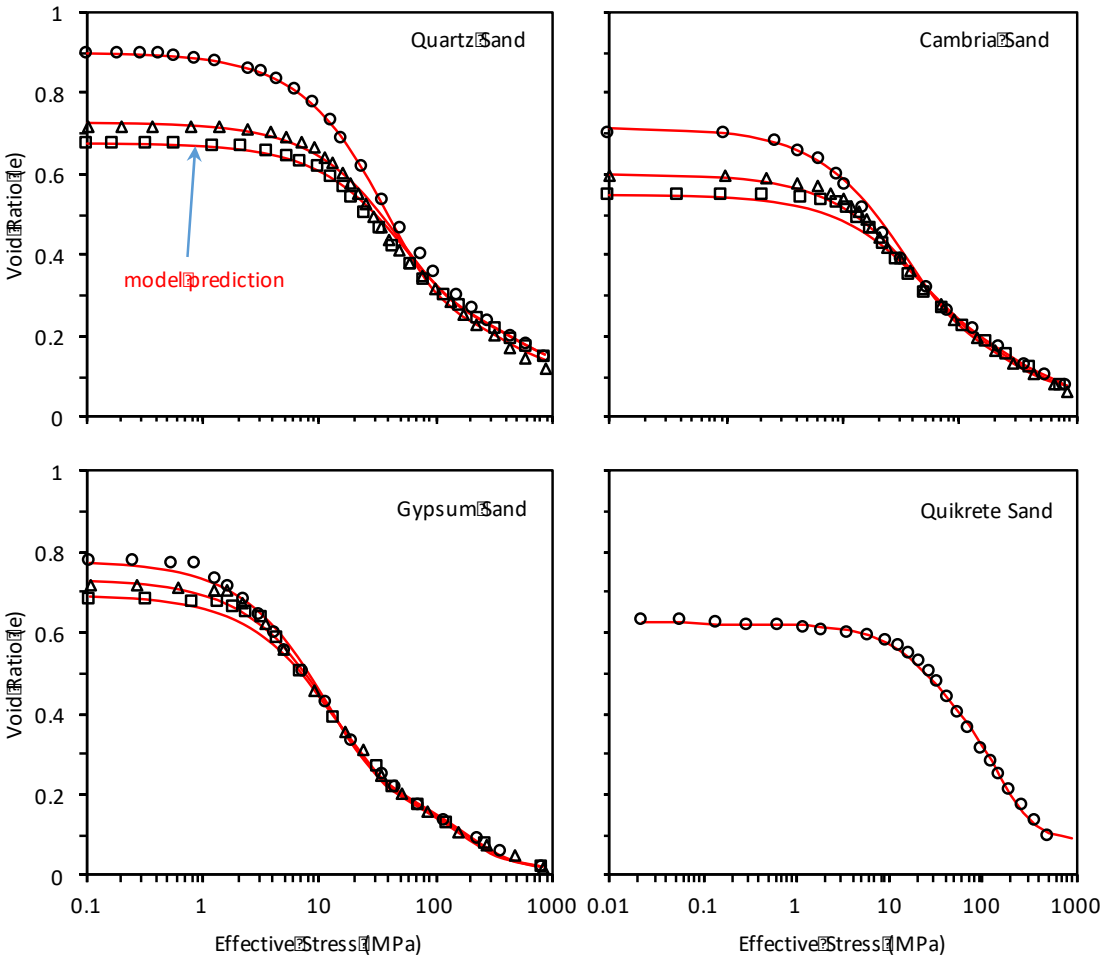

Figure 71. Measured and predicted void ratios for 4 different granular materials under very wide compressive stress ranges.

5.5. Conclusions

In this chapter, the previous postulate of active and inactive void ratios was used to develop an evolution law for the inactive void ratio change during compression with consideration of particle crushing effects. Using compression test data, it was shown that both active and inactive void ratios change during compression loading similarly, but at different stress levels. The new evolution law for inactive void ratio change during particle crushing was combined with the evolution law for active void ratio and a

compressibility model was proposed. The proposed model can predict the void ratio of granular material under isotropic and 1-D compression loading up to comminution limit of the granular material, where particle size distribution reaches an ultimate distribution and no further particle breakage occurs in the material.

The evolution of inactive void ratio is directly proportional to (1-*Breakage Index*). *Breakage Index* is a physical measure of the extent of particle breakage and varies between 0 for no crushing to 1 for the material at its fractal limit for particle size distribution. This comparison verified the physical meaning of inactive void ratio and its relation to particle crushing.

The model parameters for the evolution of inactive void ratio, as well as the parameters for active void ratio, can be directly determined from compression test data..

The advantage of the proposed model is that (1) it does not need the yield stress of the material to be known prior, (2) it is in a continuous form, (3) it needs 3-4 material parameters that are conveniently calibrated by 1-D or isotropic compression tests results.

The comparison between predicted and measured void ratios shows that the proposed model can simulate the compression line of different granular material over a very wide range of stresses.

The verified concept of active and inactive voids can now be extended to other aspects of granular material behavior for developing simple constitutive models.

Table 6. Properties of the granular material used to verify the proposed model and model parameters for each soil.

Granular Material	Test Type*	D_{50} (mm)	D_{60}/D_{10}	Particle Shape†	Mineralogy‡	e_{min}	e_{max}	Model parameters					Compression Test Data Source
								a ($\times 10^{-3}$)	b ($\times 10^{-3}$)	e_{r_t}	e_{r_b}	Upper Range of Validity¶ (MPa)	
Petroleum coke	1-D	-	1.4	R	C	-	-	23.4	2.3	1.15	0.22	130	Biarez and Hicher (1994)
Quartz sand	1-D	1.15	uniform	A	Q	0.66	1.07	3.3	0.3	0.33	0.12	600	Yamamuro et al. (1996)
Cambria sand	1-D	1.42	uniform	R	Q	0.49	0.78	4.5	0.3	0.24	0.03	560	ditto
Gypsum sand	1-D	0.63	uniform	-	Ca	0.70	0.97	15.2	1.9	0.35	0.06	220	ditto
Quikrete sand	Iso	0.32	-	A	Q	0.51	0.80	2.3	0.3	0.25	0.03	510	Martin and Cazacu (2013)

*Iso=isotropic compression test; 1-D=one dimensional compression test

†A=angular ; R=round ; sA=subangular ; sR=subround

‡Q=siliceous (quartz); Ca=calcareous; C=carbonaceous; V=volcanic ash (siliceous)

¶The compression test data was available up to this stress level. #Also known as Dogs Bay sand.

CHAPTER 6

CONCLUDING REMARKS

In this dissertation, a micromechanics-based model was developed to predict the undrained behavior of sand-silt mixtures. After predicting the undrained behavior of six different types of sand-silt mixtures, it was identified that a more comprehensive model is required to predict the compressibility of sand-silt mixtures and this model should be able to explicitly consider the amount of fines in its formulation. It was also identified that a proper compressibility model should incorporate the effects of particle crushing on the void ratio change of soil.

To address the need for a new compression model, a new hypothesis for dividing the voids of a granular material into two fractions of active and inactive voids was proposed. The new compressibility model constructed on this hypothesis can predict the behavior of granular soils for a wide range of stresses up to comminution limit and it explicitly considers the amount of fines in its formulation.

Suggested future work can be as follows:

- Extending the model to the case of unloading-reloading,
- Developing a model for shear-induced volume changes in granular material based on the concept of active and inactive voids,
- Incorporating the effects of particle crushing on the critical state model.

BIBLIOGRAPHY

- Akers, S.A. 2001. Two-Dimensional Finite Element Analysis of Porous Geomaterials at Multikilobar Stress Levels. PhD Thesis, Virginia Polytechnic Institute, Blacksburg, VA, USA.
- ASTM 4253-16. 2016. Standard test methods for maximum index density and unit weight of soils using a vibratory table. ASTM International. doi:10.1520/D4253-16
- Bartholomeeusen, G., et al., 2002. Sidere: Numerical prediction of large-strain consolidation. Géotechnique 52(9), 639–648.
- Belkhatir, M., Arab, S., Della, N., Missoum, H., and Schanz, T. 2010. Influence of inter-granular void ratio on monotonic and cyclic undrained shear response of sandy soils. Comptes Rendus Mécanique 338(5), 290-303.
- Benahmed, N., Nguyen, T.K., Hicher, P.-Y., Nicolas, M. 2015. An experimental investigation into the effects of low plastic fines content on the behaviour of sand silt mixtures. Eur. J. Environ. Civ. Eng. 19:109–128. doi: 10.1080/19648189.2014.939304
- Biarez, J., Hicher, P.-Y., 1994. Elementary Mechanics of Soil Behaviour：Saturated Remoulded Soils. Balkema, Rotterdam.
- Bobei, D.C., Lo, S.R., Wanatowski, D., Gnanendran, C.T., Rahman, M.M., 2009. Modified state parameter for characterizing static liquefaction of sand with fines. Can. Geotech. J. 46, 281–295. doi:10.1139/T08-122
- Boddy R.G.H.B. 1943. Microscope observations of the crushing of coal. Nature 151:54
- Bouckovalas, G.D., Andrianopoulos, K.I., and Papadimitriou, A.G. 2003. A critical state interpretation for the cyclic liquefaction resistance of silty sands. Soil Dyn. & Earthquake Eng. 23(2), 115-125.
- Bouville, F., Studart, A.R. 2017. Geologically-inspired strong bulk ceramics made with water at room temperature. Nature Communications 8:14655. doi: 10.1038/ncomms14655
- Bowen, R.M. 1976. Theory of Mixtures, Part I. Contin. Phys. III
- Brandes, H.G. 1999. Mine burial due to wave-induced liquefaction and other processes, in: Proc. Ninth Int. Offshore & Polar Eng. Conf., Brest, France.
- Bransby, M.F., Randolph, M.F. 1998. Combined loading of skirted foundations. Géotechnique 48(5), 637–655.

- Butterfield, R. 1979. A natural compression law for soils. Géotechnique, 29(4): 469–480.
- Cabalar, A.F. 2010. Applications of the oedometer, triaxial and resonant column tests to the study of micaceous sands. Eng Geol 112:21–28. doi: 10.1016/j.enggeo.2010.01.004
- Chang, C.S. 1988. Micromechanical modeling of constructive relations for granular material. In: Satake, M., Jenkins, J.T. (Eds.), Micromechanics of Granular Materials, 271–279.
- Chang, C.S., Hicher, P.-Y. 2005. An Elasto-plastic Model for Granular Materials with Microstructural Consideration. Int. J. Solids & Structures 42, 4258-4277.
- Chang, C.S., Meidani, M. 2012. Deformation and failure of soils under erosion. NSF Civil Eng. Innov. Conf. doi: 10.13140/RG.2.1.1964.1204.
- Chang, C.S., Meidani, M., 2013. Dominant grains network and behavior of sand-silt mixtures: stress-strain modeling. Int. J. Numer. Analyt. Methods Geomech. 37(15), 2563-2589. doi:10.1002/nag.2152
- Chang, C.S., Meidani, M., Deng, Y. 2017. A compression model for sand-silt mixtures based on the concept of active and inactive voids. Acta Geotechnica, https://doi.org/10.1007/s11440-017-0598-1
- Chang, C.S., Sundaram, S.S., Misra, A. 1989. Initial moduli of particulate mass with frictional contacts. Int. J. Numerical & Analytical Methods in Geomechanics 13(6), 626-641.
- Chang, C.S., Wang J.-Y., Ge, L. 2015. Modeling of minimum void ratio for sand–silt mixtures. Eng Geol 196:293–304. doi: 10.1016/j.enggeo.2015.07.015
- Chang, C.S., Yin, Z-Y. 2011. Micromechanical modeling for behavior of silty sand with influence of fine content. Int. J. Solids & Structures 48(19), 2655-2667.
- Chen, C., Zhang, L.M., Chang, D.S. 2016. Stress-Strain Behavior of Granular Soils Subjected to Internal Erosion. J Geotech Geoenvironmental Eng 142:6016014. doi: 10.1061/(ASCE)GT.1943-5606.0001561
- Chong, S.-H., Santamarina, J.C. 2016. Soil Compressibility Models for a Wide Stress Range. J. Geotech. Geoenvironmental Eng. 142, 6016003. doi:10.1061/(ASCE)GT.1943-5606.0001482
- Choo, H., Burns, S.E. 2015. Shear wave velocity of granular mixtures of silica particles as a function of finer fraction, size ratios and void ratios. Granul Matter 17:567–578. doi: 10.1007/s10035-015-0580-2

- Chuhan, F.A., Kjeldstad, A., Bjørlykke, K., Høeg, K. 2002. Porosity loss in sand by grain crushing - experimental evidence and relevance to reservoir quality. Marine and Petroleum Geology 19(1), 39–53. doi:10.1016/S0264-8172(01)00049-6

- Cil, M.B., Buscarnera, G. 2016. DEM assessment of scaling laws capturing the grain size dependence of yielding in granular soils. Granular Matter, 18-36. doi:10.1007/s10035-016-0638-9

- Coop, M.R., 1990. The mechanics of uncemented carbonate sands. Géotechnique 40, 607–626. doi:10.1680/geot.1990.40.4.607

- Coop, M.R., Atkinson, J.H. 1993. The mechanics of cemented carbonate sands. Géotechnique 43:53–67. doi: 10.1680/geot.1993.43.1.53

- Coop, M.R., Lee, I.K., 1993. The behaviour of granular soils at elevated stresses, in: Predictive Soil Mechanics: Proc. of the Wroth Memorial Symp. London, England, pp. 186–198.

- Costa, P.J.M., Andrade, C., Mahaney, W.C., Marquez de Silva, F., Freire, P., Freitas, M.C., Janardo, C., Oliveira, M.A., Silva, T., Lopes, V., 2013. Aeolian Microtextures in Silica Spheres Induced in Wind Tunnel Experiment: Comparison with Aeolian Quartz. Geomorphology 180–181 120–129. doi:10.1016/j.geomorph.2012.09.011

- Daouadji, A., Hicher, P.-Y., 2009. An enhanced constitutive model for crushable granular materials. Int. J. Numer. Analyt. Methods Geomech. 34, 555–580. doi:10.1002/nag.815

- Dash, H.K., Sitharam, T.G. 2011. Undrained monotonic response of sand–silt mixtures: effect of nonplastic fines. Geomech Geoengin 6:47–58. doi: 10.1080/17486021003706796

- de Bono, J.P., McDowell, G.R. 2015. An insight into the yielding and normal compression of sand with irregularly-shaped particles using DEM. Powder Technololy 271:270–277. doi:10.1016/j.powtec.2014.11.013

- Domenico, S.N., 1977. Elastic properties of unconsolidated porous sand reservoirs. GEOPHYSICS 42, 1339–1368. doi:10.1190/1.1440797

- Drucker, D.C. 1988. “Comments on the modelling of the behavior of sand.” In Constitutive Equations for Granular non-Cohesive Soils, eds. Saada and Bianchini, Balkema, Rotterdam, ISBN 9061917891.

- Einav, I. 2007. Breakage mechanics - Part II: modeling granular materials. Journal of Mechanics and Physics of the Solids 55, 1298-1320. doi:10.1016/j.jmps.2006.11.004

- Emeriault, F., Cambou, B. 1996. Micromechanical modelling of anisotropic non-linear elasticity of granular medium. Int. J. Solids & Structures 33 (18), 2591–2607.

- Field, J.E., Farhat, M., Walley, S.M. 2014. Comminution limit (CL) of particles and possible implications for pumped storage reservoirs. J Mater Sci 49:3780–3784. DOI 10.1007/s10853-014-8089-3

- Floyd, T. L., Buchla, D. M. 2009. Electronics fundamentals: circuits, devices & applications, 8th ed., Prentice Hall.

- Fourie, A. B., Papageorgiou, G. 2001. Defining an appropriate steady state line for Merriespruit gold tailings. Can. Geotech. J. 38, 695-706.

- Furnas, C.C. 1931. Grading aggregates, I-mathematical relations for beds and broken solids of maximum density. Ind. Eng. Chem. 23 (9), 1052-1058.

- Georgiannou, V.N. 2006. The undrained response of sands with additions of particles of various shapes and sizes. Géotechnique 56:639–649. doi: 10.1680/geot.2006.56.9.639

- Graton, L.C., Fraser, H.J. 1935. Systematic packing of spheres: with particular relation to porosity and permeability. J. Geology 43(8), Part I, 785-909.

- Hagan, J.T. 1981. Impossibility of fragmenting small particles: brittle–ductile transition. J Mater Sci 16:2909–2911

- Hardin, B.O. 1987. 1-D strain in normally consolidated cohesionless soils. ASCE J. Geotechnical Engineering Division 113(12), 1449-1467.

- Hendron, A.J. 1963. The behavior of sand in one-dimensional compression. Ph.D. thesis, Dept. Civil and Env.Eng., Univ. Illinois at Urbana-Champaign, Urbana, Ill.

- Hicher, P.-Y. 2013. Modelling the impact of particle removal on granular material behaviour. Geotechnique 63:118–128. doi: 10.1680/geot.11.P.020

- Hicher, P.-Y., Chang, C.S. 2005. Evaluation of two homogenization techniques for modeling the elastic behavior of granular materials. ASCE J. Eng. Mech. 131(11), 1184-1194.

- Hong, Z.S., Zeng, L.L., Cui, Y.J., Cai, Y.Q., Lin, C. 2012. Compression behaviour of natural and reconstituted clays. Geotechnique 62(4), 291–301.

- Houlsby, G.T., Kelly, R.B., Huxtable, J., Byrne, B.W. 2005. Field trials of suction caissons in clay for offshore wind turbine foundations. Géotechnique 55(4), 287–296.

- Hyodo, M., Nakata, Y., Aramaki, N., Hyde, A.F.L., Inoue, S. 2000. Liquefaction and particle crushing of soil. Proc. 12th World Conf. on Earthqauke Engrg.

- Hyodo, M., Nakata, Y., Yoshimoto, N., Kato, Y., Okabayashi, T. 2001. The role of fines in the shear and liquefaction of a volcanic soil "Shirasu" as a reclamation

material, in: Proc. 11th Int. Offshore and Polar Engineering Conf. Norway, pp. 501–507.

- Jenkins, J.T. 1988. Volume change in small strain axisymmetric deformations of a granular material. In: Satake, M., Jenkins, J.T. (Eds.), Micromechanics of Granular Materials, 143-152.

- Jenkins, J.T., Strack, O.D.L. 1993. Mean-field inelastic behavior of random arrays of identical spheres. Mechanics of Material 16, 25–33.

- Juárez-Badillo, E., 1981. General compressibility equation for soils, in: Proc. 10th Int. Conf. on Soil Mechanics and Foundation Engineering. Stockholm, Sweden, pp. 171–178.

- Ke, L., Ouyang, M., Horikoshi, K., Takahashi, A. 2016. Soil deformation due to suffusion and its consequences on undrained behavior under various confining pressures. Japanese Geotech Soc Spec Publ 2:368–373. doi: 10.3208/jgssp.JPN-083

- Ke, L., Takahashi, A. 2015. Drained Monotonic Responses of Suffusional Cohesionless Soils. J Geotech Geoenvironmental Eng 141:1–8. doi: 10.1061/(ASCE)GT.1943-5606.0001327

- Kendall, K. 1978 The impossibility of comminuting small particles by compression. Nature 272:710–711.

- Kendall, K. 1978. Complexities of compression failure. Proc R Soc Lond A 361:245–263

- Khalil, T., Saiyouri, N., Muresan, B., Hicher, P.-Y. 2013. Internal erosion of chemically reinforced granular materials: a mathematical modeling approach. Int J Numer Anal Methods Geomech 37:491–502. doi: 10.1002/nag.1108

- Kikumoto, M., Muir Wood, D., Russel, A. 2010. Particle crushing and deformation behavior. Soils and Foundations 50(4), 547-563.

- Kolymbas, D., 2012. The misery of constitutive modelling. In Consitutive modelling for granular materials, Kolymbas, D. (ed.), Springer Berlin Heidelberg. ISBN: 978-3-642-57018-6. doi: 10.1007/978-3-642-57018-6_1

- Konishi, Y., Hyodo, M., Ito, S. 2007. Compression and undrained shear characteristics of sand-fines mixtures with various plasticity. JSCE J Geotech Geoenvironmental Eng 63:1142–1152. doi: 10.2208/jscejc.63.1142

- Krost, K., Gourvenec, S.M., White, D.J., 2011. Consolidation around partially embedded seabed pipelines. Géotechnique 61(2), 167–173.

- Kruyt, N.P., Rothenburg, L. 2002. Micromechanical bounds for the effective elastic moduli of granular materials. Int. J. Solids & Structures 39 (2), 311-324.

- Kuerbis, R.H. 1989. The effect of gradation and fines content in the undrained loading response of sand, Master of App. Sci. dissertation, Univ. of British Columbia, Vancouver, Canada.

- Lade, P.V., Abelev, A.V. 2005. Characterization of cross-anisotropic soil deposits from isotropic compression tests. Soils Found. 45, 89–102.

- Laufer, I. 2015. Grain crushing and high-pressure oedometer tests simulated with the discrete element method. Granular Matter 17:389–412. DOI 10.1007/s10035-015-0559-z

- Lee, K.L., Seed, H.B. 1967. Drained strength characteristics of sands. J. Soil Mech. Found. Div 93, 117–141.

- Lehane, B., Fahey, M., 2002. A simplified nonlinear settlement prediction model for foundations on sand. Can. Geotech. Journal, 39, 293–303. doi:10.1139/T01-091

- Liao, C.L., Chan, T.C., Suiker, A.S.J., Chang, C.S. 2000. Pressure-dependent elastic moduli of granular assemblies. Int. J. Analytical & Numerical Methods in Geomechanics 24, 265-279.

- Liu, M., Gao, Y. 2016. Constitutive modeling of coarse-grained materials incorporating the effects of particle breakage on critical state behavior in a framework of general plasticity. Int. J. of Geomechanics. doi:10.1061/(ASCE)GM.1943-5622.0000759

- Maleej, Y., Dormieux, L., Sanahuja, J. 2009. Micromechanical approach to the failure criterion of granular media. European J. Mechanics A/Solids 28, 647-653.

- Marachi, N.D., Chan, C.K., Seed, H.B., Duncan, J.M. 1969. "Strength and deformation characteristics of rockfill materials," Dept. of Civil Engineering, University of California, Berkeley, California.

- Martin, B.E., Cazacu, O., 2013. Experimental and theoretical investigation of the high-pressure, undrained response of a cohesionless sand. Int. J. Numer. Analyt. Methods Geomech. 37, 2321–2347. doi:10.1002/nag.2143

- Matsuoka, H., Takeda, K. 1980. A stress–strain relationship for granular materials derived from microscopic shear mechanisms. Soils & Foundation 20 (3), 45-58.

- McDowell G.R., Bolton, M.D., Robertson, D. 1996. The fractal crushing of granular materials. J. Mech. Phys. Solids, 44(12), 2079-2102.

- McKeon, R. (translator) 1963. Posterior Analytics. Aristotle.

- Meidani, M., Chang, C.S., Deng, Y. 2017. On active and inactive voids and a compression model for granular soils (In Press). Eng Geol. doi: 10.1016/j.enggeo.2017.03.006

- Mesri, G., Vardhanabhuti, B., 2009. Compression of granular material. Can. Geot. J. 46, 369-392. doi:10.1139/T08-123

- Minh, N.H., Cheng, Y.P. 2013. A DEM investigation of the effect of particle-size distribution on one-dimensional compression. Geotechnique 63, 44–53. doi:10.1680/geot.10.P.058

- Misra, A. Yang, Y. 2010. Micromechanical model for cohesive materials based upon pseudo-granular structure. Int. J. Solids & Structures 47, 2970-2981.

- Mitchell, J.K., 1993. Fundamentals of soil behavior, Second ed., Wiley Interscience Publ.

- Miura, N., Murata, H., Yasufuku, N. 1984. "Stress-strain characteristics of sand in a particle-crushing region." Soils and Foundations 24(1), 77-89.

- Murthy. T.G., Loukidis D., Carraro. J.A.H. 2007. Undrained monotonic response of clean and silty sands. Géotechnique 57:273–288. doi:10.1680/geot.2007.57.3.273

- Ni, Q., Tan, T. S., Dasari, G. R., Hight, D. W. 2004. Contribution of fines to the compressive strength of mixed soils. Géotechnique 54(9), 561-569.

- Nicot, F. Darve, F. 2007. Basic features of plastic strains: From micro-mechanics to incrementally nonlinear models. Int. J. Plasticity 23, 1555-1588.

- Oakeshott, R.B.S., Edwards, S.F. 1994. Perturbative theory of the packing of mixtures and of non-spherical particles. Physica A (202), 482-498.

- Oda, M. 1977. Coordination number and its relation to shear strength of granular material. Soils & Foundations 17(2), 29-42.

- Oldecop, L.A., Alonso, E.E. 2001. A model for rockfill compressibility. Géotechnique 51(2), 127-139. doi:10.1680/geot.51.2.127.40283

- Pestana, J.M., Whittle, A.J. 1995. Compression model for cohesionless soils. Geotechnique 45:611–631. doi: 10.1680/geot.1995.45.4.611

- Podcreck, F. Sharma, M. 1996. The influence of particle size and shape of components of binary powder mixtures on the maximum volume reduction due to packing. Int. J. Pharmaceutics 137, 41-47.

- Polito, C.P., Martin, J.R. 2001. Effects of Nonplastic Fines on the Liquefaction Resistance of Sands. 127:408–415. doi:10.1061/(ASCE)1090-0241(2001)127:5(408)

- Puttick, K.E. 1979. Energy scaling, size effects and ductile-brittle transitions in fracture. J Phys D Appl Phys 12:L19–L23

- Rahman, M.M., Lo, S.R., Gnanendra, C.T. 2008. On equivalent granular void ratio and steady state behavior of loose sand with fines. Can. Geotech. J. 45, 1439-1456.
- Rassouly, S.M.K. 1999. The packing density of perfect binary mixtures. Powder Technol. 103, 145-150.
- Rees, S.D. 2010. Effects of fines on the undrained behavior of Christchurch sandy soils. Ph.D dissertation, Univ. of Canterbury, Christchurch, New Zealand.
- Ren, W., Zhang, Z., Wang, Y., Kan, G., Tan, Q., Zhing, Z., Su, F. 2015. Preparation of porous carbon microspheres anode materials from fine needle coke powders for lithium-ion batteries. RSC Adv. (5), 11115-11123. doi:10.1039/C4RA15321A
- Reuss, A. 1929. lsquoBerechnung der Fließgrenze von Mischkristallen auf Grund der Plastizitätsbedingung für Einkristalle. Z. Angew. Math. Mech. 9, 49-58.
- Roscoe, K.H., Burland, J.B. 1968. On the generalized stress–strain behaviour of 'wet' clay, in: Heyman, J., Leckie, F. A. (Eds.), Engineering Plasticity. Cambridge University Press, London, U.K., 535-609.
- Rothenburg, L. Selvadurai, A.P.S. 1981. Micromechanical definitions of the Cauchy stress tensor for particular media. In: Selvadurai, A.P.S. (Ed.), Mechanics of Structured Media. Amsterdam, Elsevier, 469-486.
- Rumpf, H., Schönert, K. 1972. Die Brucherscheinungen in Kugeln bei elastischen sowie plastischen Verformungen durch Bruck- beanspruchung. Dechema Monograph 69:51–86.
- Russell, A.R., Khalili, N. 2004. A bounding surface plasticity model for sands exhibiting particle crushing. Can Geotech J 41:1179–1192. doi: 10.1139/t04-065
- Salgado, R., Bandini, P., Karim, A. 2000. Shear strength and stiffness of silty sand. ASCE J. Geotech. & Geoenviron. Eng. 126(5), 451-462.
- Schofield, A.N., Wroth, C.P. 1968. Critical state soil mechanics. Maidenhead, England.
- Shaebani, M.R., Madadi, M., Luding, S., Wolf, D.E. 2012. Influence of polydispersity on micromechanics of granular materials. Physical Review E 85, 011301.
- Shahnazari, H., Rezvani, R. 2013. Effective parameters for the particle breakage of calcareous sands: An experimental study. Eng. Geol. 159, 98–105. doi:10.1016/j.enggeo.2013.03.005
- Sherwood, J.D., Meeten, G.H. 1997. The filtration properties of compressible mud filtercakes. J. Pet. Sci. Eng. 18, 73–81. doi:10.1016/S0920-4105(97)00005-3

- Sladen, J.A., Hollander, D.R.D., Krahn, J. 1985. The liquefaction of sands, a collapse surface approach. Can. Geotech. J. 22(4), 564-578.
- Spagnoli, G., Doherty, P., Wu, D., Doherty, M. 2015. Some mineralogical and geotechnical properties of carbonate and silica sands in relation to a novel mixed-in-place pile. in Offshore Mediterranean Conference and Exhibition, Ravenna, Italy.
- Stamatopoulos, C.A. 2010. An experimental study of the liquefaction strength of silty sands in terms of the state parameter. Soil Dyn Earthq Eng 30:662–678. doi: 10.1016/j.soildyn.2010.02.008
- Stark, T.D., Choi, H., Schroeder, P.R. 2005. Settlement of Dredged and Contaminated Material Placement Areas. II: Primary Consolidation, Secondary Compression, and Desiccation of Dredged Fill Input Parameters. J. Waterw. Port, Coastal, Ocean Eng. 131, 52–61. doi:10.1061/(ASCE)0733-950X(2005)131:2(52)
- Taylor, D.W. 1948. Fundamentals of Soil Mechanics. John Wiley and Sons, New York, NY.
- Tengattini, A., Das, A., Einav, I. 2016. A constitutive modelling framework predicting critical state in sand undergoing crushing and dilation.
- Terzaghi, K. 1956. Varieties of submarine slope failures. Proc. 8th Texas Conference on Soil Mech. Found. Eng., Univ. of Texas, Austin, TX, USA.
- Terzaghi, K., Peck, R.B., 1948. Soil mechanics in engineering practice. Wiley, New York.
- Thevanayagam, S., 1998 Effect of fines and confining stress on undrained shear strength of silty sands. ASCE J. Geotech. & Geoenviron. Eng. 124(6), 479-491.
- Thevanayagam, S., Mohan, S. 2000. Intergranular state variables and stress-strain behavior of silty sands. Geotechnique 50(1), 1-23.
- Thevanayagam, S., Shenthan, T., Mohan, S., Liang, J. 2002. Undrained Fragility of Clean Sands, Silty Sands, and Sandy Silts. J Geotech Geoenvironmental Eng 128:849–859. doi: 10.1061/(ASCE)1090-0241(2002)128:10(849)
- Tran, T-H, Monchiet, V., Bonnet, G. 2012. A micromechanics-based approach for derivation of constitutive elastic coefficients of strain-gradient media. Int. J. Solids & Structures 49(5), 783-792.
- Troncoso, J. H., 1988. Evaluation of seismic behavior of hydraulic fill structures, in: Geotech. Spec. Publ. 21, ASCE, New York, 475-491.
- Vaid, Y.P. 1994. Liquefaction of silty soils. In: Proc. of Ground failures under seismic conditions. Geotech. Spec. Publ. 44, ASCE, New York, 1–16.

- Vesic, A.S., Clough, G.W. 1968. Behavior of granular materials under high stresses. J. Soil Mech. Found. Div 94, 661–688.
- Voigt, W. 1910. Lerrbuch der Kristallphysik, Teubner-Verlag, Leipzig.
- Walton, K. 1987. The effective elastic moduli of a random packing of spheres. J. Mechanics & Physics of Solids 35, 213-226.
- Wilson, T. M., Jenkins, S. F., Stewart, C. 2015. Volcanic ash fall impacts. In. S.C. Loughlin, R.S.J. Sparks, S.K. Brown, S.F. Jenkins & C. Vye-Brown (eds) Global Volcanic Hazards and Risk, Cambridge: Cambridge University Press.
- Wu, Y., Yamamoto, H., Izumi, A. 2016. Experimental investiogation on crushing of granular material in one-dimensional test. Period. Polytech. Civil Eng. 60(1), 27-36. doi:10.3311/PPci.8028
- Yamamuro, J.A., Bopp, P.A., Lade, P. V. 1996. One-Dimensional Compression of Sands at High Pressures. J. Geotech. Eng. 122, 147–154. doi:10.1061/(ASCE)0733-9410(1996)122:2(147)
- Yamamuro, J.A., Covert, K.M. 2001. Monotonic and cyclic liquefaction of very loose sands with high silt content. J Geotech Geoenvironmental Eng 127:314–324. doi: 10.1061/(ASCE)1090-0241(2001)127:4(314)
- Yamamuro, J.A., Lade, P.V. 1999. Experiments and modelling of silty sands susceptible to static liquefaction. Mech Cohesive-frictional Mater 4:545–564. doi: 10.1002/(SICI)1099-1484(199911)4:6
- Yang, S. L. 2004. Characterization of the properties of sand–silt mixtures. Ph.D. dissertation, Norwegian Univ. Sci. Tech., Trondheim, Norway.
- Yang, S. L., Sandven, R., Grande, L. 2006. Instability of sand silt mixtures. Soil Dyn. & Earthquake Eng. 26, 183-190.
- Yang, S., Lacasse, S., Sandven, R. 2006. Determination of the transitional fines content of mixtures of sand and non-plastic fines. Geotech Test J 29:1–6. doi: 10.1520/GTJ14010
- Yu, A.-B., Standish, N., McClean, A. 1993. Porosity calculation of binary mixtures of nonspherical particles. J. Am. Ceram. Soc. 76(11), 2813-2816.
- Zhang, W., Zhao, C. 2011. Micromechanics analysis for unsaturated granular soils. Acta Mechanica Solida Sinica 24(3), 273-281.
- Zheng, W., Tannant, D. 2016. Frac sand crushing characteristics and morphology changes under high compressive stress and implications for sand pack permeability. Can. Geotech. J. 53, 1412-1423. doi:10.1139/cgj-2016-0045

- Zhu, Q.Z., Shao, J.F., Mainguy, M. 2010. A micromechanics-based elastoplastic damage model for granular materials at low confining pressure. Int. J. Plasticity 26, 586-602.

- Zimbardo, M. 2016. Mechanical behaviour of Palermo and Marsala calcarenites (Sicily), Italy. Engineering Geology 210, 57-69.

- Zlatovic, S. 1994. Residual strength of silty soils. D.Eng dissertation, Univ. of Tokyo, Japan.

- Zlatovic, S. Ishihara, K. 1997. Normalized behavior of very loose non-plastic soils: effects of fabric. Soils & Foundations 37(4), 47-56.

- Zlatović, S., Ishihara, K. 1995. On the influence of nonplastic fines on residual strength. In: First Int. Conf. Earthq. Geotech. Eng., Tokyo, Japan, 239–244